COMPARATIVE EVALUATION
OF A
A HYDROFOIL-ASSISTED TRIMARAN

Thesis presented in partial fulfillment of
the requirements for the degree

MASTER OF SCIENCE IN ENGINEERING

By

Ryno Moolman

Supervisor
Prof. T.M. Harms
Department of Mechanical Engineering
University of Stellenbosch

Co-supervisor
Dr. G. Migeotte
CAE Marine

December 2005

Declaration

I, the undersigned, declare that the work contained in this thesis is my own original work and has not previously, in its entirety or in part, been submitted at any University for a degree.

Signature of Candidate

Date

Abstract

This work is concerned with the design and hydrodynamic aspects of a hydrofoil-assisted trimaran. A design and configuration of a trimaran is evaluated and the performance of a hydrofoil-assisted trimaran is effectively compared to the performance of a hydrofoil-assisted catamaran with similar overall displacement and same speed. The performance of the trimaran with different outrigger clearances are also evaluated and compared. The hydrodynamic aspects focuses mainly on the performance and to a lesser extend on the sea-keeping and stability of a hydrofoil-assisted trimaran. The results were determined by means of experimental testing, theoretical analysis and numerical analysis. The project was initiated as a result of the success of the hydrofoil-assisted catamarans and due to the fact that there does not exist a hydrofoil-assisted trimaran (to the author's knowledge) where the main focus of the foils is to significantly reduce the resistance.

A brief history, recent developments and associated advantages regarding trimarans are discussed. A complete theoretical model is presented to evaluate the lift and drag of the hydrofoils, as well as, the resistance of the trimaran. The data so obtained is then used to compare the reliability and feasibility of the numerical and experimental predicted values.

The design of the trimaran and hydrofoil system is explained, together with the problems associated with the final design of the trimaran. The design of a trimaran is much more complicated than a catamaran due to more design variables being associated with trimarans. The selection of the trimaran configuration is done in a logical manner considering stability and hydrodynamics. However, the hydrofoil-assisted trimaran is closely adapted to the main dimensions of the comparable hydrofoil-assisted catamaran.

An in-depth discussion of the testing technique used and the problems that are associated with towing tank testing will facilitate similar tests in the future. The scaling method of Froude was modified to account for the different sized hulls. The numerical methods are explained, with emphasis on accuracy, limitations, feasibility and the time required to complete a calculation.

The results are presented in an order suggested by the experimental and numerical work carried out. The resistance, trim and rise/sinkage results are presented with speed for both the trimaran and catamaran with and without the addition of foils. The addition of the foils supplies results based on the amount of lift the foils carry and therefore can easily clarify the significant resistance advantage the foils offer the trimaran and the catamaran evaluated in this project.

The final design and results of the evaluated trimaran are discussed. It is concluded that the catamaran with similar displacement and speed is still superior to the trimaran, with and without foils in both cases. The addition of foils to the trimaran does decrease the resistance significantly. The conclusions regarding these results are presented, together with recommendations for future work.

Opsomming

Hierdie studie is gerig op die ontwerp en hidrodinamiese aspekte van ‘n hidrovleuel-gesteunde drierompskuit. ‘n Ontwerp en konfigurasie van ‘n drierompskuit is ge-evalueer en dan is die werksverigting van ‘n hidrovleuel-gesteunde drierompskuit effektief vergelyk met die werksverigting van ‘n hidrovleuel-gesteunde katamaran met dieselfde algehele verplasing en dieselfde spoed. Die werksverigting van ‘n drierompskuit met verskillende hulpskuit posisies is ook geëvalueer en vergelyk. Die hidrodinamiese aspekte fokus meestal op die werksverigting en tot ‘n minder mate op die see-vaardigheid en stabiliteit van ‘n hidrovleuel-gesteunde drierompskuit. Die resultate is verkry deur gebruik te maak van model toetse, teoretiese en numeriese motodes. Die projek is geloods na aanleiding van die sukses van hidrovleuel-gesteunde katamarans en ook as gevolg van die feit dat aar geen hidroveuel-gesteunde drierompskuit (so ver soos die outeur se kennis strek) waar die fokus van die hidroveuel meestal gerig is om die weerstand beduidend te verminder.

‘n Vlugtige geskiedenis, die nuutste ontwikkelings en the gepaardgaande voordele van ‘n drierompskuit word bespreek. ‘n Volledige teoretiese model is vertoon en word gebruik om die hefkrag en die sleurkrag te evalueer, asook, die weerstand van die drierompskuit. Die verwerkte data word gebruik om die betroubaarheid en uitvoerbaarheid van die numeriese en eksperimentele voorspelde waardes te vergelyk.

Die ontwerp van die drierompskuit en hidrovleuel sisteem word verduidelik, tesame met die probleme wat gepaard gaan met final ontwerp van buide die drierompskuit. Die ontwerp van die drierompskuit is baie meer gekompliseerd as die van ‘n katamaran as gevolg van meer ontwerp veranderlikes wat geassosieer is met ‘n drierompskuit. Die keuring van die drierompskuit se konfigurasie is gedoen op ‘n logiese manier wat die stabiliteit en hidrodinamika in aanmerking neem. Nogtans, is die hidrovleuel-gesteunde drierompskuit naastenby aangepas om by die hoof vernaamste dimensies van ‘n vergelykbare hidrovleuel-gesteunde katamaran te pas.

‘n Diepgaande studie van die toets tegniek wat gebruik is, laat die moontlikheid van toekomstige studie van ‘n soortegelyke toets te onderneem asook om bewus te wees van die probleme wat gepaard gaan met sleeptenk toetse. Die skalering metode wat gebruik was is ‘n gewysigde Froude metode wat die verskillende grotes van die rompe in agneem. Die numeriese metodes se akkuraatheid, beperkings, uitvoerbaarheid en die tyd benodig om ‘n berekining te doen word ook in aanmerking geneem.

Die resultate word in ‘n ordelikke manier voorgestel wat hoofsaaklik deur eksperimentele werk en numeriese werk bereken was. Die weerstand, trim en styging/sakking resultate word voorgestel saam met spoed vir beide die drierompskuit en die katamaran met en sonder hidrovleuels in beide gevalle. Die byvoeging van hidrovleuels weergee die resultate wat gebaseer is op die hoeveelheid hefkrag wat die hidrovleuels drae en daarvoor kan maklik verklaar word die beduidende weerstands voordeel wat die hidrovleuels die drierompskuit en die katamaran wat geëvalueer was in die projek bied.

Die finale ontwerp en resultate van die geëvalueerde drierompskuit word bespreek. Dis afgelei dat die katamaran met dieselfde verplasing en spoed beter is as die drierompskuit, met en sonder hidrovleuels in beide gevalle. Die byvoeging van hidrovleuels aan die drierompskuit verminder die weerstand beduidend. Die gevolgtrekking aangaande die resultate word voorgelê saam met toekomstige verwante werk.

Acknowledgements

A number of different people need to be acknowledged and thanked for their guidance and support in this study. Thank you to the promoter of this project Prof. T.M Harms for continuously guiding the project in the right direction. Thank you to the co-supervisor Dr G. Migeotte. The unlimited knowledge that was extended towards this project is greatly appreciated. Special thanks to Dr. N. Kornev that made the software of Autowing Version 3.0 available. Thanks to Mr. S. Tannous, Mr. L. Kababula, Mr. C. Zietsman and Mr. F. Zietsman for assisting in testing and manufacturing. Lastly, thanks to the National Research Foundation and CAE-Marine for the financial support.

Contents

Nomenclature

A	Pankhurst constant [-]
A_x	Maximum cross sectional area [m^2]
a_f	Horizontal distance between struts [m]
AR	Aspect ratio [-]
B	Center of buoyancy [m]
b	Outrigger transverse clearance distance [m]
b_c	Channel width [m]
b_f	Foil span length [m]
c	Chord Length [m]
C_A	Correlation coefficient [-]
C_B	Block coefficient [-]
C_D	Hydrofoil total drag coefficient [-]
C_{Di}	Hydrofoil induced drag coefficient [-]
C_{Dint}	Hydrofoil interference drag coefficient [-]
C_{DP}	Hydrofoil profile drag coefficient [-]
C_{DS}	Strut drag coefficient [-]
C_{DW}	Hydrofoil wave drag coefficient [-]
C_F	Frictional drag coefficient [-]
C_L	Hydrofoil lift coefficient [-]
$C_{L\alpha}$	Hydrofoil lift curve slope [-]
C_P	Pressure coefficient [-]
C_R	Residuary resistance coeffcient [-]
C_T	Total resistance coeffcient [-]
ΔC	Correlation coefficient [-]
d	Water depth [m]
Fn	Froude number [-] $\{V/\sqrt{gL}\}$
Fn_c	Chord Froude number [-] $\{V/\sqrt{gc}\}$

Fn_d	Depth Froude number [-] $\{V/\sqrt{gd}\}$
Fn_h	Depth Froude number [-] $\{V/\sqrt{gh}\}$
G	Center of gravity [m]
h	Submerged depth of foil [m]
h'	Twice the submerged depth of foil [m]
h_c	Channel depth [m]
I	Dubrovsky's interaction coefficient [-]
k_φ	Lift curve slope correction factor [-]
$(1+k)$	Form factor [-]
L	Length of vessel [m]
L^*	Length of model [m]
L_p	Lower surface ordinates of foil profile [m]
L_{pp}	Length between perpendiculars [m]
L_{MH}	Length of main-hull [m]
L_{wl}	Water line length [m]
M	Meta-centric height [m]
m_p	Emperical correction factor [-]
P	Free surface correction factor [-]
p	Vessels wetted perimeter [m^2]
Rn	Reynolds number [-] $\{VL/v\}$
Rn^*	Model Reynolds number [-] $\{VL^*/v\}$
R_F	Friction resistance [N]
R_H	Hydraulic radius [m]
R_R	Residual resistance [N]
R_T	Total resistance [N]
R_O	Total outriggers resistance [N]
S	Planform area of foil [m^2]
Sw	Wetted surface area [m^2]
t	Maximum foil thickness [m]
t_c	Catamaran clearance [m]

t_o	Outrigger clearance [m]
U_p	Upper surface ordinates of foil profile [m]
V	Velocity [m/s]
V_{crit}	Critical velocity [m/s]
V_H	Speed in restricted channel [m/s]
V_∞	Corresponding speed in deep water [m/s]

Greek Symbols

α	Angle-of-attack [measured in radians]
α_0	Zero lift angle-of-attack [measured in radians]
β	Strut free surface angle [degrees]
ξ	Planform correction factor [-]
ρ	Density [kg/m^3]
σ	Munk's interference factor [-]
φ	Free surface correction factor [-]
∇	Trimaran displacement [m^3]
Γ	Dihedral [measured in radians]
Λ	Sweep [measured in radians]

Subscripts

MH	Main-hull
O	Outriggers

Superscripts

*	Ship model

Abbreviations and Acronyms used in text and references

AAC	Average Aerodynamic Chords
CAE	Stellenbosch Automotive Engineering
COP	Closest Outrigger Position
DAQ	Data Acquisition Device
FOP	Furthest Outrigger Position
HSC	High-Speed Craft
ITTC	International Towing Tank Conference
LCB	Longitudinal Center of Buoyancy
LCF	Longitudinal Center of Floatation
LCG	Longitudinal Center of Gravity
MOP	Middle Outrigger Position
NACA	National Advisory Committee for Aeronautics
NWBS	North West Bay Ships
WPA	Water plane area
WSA	Wetted surface area

List of Figures

p.

List of Tables

Chapter 1 Introduction

1.1 History of Trimarans

The first recorded date of both proas and boats with outriggers used by the Polynesians are as early as the 1800. These native hollowed-out tree trunks had a high length-to-beam ratio and the outriggers supplied the stability of the canoe. The concept has, however, developed over the last couple of years to become today what we called a trimaran. According to Armstong (2004), only from 1970 onwards has research been conducted in Russia when the concept of outriggers was re-discovered that led to a number of patents (Lyakhovitsky, 1976).

The Russians are responsible for the term "*trimaran*" that we still use today. In Russia the term "*trimaran*" is specifically used for a vessel with three identical hulls, whereas in the USA and UK this term has more often been associated with a larger central hull and two smaller side hulls (Dubrovsky, 2004). In this document, the latter definition will be used.

Figure 1.1: Nigel Irens "*Cable and Wireless Adventurer*" (Irens, 2005)

Major advances in ships with outriggers emerged in the 1970's from innovative designs and pioneering studies at the Zelenodesk Design Bureau on the Volga River where naval ships were

designed and built for the Soviet Navy (Dubrovsky, 2004). In 1986, the Super-Outrigger was built in Hawaii that introduced the advantages of the larger deck area and higher safety created by the outriggers. In 1989, Nigel Irens demonstrated the advantages of a trimaran, which more correctly should be called a stabilized mono-hull. This stabilized mono-hull, *Ilan Voyager* won a race that circled Britain and in 1998 he won the circumnavigation race around the world with a world record of 74 days with a 35 m trimaran called *Cable and Wireless Adventurer* illustrated in figure 1.1 (Armstrong, 2004).

1.2 Recent Developments of Trimarans

The passenger and vehicle transport industry also realized the advantages of the trimaran concept and a number of passenger ferries with outriggers were built in 2001. The 55 m ferry *Dolphin Ulsan* was built by North West Bay Ships (NWBS) in Australia and is shown in figure 1.2. This ferry is capable of achieving an operating speed of 40 knots with three MTU 16V4000 marine diesel engines delivering 2 320 kW each, while an equivalent catamaran or mono-hull would require four engines of equal capacity to achieve the same speed. Therefore, adding US$550 000 to annual operating fuel and engine maintenance costs (Dolphin Ulsan, 2005).

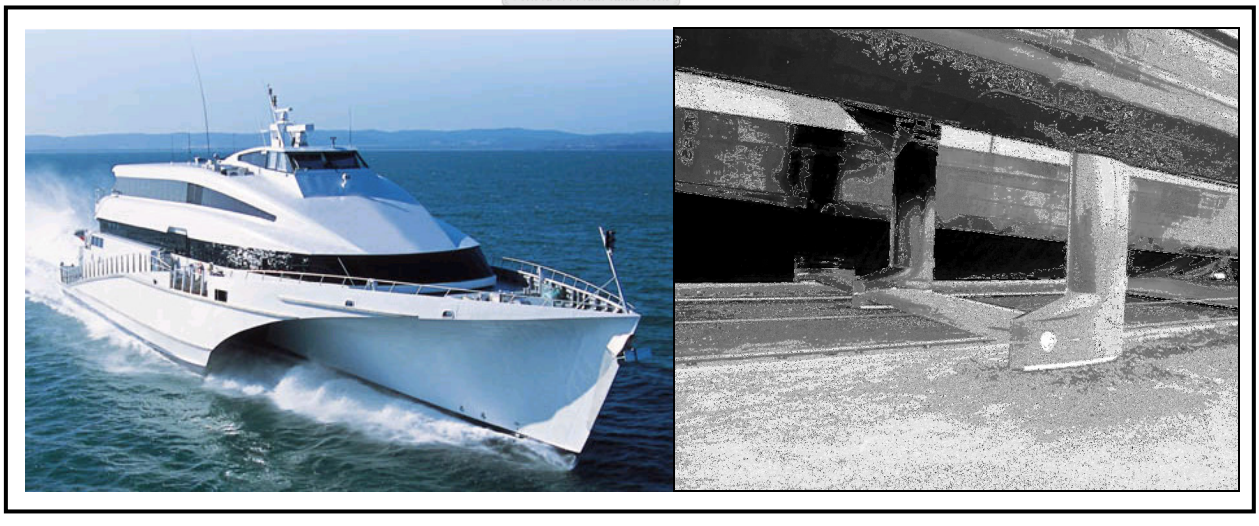

Figure 1.2: Passenger trimaran ferry, "*Dolphin Ulsan*" and its ride-control system (Dolphin Ulsan, 2005)

Overall length, m	54.5	Power, kW	3 x 2320
Beam, m	15.3	Service Speed, kn	40
Depth, m	5.5	Full Speed, kn	44.5
Deadweight, tonnes	57	Passenger Capacity	484

Table 1.1: Principle characteristics of the *Dolphin Ulsan*

The 127 m trimaran "*Benchijigua Express*" was built by West Australia Shipyard, Austal and launched in 2004 and is illustrated in figure 1.3. The "*Benchijigua Express*" is the world's largest all-aluminum ship and the most significant vessel to arrive on the fast ferry stage that will improve fast sea transportation. The trimaran offered an improvement of more than 35 % in terms of passenger capacity, deadweight and freight lane meters compared to other vessel types and at the same time the passenger comfort increased by 25 % to 40 % depending on sea conditions as claimed by the manufacturers (Fast, 2005). A major novelty of the trimaran concept is the separation of stability from comfort that has not been possible on any other type of craft supported by buoyancy forces (Armstrong and Holden, 2003). During sea trials with operating ride control "*Benchijigua Express*" achieved a speed of 40.4 knots whilst carrying deadweight of 500 tonnes with a propulsion system of 32.8 MW. This ferry operates in the Canary Islands with a capacity to carry 1 350 passengers and 341 cars.

Figure 1.3: The largest diesel-powered fast ferry, "*Benchijigua Express*" (Austal, 2005)

Yachts are also using the advantages that the trimaran hull concept has to offer. NWBS designed an *e-motion* series of different size motorized yachts ranging between 30 to 100 meters. An *e-*

motion series yacht is illustrated in figure 1.4. The vessels vertical acceleration was decreased by 50 % compared to an equivalent length mono-hull at 20 knots in 2 m bow waves.

Figure 1.4: A yacht from the *e-motion* series (e-motion, 2005a)

The upper deck area was also increased as shown in figure 1.5. The 61 m *e-motion* provides main and upper deck areas equivalent to a 75 m mono-hull. Trimarans have significantly less resistance and outperform comparable mono-hulls throughout the entire speed range as results of the *e-motion* series show in figure 1.6.

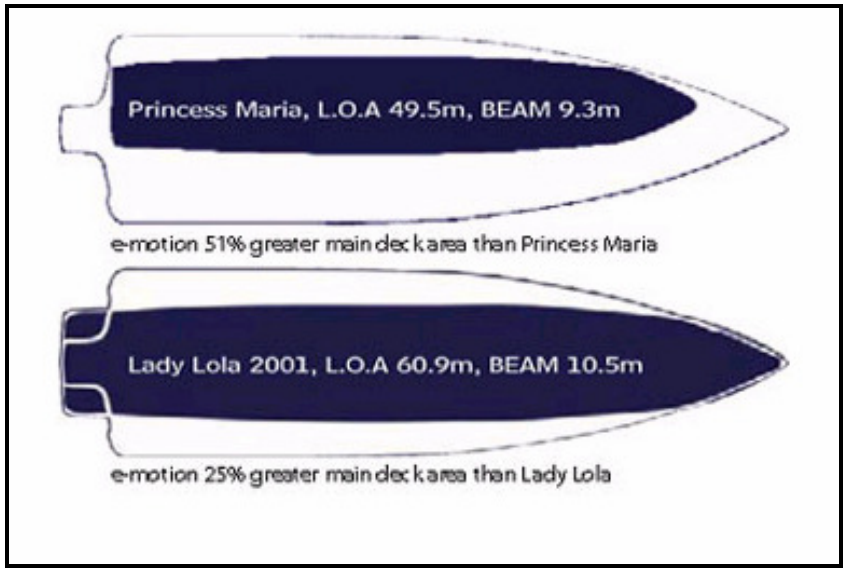

Figure 1.5: The *e-motion* series larger deck area (e-motion, 2005b)

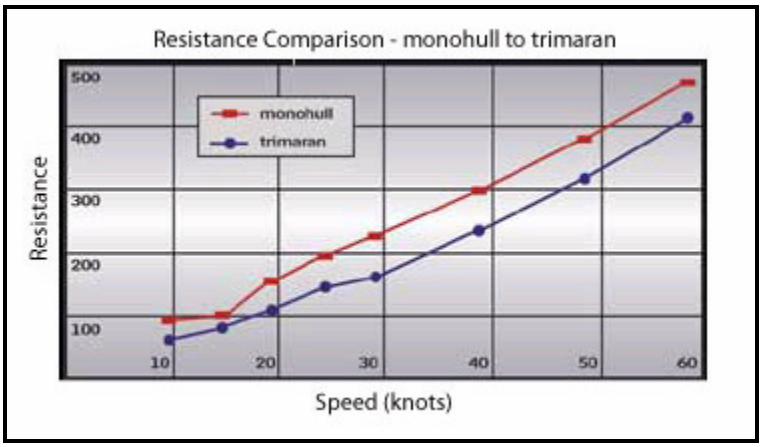

Figure 1.6: Resistance data of the *e-motion* series comparing equivalent mono-hull and trimaran (e-motion, 2005c)

"The trimaran configuration offers, above mono-hull and twin-hull vessels, many hydrodynamic and layout advantages for ship types that require a relative high performance, seaworthiness, maneuverability, large deck area (as shown), stability, while having a low speed loss in waves and minimizing the drag at high speeds" (Bricknell and Carlisle, 2004). These are very important characteristics for military purpose and fast ferries due to increased cargo capacity and passenger comfort. The trimaran concept offers a certain arrangement that can be made on the upper deck that in the past could not. This is especially beneficial to warships.

There is very little research done and not much available information on hydrofoil-assisted trimarans. Though, the research that has been done by NWBS on an active foil ride control system shows a significant decrease in total resistance for speeds above 25 knots (Tulk and Quigley, 2004). The hydrofoil system shown in figure 1.2 operates mainly as a ride control system that has the benefit of reducing the vessels drag due to the dynamic lift created by the foils, while still enhancing the ride comfort. The foil system produces a lift that is approximately 30 % of the vessel's full-load displacement and is an active component on the trimaran *Dolphin Ulsan* and increased the vessels speed by 3 to 4 knots. Figure 1.7 illustrates the results obtained by NWBS for a trimaran with and without foils (Tulk and Quigley, 2004).

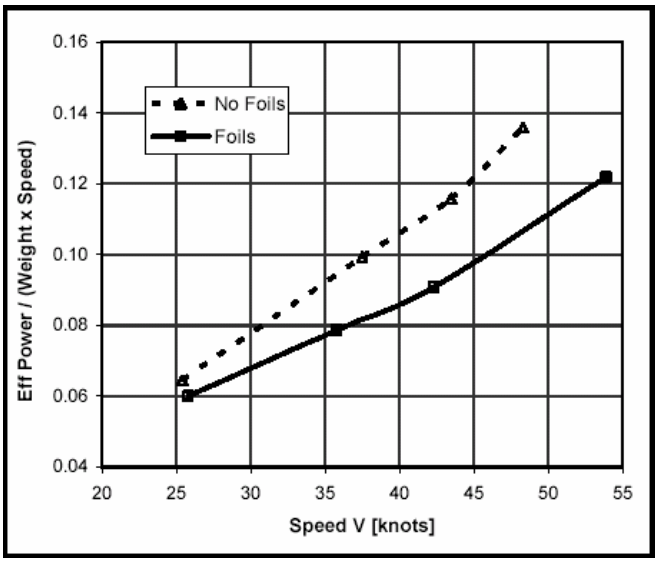

Figure 1.7: NWBS results for a trimaran with and without foils (Tulk and Quigley, 2004)

One of the significant benefits of adopting the trimaran hull-forms was the capability to solve the drag versus transverse stability conflict, through the adoption of long thin hulls for low resistance, while achieving a greater second moment of inertia by moving the waterplane area further from the ship center-line. A trimaran can maintain speed in significantly greater sea states than either similarly sized catamarans or mono-hulls regarding safety. This is because there is no tunnel roof and therefore slamming is reduced, which is a major advantage over a catamaran. The positioning of the outrigger influences not only the wave interaction between the hulls, but also the transverse stability.

It is also well known that the wave resistance, that is the main part of the residual resistance, drops as the length-displacement ratio $L/\nabla^{1/3}$ of the hull increases (Bricknell and Carlisle, 2004). Therefore, to achieve greater speeds the resistance should obviously be decreased. The resistance can be decreased in a number of ways. Increasing the length of the vessel will decrease the wave resistance, due to a more slender hull while keeping the displacement constant. The addition of foils that act as lifting devices will decrease the wetted surface area above certain speeds and will also dampen the wave system created by the vessel.

Results regarding the ongoing trimaran-catamaran debate concluded that the predicted resistance data obtained by NWBS proved that the resistance of a 55 m trimaran was also less than a

catamaran with similar capacity (Tulk and Quigley, 2004). The trimaran offers above catamaran enhanced sea-keeping ability that allows for other sea routes to be used that in the past could not due to the difficult sea conditions (Fast, 2005). According to Armstrong (2004), the operability of the trimaran provides the best features of both catamaran and mono-hull, without the disadvantages.

1.3 Aim and Objectives

Design and manufacture a trimaran model that is suitable for experimental model testing with and without the addition of foils: Chapter 2 presents a theoretical background to obtain a clear understanding of the different resistance components of a trimaran that will allow for of a suitable trimaran design. A complete and logical design procedure, together with the limitations set by the catamaran design that the trimaran is compared with, is therefore presented in chapter 3.

Supervising the manufacturing of a hydrofoil system based on the design of Dr. G. Migeotte, managing director of CAE-Marine (South Africa): The theoretical method to determine the lift and drag forces of a hydrofoil is supplied in chapter 2 and can be used to obtain a suitable trimaran configuration based on the theoretical knowledge of hydrofoils. A background of the basic hydrofoil design variables is discussed in chapter 3.

Test experimentally the resistance, trim and rise/sinkage of a trimaran with three different outrigger transverse clearance distances and with three different longitudinal center of gravity (LCG) positions: The results are compared to determine the outrigger transverse clearance position with the least amount of resistance. The experimental testing technique and procedure are described in Chapter 4, together with the limitations resulting from the towing tank and model dimensions. A numerical analysis and theoretical analysis is conducted based on the same outrigger transverse clearance positions. The three methods are compared to determine the feasibility of each method. These methods are presented in Chapter 5.

Determine a feasible scaling procedure for a trimaran without foils: A modified Froude scaling method must therefore be developed to account for the different sized hulls of the trimaran. A complete scaling procedure for a trimaran with and without foils is presented in appendix C.

Test experimentally the hydrofoil-assisted trimaran with three different LCG positions to determine if the addition of foils can reduce the vessels total resistance significantly. An aim of at least 40 % reduction of resistance at 50 knots would be acceptable: The hydrofoil system does not have to act as an active ride control system improving the ride comfort and the sea-keeping abilities, but rather a system that decreases the resistance of the vessel significantly. The angle-of-attack of the front and rear foils of the hydrofoil system are determined experimentally to obtain an idea about the optimum with regards to safety and stability. These results are compared to a numerical analysis and the deviations that would be expected are discussed.

Investigate any instabilities and other problems that occurred during towing tank testing: Provide a numerical based analysis to support explanations of any instabilities and other problems that occured.

Compare the resistance, trim and rise/sinkage results of a trimaran with a catamaran with similar overall displacement of 161 tonnes and speed with and without the addition of foils in both cases: The design of the trimaran should be closely adapted to the main dimensions of the catamaran to facilitate a performance comparison.

Evaluate the lifting capability of the hydrofoil system of the hydrofoil-assisted trimaran over a speed range of 0 knots to 50 knots: These results give an understanding of the amount of lift the hydrofoil system generates and the forces associated due to planing of the vessel. A numerical analysis is used to determine the lifting force of the hydrofoil system taking into account the trim and rise/sinkage of the hydrofoil-assisted trimaran. The validity of the numerical method used to calculate the lifting capability of the hydrofoil system is presented in chapter 5.

Chapter 2 Hydrodynamics and Resistance

2.1 Hydrodynamics of a Fast Ships

2.1.1 Operating Regimes

There are three distinct operating regimes for a fast ship: displacement, transition and planing. These regimes are shown in figure 2.1 (Marshall, 2002). A vessel's hydrodynamic characteristics differ in each of these three regimes. The boundaries of the different regions differ for each vessel due to the different lifting capabilities created by the hydrofoil system and the hull shape of each vessel. The planing phase for hydrofoil-assisted craft generally tend to be earlier than compared to conventional vessels (Migeotte, 2001). The effect of hydrofoil assistance to a craft will be discussed later in the report.

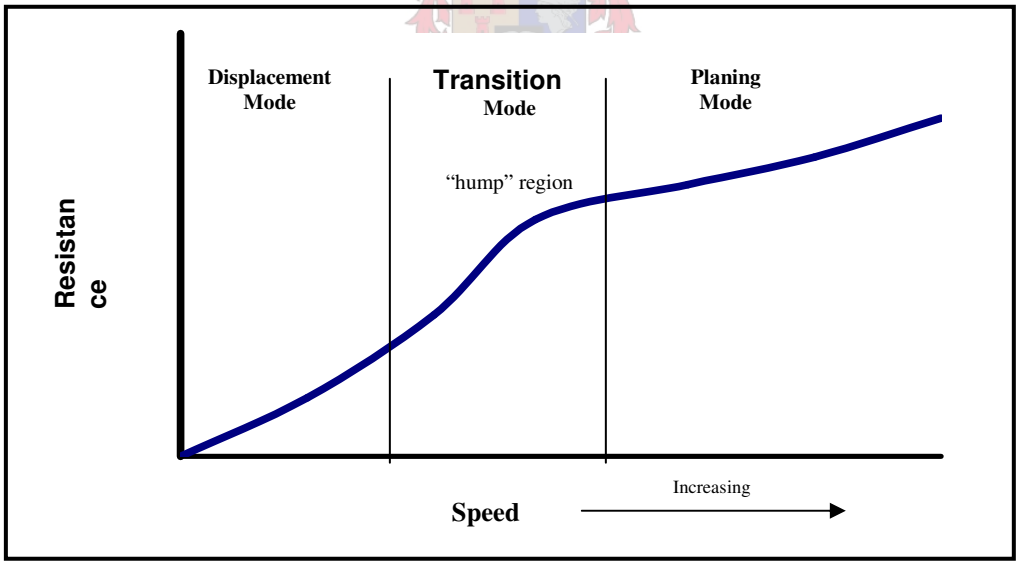

Figure 2.1: Operating regimes for conventional crafts (Marshall, 2002)

Displacement phase

In the displacement phase the lift for all craft including hydrofoil-assisted craft is mostly generated by buoyancy forces, rather than lifting forces created by a hydrofoil system and the dynamic forces created by the hull. Strong wave-making characteristics are present for both conventional vessels and hydrofoil-assisted vessels. The hydrofoils can either increase or decrease the resistance of the vessel in this phase. The hydrofoil decreases the wave build-up in the tunnel (if the foil spans the width of the tunnel) and therefore, decreases the vessel's total resistance. The hydrofoil, however also increases the vessel's total resistance due to the extra friction and profile resistance. It has been shown that there is not much difference hydro-dynamically between a hydrofoil-assisted catamaran and a conventional catamaran in the displacement phase (Migeotte, 2002). This will also probably be the case for a hydrofoil-assisted trimaran. Vessels are associated with a low trim angle in this phase.

Transition phase

This phase is associated with the hump resistance that is caused by the wave-making of the vessel. To break free from the displacement phase to the planing phase the vessel has to overcome the hump resistance. The shape of the hull and the foil-hull interaction is responsible for the wave-making and dynamic suction. The transition phase is hydro-dynamically the most complicated due to foil-hull interaction, especially for foils carrying more than 70 % of the weight (Migeotte, 2002). A relatively high trim angle can be expected in this phase. The hydrofoils allow the trim of the vessel to be regulated in order to reduce the hump resistance. The transition hump region for hydrofoil-assisted vessels occurs at higher Froude numbers compared to traditional displacement vessels. This is due to the hull-foil interactions where the hull suction force is of the same magnitude as the foil lift (Migeotte, 2005).

Planing phase

This phase is associated with the lift created mostly by the foil system and also assisted by the dynamic lifting force of the hull. The transition hump resistance has been overcome with lifting

forces. The increase of resistance with speed is fairly constant. The transition to planing for a hydrofoil-assisted craft of the hydrofoil-supported watercraft (HYSUWAC) type results in a rapid increase in trim due to the lift generated by the front foil. This, however, also reduces the suction forces. The wave-making is also effectively lower. The depth of the front foil influences the trim. A moderate trim is associated with conventional vessels in this phase.

The most common instability found in this phase is when the front foil breaks through the free surface and re-submerges due to no lift being generated above the free surface. The cycle is repeated and results in a pitch-heave instability (Migeotte, 2002).

2.1.2 Hydrodynamics and Resistance of a Trimaran

The trimaran is a new concept only for large fast ferries in Naval Architecture. Sailing trimarans have existed for a reasonable time. The first operating vehicle-carrying trimaran fast ferry was built and then launched in 2004 by Austal Ships in Australia. The concept of trimaran represented a shift in technology for high-speed craft offering improvements in fuel consumption and a noticeable improvement in comfort and sea-keeping ability (Armstrong and Holden, 2003).

Hydrodynamics of a trimaran

The resistance components of a trimaran are similar to that of a mono-hull with a very slender hull but with additional components for the viscous and wave-making interference resistance due to the addition of the outriggers. The dimensions and shape of the main hull and the outriggers do not only determine the hydrodynamic interaction, but also the mutual positioning of the outriggers with respect to the main-hull.

For an outriggered ship as compared to a mono-hull, the initial transverse stability is provided mainly by the outriggers position and displacement rather than the main-hull's width. Thus, there are no stability limits for the width and shape of a trimaran main-hull (Dubrovsky, 2004). The width of the main hull is limited by the propulsion system that is used. A trimaran is a super

slender unstable mono-hull with outriggers. The more slender a hull, the less wave-making resistance the hull generates. Higher speeds require a significant reduction of wave-making resistance that is the most important component of the vessel's resistance when the speed increases (Migali et al., 2001). According to Migeotte (2005), the wave-making resistance is only the most important component at the hump speed, therefore for a 127 m trimaran it is important but less for smaller trimarans. The whole concept of a trimaran is to obtain a lower total resistance to a comparable mono-hull or catamaran. The super slender main-hull decreases the wave resistance, but the addition of the outriggers results in viscous and wave interference resistance that increases the total resistance. The amount of decrease and increase of the wave resistance and the interference resistance respectively should result in an overall decrease of the total resistance for a trimaran to be superior. The viscous interference resistance is due to two factors (Migeotte, 1997): Firstly the change in pressure around a hull affects the form factor (1 + k) that is used in the calculation of the frictional resistance. Secondly the velocity increase in the tunnel between the main-hull and the outrigger disturbs the potential flow field of both hulls resulting in additional resistance.

Outrigger length, position and displacement

The length of the outriggers has an influence on the stability and the resistance of the vessel. Increasing the length not only reduces the residual resistance but also increases the deck area and improves the dynamic buoyancy (lift) as the vessel is heeled (Tulk and Quigley, 2004). The increased length does however also increase the frictional resistance, but can be reduced by the addition of foils.

The transverse and longitudinal position of the outriggers with regards to the main-hull is very important. The position will have a major influence on the magnitude of the viscous and wave-making interference resistance (Dubrovsky, 2004). The wave interaction of a slender hull and outriggers can either increase or decrease the total wave interference resistance, depending on their dimensions and mutual positions. If the outriggers are positioned far apart, then the wave interaction can be very small and have no influence on the total resistance (Lyakhovitsky, 1973).

The outrigger displacement influences not only the stability, but also the wave resistance. The optimum value for the outrigger displacement can be determined in the consideration of the actual ship dimensions, center and side hull forms and side hull position (Mizine and Amromin, 1999).

Length-displacement ratio of main-hull

The length of the vessel is perhaps the most influential dimension in ship design and has a significant impact on economics, seakeeping and powering (Roy and Gee, 2003). Previous studies of high-speed slender vessels have shown that a longer vessel will require a lower installed power for a constant displacement due to a higher length-displacement ratio and lower Froude number (Roy and Gee, 2003). However, the wetted surface area will increase and therefore increase the viscous resistance, but the wave-making resistance will decrease if the displacement is kept constant. This characteristic is especially suitable for vessels operating in the transition phase.

Resistance of a trimaran

The resistance of a trimaran can be estimated theoretically by the following equation (Dubrovsky, 2004),

$$R_T = 0.5\rho V^2 Sw_{MH}\left(C_F + \Delta C + C_R I\right) + R_O \qquad (2.1)$$

where C_F, ΔC, C_R and I are the frictional resistance coefficient of the main-hull, correlation factor, the residuary resistance coefficient of the main-hull and the interaction coefficient respectively. R_O is the total resistance of the outriggers without the main-hull and Sw_{MH} is the wetted surface area of the main-hull. The water density and vessel speed are denoted as ρ and V respectively. The frictional coefficient for the main-hull can be determined according to the International Towing Tank Conference (ITTC) 1957 correlation as follows,

$$C_F = \frac{0.075}{(\log_{10} Rn - 2)^2} \tag{2.2}$$

where *Rn* is the Reynolds number of the main-hull. As a correlation line, the ITTC 1957 line already contains some allowance for 3-dimensional effects, and two recent ITTC Committees have recommended that additional form correction should not be made in routine resistance predictions of high-speed craft (Insel and Molland, 1991).

The interaction coefficient *I* between the main-hull and the outriggers can be determined according to figure 2.2. The dimensions and position of the outriggers have a significant effect on the interference effects of the vessel. Two kinds of interference effect are recognized, from the wave and from the body. Each hull creates a wave system that may increase or decrease the wave-making resistance in conjunction with the wave systems created by the other two hulls. The viscous interference is concerned with the change of flow about one hull due to the presence of the other two hulls (Deguili et al., 2005). Figure 2.2 illustrates the interaction coefficient for a trimaran with the following parameters (Dubrovsky, 2004):

- $\ell = L_{MH}/\nabla^{1/3} = 8$
- 2b/L = 0.207, 0.31 and 0.47
- 2 x 2.5 % outrigger displacement

where L, b and ∇ are the length of the main-hull, the transverse clearance of an outrigger and displacement (in cubic meters) of the vessel respectively.

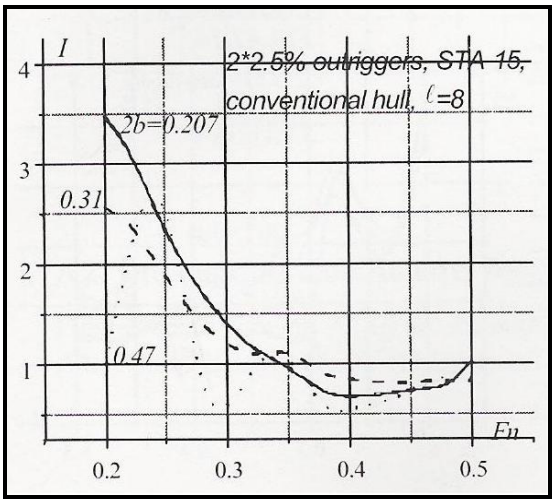

Figure 2.2: Dubrovsky's interaction coefficient for three different outrigger clearance distances (Dubrovsky, 2004)

The specified parameters used to determine figure 2.2 are assumed to be applicable due to the rough similarity of the dimensions of the trimaran used in this project. A note worth mentioning regarding the interaction coefficient is at particular *Fn* numbers the interaction can be less than 1; indicating that the outriggers can help to reduce the total resistance. The graph illustrates the values for the interaction coefficient based on the main-hull's length based Froude number. The wave interference occurs generally at low speeds where the angle of the bow wave of the main-hull is large and will have an interference effect with the outriggers. As speed increases, the angle of the bow wave decreases and the interference between the hulls decreases and disappears similar to catamarans (Insel, 1991). Therefore, it is assumed the interaction coefficient values above Fn = 0.5 will be taken as unity. The residuary resistance coefficient C_R of the main-hull or the outrigger can be determined according to figure 2.3 (Dubrovsky, 2004).

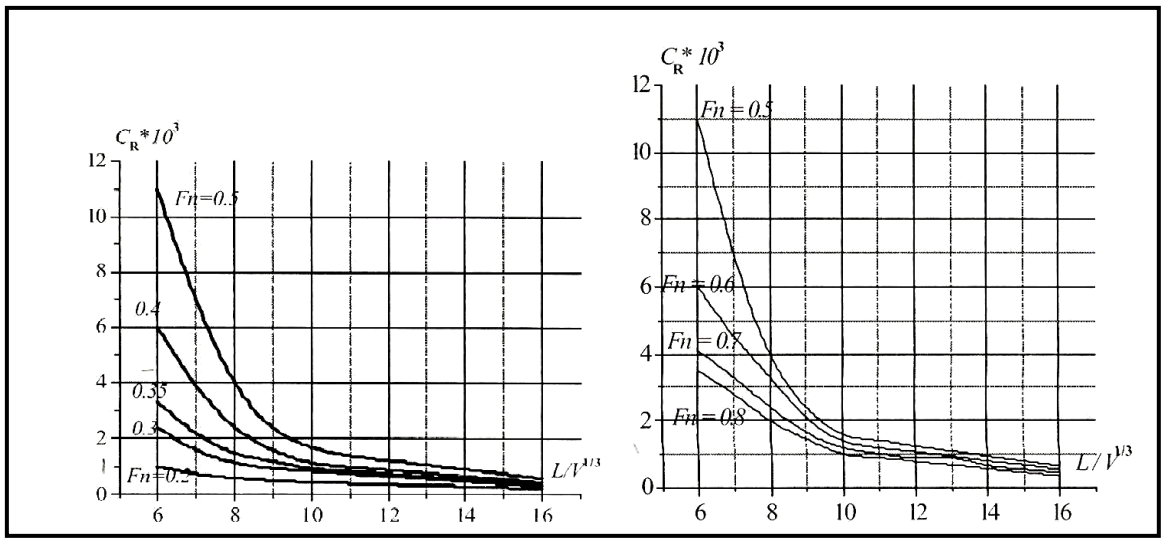

Figure 2.3: Residuary coefficient of a single hull (main-hull or outrigger) (Dubrovsky, 2004)

2.2 Hydrodynamics of Hydrofoils

The hydrodynamic principles of a hydrofoil can be compared to the aerodynamics of an aerofoil section. However, the hydrofoil's environment differs from the airfoils in two important ways (Daskovsky, 2000): firstly, the hydrofoil operates in proximity to a free surface and secondly, the hydrofoil operates in a liquid of higher density that will boil if the pressure drops below a critical value (cavitation). The airfoil sections are normally NACA profiles, where some of the hydrofoils are often circular arcs (as in the case of this project). The foil should provide a large enough force normal to the flow direction with as little drag as possible, therefore, not to increase the overall resistance of the vessel. At low Froude numbers, generally, the addition of foils does result in an increase in the total resistance of the vessel. Only at higher Froude numbers $Fn_{\nabla} \approx 2.0$ will the addition of foils decrease the "hump" resistance and also the high-speed resistance (Hoppe, 1991). This lifting force, at a certain speed, will be able to lift a major part of the vessel above the water surface and therefore, decrease the viscous resistance and wave resistance. The foil thickness, chord length, aspect ratio, camber line and angle of attack are some of the parameters that influence the lift-to-drag ratio of a hydrofoil. These parameters are shown in figure 2.4. The positive and negative effects resulting from foil addition will be discussed in this section.

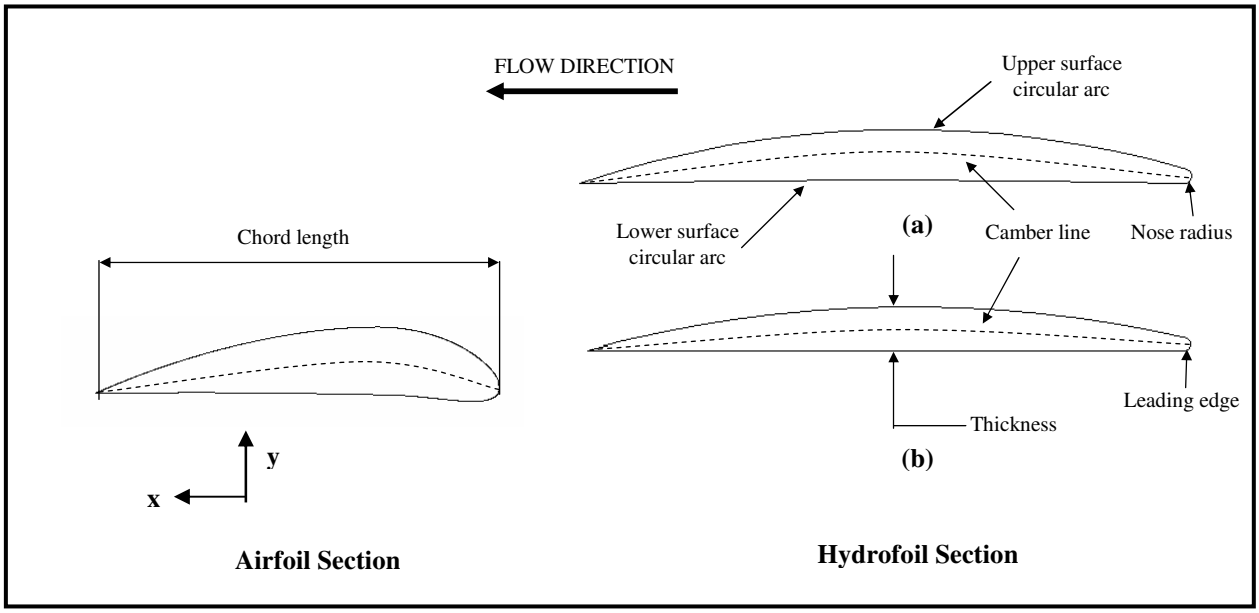

Figure 2.4: Airfoil section versus hydrofoil section

The airfoil section, for subsonic use, has a rounded leading edge with a definite radius of curvature. The hydrofoils rounded leading edge is much smaller compared to the airfoil section, because of higher density of water and also to avoid cavitation. Hydrofoil sections can either contain a circular arc for the upper surface with a flat lower surface or both surfaces being circular arcs as shown in figure 2.4. Concave lower surfaces give higher efficiencies in close surface approach (Hoppe, 1999). The camber line is the curve that is formed by adjoining the points that are located mid-way between the upper and the lower surface from the nose to the trailing edge of the foil (Houghton and Carpenter, 1993). The maximum thickness of hydrofoils is located near the midchord. Generally, the foil needs to be as thin as possible to prevent cavitation (Hoppe, 1999) depending on the speed and load.

The aspect ratio is a measurement of the narrowness of the foil planform and can be determined by the following equation,

$$AR = \frac{(span)^2}{area} = \frac{b_f}{c} \tag{2.3}$$

where the *span* is the overall length along the wing in the z-direction. The *area* is the planform area as seen from the top. A higher aspect ratio results in a higher efficiency of the foil. The aspect ratio can be increased with the addition of struts as will be shown later in this chapter.

The surface quality of the foil has a big influence on the drag (if surface is rough) and is associated with a loss in maximum lift (Migeotte, 1997). To eliminate such problems the hydrofoils should have a very smooth and accurate surface finish.

2.2.1 Hydrofoil Lift

The hydrofoil lift is determined by the same principles as used in aeronautical practice. The overall lifting property of the two-dimensional aerofoil depends on the circulation it generates and this has been assumed to be concentrated at a point within the aerofoil profile, and to have a magnitude related to the incidence, camber and thickness of the aerofoil (Houghton and Boswell, 1969). The same will apply for hydrofoils except that the hydrofoil lift also depends on the submergence of the foil below the free surface. The lift force created by a hydrofoil can be determined by using the lift coefficient C_L as shown in the following equation (Houghton and Carpenter, 1993),

$$Lift = C_L \cdot \left(\tfrac{1}{2} \rho V^2 S\right) \tag{2.4}$$

where S is invariably the planform area. The lift coefficient can be determined by the three-dimensional lifting surface equation as shown in equation 2.5 given by Migeotte (1997).

$$C_L = C_{L\alpha}(\alpha - \alpha_0) \tag{2.5}$$

where $C_{L\alpha}$ and α are the 3-dimensional lifting curve slope and the foil angle-of-attack measured in radians respectively. The zero lift angle-of-attack is denoted as α_0 and also measured in radians.

The three-dimensional lift curve slope depends on factors that are mostly associated with airfoils and wings of aircrafts such as: sweep angle, dihedral, aspect ratio but also submergence. There is at present no unified theory for hydrofoils and a number of equations exist for determining the lift curve slope. The following equation is a combination of those equations and also takes into account the effect of a hydrofoil operating in close proximity of a free surface given by Migeotte (1997),

$$C_{L\alpha} = \frac{2\pi \cdot P \cdot AR \cdot \cos\Lambda \cos^2\Gamma}{AR + 2P(1+\sigma)(1+\xi)\cos\Lambda\cos^2\Gamma\left[1+\left[1+\left(\frac{AR}{2P\cos\Lambda\cos^2\Gamma}\right)^2\right]^{0.5}\right] - AR(1+\sigma)(1+\xi)} \tag{2.6}$$

where Λ and Γ are respectively the sweep angle (in radians) and the dihedral angle (in radians). Munk's interference factor and the planform correction factor are represented by σ and ξ respectively.

The free surface correction estimated for high-speeds can be determined as follows (Lewis, 1988),

$$P = \frac{16\left(\frac{h}{c}\right)^2 + 1}{16\left(\frac{h}{c}\right)^2 + 2} \tag{2.7}$$

where h is the submergence of the quarter chord. Equation 2.7 is applicable for the operating speed range for hydrofoils of high-speed catamarans. Therefore, it can be assumed that this equation is valid for hydrofoils that are fitted to high-speed trimarans, due to a similar speed range.

The Munk's interference factor is determined by bi-plane theory and the effect is similar to the interference effect created by bi-planes (Korvin-Kroukovsky and Wernick, 1952). The factor corrects for the error created by the free surface on the trailing vortex system associated with 3-

dimensional flow around a hydrofoil with infinite span. The factor is reproduced (Korvin-Kroukovsky and Wernick, 1952) and shown in figure B.1 in appendix B. The following curve fit provides a sufficient approximation to the reproduced factor,

$$\sigma = 1.4733\left(\frac{h'}{b_f}\right)^4 - 4.2929\left(\frac{h'}{b_f}\right)^3 + 4.8849\left(\frac{h'}{b_f}\right)^2 - 2.9007\left(\frac{h'}{b_f}\right) + 0.9024 \tag{2.8}$$

where *h'* and b_f are the vertical distance between the two spans (equal to *2h*) and the span length respectively.

Two different methods can be used to determine the planform correction factor which corrects the elliptical foil lift distribution for rectangular foils. These two methods will be compared to the numerical values determined in Autowing Version 3.0. The first method is given by Du Cane (1973) where a general aerodynamic empirical relationship for rectangular wings is used.

$$\xi = 1 + \frac{2}{AR^2} \tag{2.9}$$

The second method uses a curve fit that was created using the original supplied data of Korvin-Kroukovsky et al. (1952) shown in figure B.2. This method provides an equation that also determines the planform factor for rectangular foils,

$$\xi = a + b \cdot AR + c \cdot AR^2 + d \cdot AR^3 \tag{2.10}$$

where

$$a = -0.0006, b = 0.0085, c = -4 \cdot 10^{-6}, d = -2 \cdot 10^{-6}$$

The zero lift angle-of-attack is the angle at which the foil provides zero lift and can be determined by using thin aerofoil theory. It is assumed that hydrofoil sections fall within the limitations of

the theory. The Pankhurst approximated solution for the zero lift angle-of-attack can be determined as follows (Abbott and Von Doenhoff, 1958),

$$\alpha_0 = \sum A\left(U_p + L_p\right) \tag{2.11}$$

where U_p and L_p are the upper and lower ordinates of the foil section in fractions of chord respectively. The constant A is given for stations at which the ordinates are usually specified as shown in table 2.1.

x	A
0	1.45
0.025	2.11
0.05	1.56
0.1	2.41
0.2	2.94
0.3	2.88
0.4	3.13
0.5	3.67
0.6	4.69
0.7	6.72
0.8	11.75
0.9	21.72
0.95	99.85
1	-164.9

Table 2.1: Constant A for Pankhurst solution (Abbott and Von Doenhoff, 1958)

The solution is based on the assumptions that the mean line ordinates are represented satisfactorily by $(U_p + L_p)/2$ and that the tangent of the mean line at the trailing edge coincides with the last two points. The accuracy is accordingly expected to be limited for sections with large curvatures of mean line near the trailing edge, or for thick, highly cambered sections.

2.2.2 Hydrofoil Drag

No theory or any prediction method exists for the determination of the drag of the hydrofoils concerning hydrofoil-assisted trimarans due to the unknown interference effects between hull and

foil. However, well-developed theory does exist for hydrofoil drag independently. The assumption that similarity exists between hydrofoil drag regarding hydrofoil-assisted catamarans and hydrofoil-assisted trimarans are made. Therefore, the hydrofoil drag components used for catamarans by Migeotte (1997) can be used for trimarans as well. The interference effect is assumed to be fairly similar between the two multi-hull configurations, but is strongly dependent on 3-dimensional shapes.

The total drag coefficient for a hydrofoil can be separated into the following components shown in the following equation (Korvin-Kroukovsky and Wernick, 1952),

$$C_D = C_{DP} + C_{DW} + C_{Di} + C_{DS} + C_{D\,\mathrm{int}} \tag{2.12}$$

where C_{DP}, C_{Di} and C_{DW} are the profile drag coefficient, induced drag coefficient and the wave drag coefficient respectively. C_{DS} and C_{Dint} are the strut drag coefficient and the interference drag coefficient respectively and are added to the original equation of Korvin-Kroukovsky and Wernick (1952) for completeness.

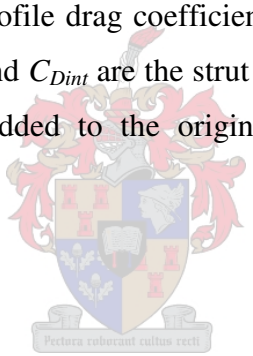

Profile drag

The profile drag can be estimated from the velocity profile in the foil wake. At the trailing edge of a foil immersed in a fluid stream, there exist boundary layers from the upper and lower surfaces. These boundary layers will join up and move downstream in the form of a wake of retarded velocity; the velocity profile will change with distance downstream, the wake cross-section increasing in size as the magnitude of its mean velocity defect (relative to the free stream) decreases. At a sufficient distance downstream, the streamlines will all be parallel and the static pressure across the wake will be constant with those in the undisturbed stream value. If conditions at this station are compared with those in the undisturbed stream ahead of the foil, will equate to the drag force on the body. The drag force so obtained will include both surface friction, pressure drag and separation drag components, since these together will produce the overall momentum change and therefore, the profile drag (Houghton and Boswell, 1969).

The hydrofoil drag will decrease as the foil approaches the free surface (Migeotte, 2001). The following formula, determined by Egorov and presented by Migeotte (2001), accounts for the influence of the free surface with regards to the profile drag coefficient:

$$C_{DP} = C_F \left[1 + \left[\left(m_p + 0.5 \right) \frac{\varphi}{k_\varphi} - 0.5 \right] C_L \right] \tag{2.13}$$

where m_p is an empirical correction factor and ranges between 0.5 and 0.75. The smaller value corresponds to $C_L = 0.175$ and its larger value to $C_L = 0.55$. A linear interpolation can be done to determine other values of m_p regarding C_L. The free surface correction factor φ can be determined as follows,

$$\varphi = 1 - e^{-2\left(\frac{h}{c}\right)^{0.6}} \tag{2.14}$$

and the lift curve slope correction factor k_φ as follows,

$$k_\varphi = 1 - \left(0.5 + \frac{t}{c} \right) \cdot e^{-2\left(\frac{h}{c}\right)^{0.6}} \tag{2.15}$$

where t, c and h are the thickness, the chord length and the submerged height of the foil respectively. C_F is the frictional coefficient of the hydrofoil and can also be determined according to the ITTC 1957 approach as follows,

$$C_F = \frac{0.075}{\left(\log_{10} Rn - 2 \right)^2} \tag{2.16}$$

where Rn is the Reynolds number based on chord length.

Wave drag

The hydrofoil in steady motion generates low pressure and high pressure on its top and bottom surfaces respectively. This pressure difference results in a net upward force, the foil lift. The pressure distribution on the top surface of the foil deforms the free surface, when the foil is in close proximity of the free surface. This deformation of the free surface results in a transverse wave following the foil. This, however, results in a drag force; more commonly known as the wave drag and curves the flow (Daskovsky, 2000). The wave drag coefficient is a function of the depth Froude number and the lift coefficient and can be determined as follows (Daskovsky, 2000),

$$C_{DW} = \frac{C_L^2}{2Fn_h^2} \cdot e^{-\left[\left(\frac{2h}{c}\right)/Fn_h^2\right]} \tag{2.17}$$

where Fn_h is the depth Froude number of the quarter chord. The wave drag is a component of drag due to lift and can therefore be considered as an additional component of induced drag (Migeotte, 1997).

Induced drag

The induced drag, also known as the trailing vortex drag, arises essentially from the downward velocity induced over the foil by the foil-tip vortices (Houghton and Carpenter, 1993). The induced drag can be determined due to standard aeronautical practice, which takes into account the bi-plane interference effect,

$$C_{Di} = \frac{C_L^2}{\pi \cdot AR \cdot P \cdot \cos\Lambda \cos^2\Gamma}(1+\sigma)(1+\xi) \tag{2.18}$$

Equation 2.18 uses the same variables as used in equation 2.6.

Strut drag

Full chord struts prevent spanwise flows and increase the effective aspect ratio of a foil (Du Cane, 1973) and can be determined according to the following equation,

$$AR = \frac{b_f}{c}\left[1+\left(\frac{a_f}{b_f}\right)^3 \frac{h}{b_f}\right]. \tag{2.19}$$

where a_f and b_f are the horizontally and laterally projected spans shown in figure 2.5.

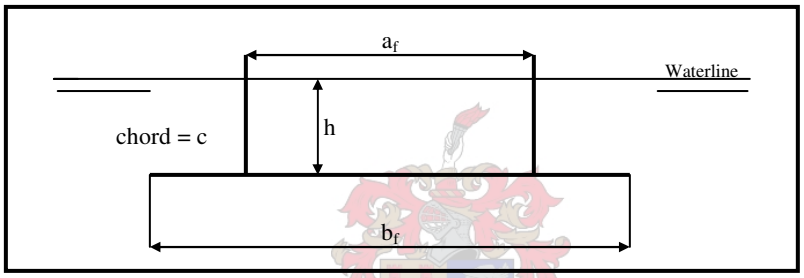

Figure 2.5: Fully submerged foil with struts

The strut drag comprises of profile strut drag, spray drag, wave-making drag and interference drag (due to the junction with the foils). The wave-making drag can be ignored for speed above the chord Froude number $Fn_c > 0.7$, due to the wave-making that drops off rapidly at high speeds (Migeotte, 2001). The spray drag can be determined by the following equation (Lewis, 1988),

$$C_{DS} = C_F\left[7.68 - 6.4\left(\frac{t\cos\beta}{c}\right)\right] \tag{2.20}$$

where β is the angle of the strut with a line normal to the free surface. A significant reduction in spray drag can be made if the struts are angle backwards (Migeotte, 1997), but taking into account that an additional friction resistance will be present.

Interference drag

Interference drag arises when a foil and struts adjoins a hull or a foil (for the case of a strut). The boundary layers of both, foil and hull or strut and foil, joins together and this results in the boundary layers being further retarded (Hoerner, 1965). Therefore, an increase in pressure drag (interference drag) arises due to the adverse pressure gradient at the rear of the foil. This drag coefficient is mostly based upon the dimensions of the foil section and can be determined with the following equation (Hoerner, 1965),

$$C_{D\,\mathrm{int}} = 0.75\left(\frac{t}{c}\right) - 0.0003\left(\frac{t}{c}\right)^2 . \tag{2.21}$$

The angle of attachment influences the magnitude of the interference drag. An angle of 90 degrees or larger is regarded as optimum. For smaller acute angles a fillet must be incorporated. Due to the interference coefficient that is dependent on the dimensions of the foil and angle of attachment to the hull therefore the assumption can be made that the interference coefficient is independent of the type of multi-hull configuration.

Another interference drag that should be mentioned is the interference the front foil creates upon the rear foil. The rear foil will operate in a downwash or upwash depending on the speed of the vessel and position of the rear and front foil, due to the wave wake created by the front foil. This interference affects the lift and drag of the rear foil. However, simple empirical equations can be used to calculate the angle of the downwash at a certain distance behind the foil to account for the change in lift and drag of foils operating in the wave wake of a leading foil (Li, 1981). The front foil also creates a wave trough behind itself above a certain speed and therefore affecting the submergence depth of the rear foil. This also affects the lift and drag of the rear foil.

2.2.3 Cavitation

Cavitation takes place when the liquid pressure drops below the vapor pressure due to the flow phenomenon and vapor bubbles form. When these vapor bubbles move into a higher-pressure region, they collapse implosively and produce strong shock waves. If this occurs in close proximity of the foil, then not only will the shock waves produce noise and vibrations, but will also physically damage the foil. Cavitation decreases the lift and increases the drag of a foil and will typically occur for conventional hydrofoil craft above 50 knots (Migeotte, 2001). Overloading a foil will also result in cavitation (Migeotte, 1997).

2.2.4 Free Surface Effects

Most theories developed to date state that the effect of surface proximity is primary a function of submergence depth to chord length ratio and very little effect is seen at depths greater than two chord lengths (Daskovsky, 2000). If the foils operate in close proximity of the free surface the lift will decrease and the drag will increase (Migeotte, 1997). This effect can be useful in some natural stabilizing applications.

2.3 Hydrodynamics and Resistance of a Hydrofoil-Assisted Trimaran

The addition of a hydrofoil system to a trimaran will result in several additional resistance components of the vessel. Not only will the foils create a drag due to their profile, but also an interference drag between the hulls and the struts. The struts too cause additional drag components. The beneficial lifting force generated by the foils creates an induced drag and this also increases the total drag of the vessel. The resistance of the vessel will, however be decreased due to the lift that the foils generate which lifts the hull partially out of the water therefore resulting in a decrease of wetted surface area, decrease of waterline length, a change in trim angle, a less significant bow wave and a considerable reduction of the wave and viscous interference between the outriggers and the main-hull. Foils are only successful if the lift-to-drag

ratio of the foil system is greater than the lift-to-drag ratio of the vessel itself (Tulk and Quigley, 2004).

The resistance in calm water can be broken down into the following components illustrated in the flow chart reproduced from Migeotte and shown in figure 2.6 (Migeotte and Hoppe, 1999). This resistance breakdown is actually for hydrofoil-assisted catamarans, but it is assumed that the interference and viscous resistance components that are found in trimarans are similar, but with different magnitudes and characteristics. The interference and viscous effects are summed for both port and starboard side of the trimaran to obtain the total interference and viscous resistance. Therefore it can be assumed that the resistance breakdown is applicable and can be used for trimaran resistance predictions or evaluations. The total resistance can be broken down into the usual frictional and residual resistance. Each of the different resistance components of the flowchart is discussed in further detail below.

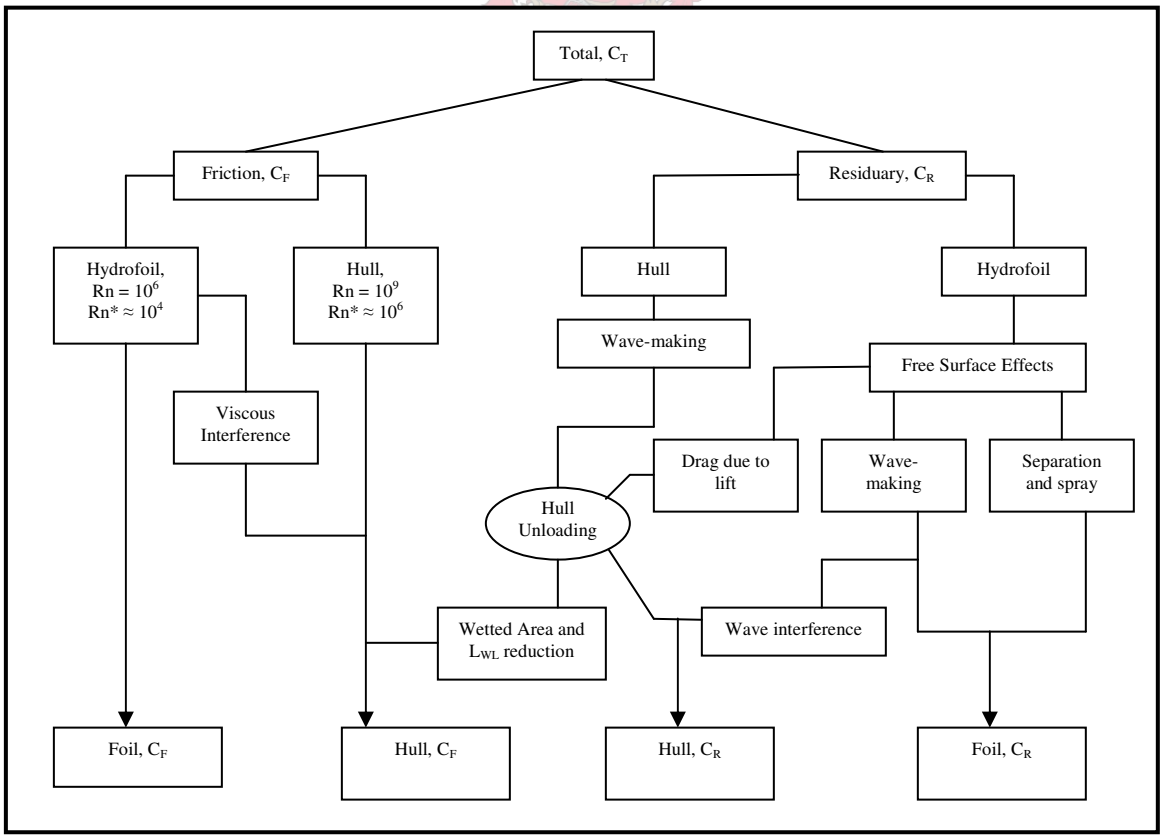

Figure 2.6: Resistance breakdown for hydrofoil-assisted craft (Migeotte and Hoppe, 1999)

2.3.1 Frictional Resistance

The flow chart illustrates that the frictional resistance of a hydrofoil-assisted trimaran can be divided into hull and foil friction components and also the viscous interference between the two. The frictional resistance component is the largest part of the total resistance for all high-speed catamarans (Migeotte and Hoppe, 1999).

A problem arises when doing model testing due to the lack of turbulent flow over the foils and this highlights the importance of accurately calculating the foil friction. The Reynolds number of the foils in model testing is too low ($Rn^* \approx 10^4$) and therefore might yield excellent results, which may not occur at full-scale. The laminar flow at model scale causes separation of flow on the foil. The foil's attributed forces do not scale with the vessel (Tulk and Quigley, 2004). The Reynolds number also has an affect on the lift of the foils by influencing the lift curve slope and zero angle-of-attack (Migeotte and Hoppe, 1999).

The frictional resistance of a hull can be calculated using the ITTC 1957 correlation line.

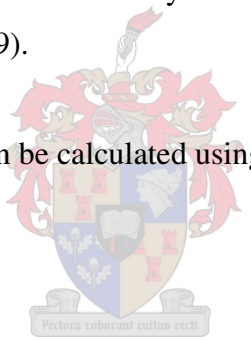

2.3.2 Residual Resistance

The residual resistance of a vessel comprises all the other influential components, excluding the frictional resistance. These components include the wave making of the hull, the wave interference between the main-hull and the outriggers and the free surface effects on the foil system (wave resistance, induced drag, separation and spray).

It is very difficult to determine the residual resistance of a hydrofoil-assisted craft due to many interference effects that cannot be accounted for and the difficulty with free surface effects. Any resistance prediction method would have to include the effects of large changes in trim and sinkage on the resistance of the hull (Migeotte and Hoppe, 1999). According to figure 2.6, the residual resistance of the vessel changes with a certain applied load.

Well-developed hydrofoil theory allows for the prediction of the residual resistance of the foils. Good preliminary foil sizing and positioning on the hull can however be achieved due to the theory (Migeotte and Hoppe, 1999).

The wave interaction between the wave system generated by the foils and that generated by the hulls of the trimaran can either be positive or negative concerning the residual resistance. The trailing vortices of the foils create suction forces on the hull. These suction forces are in the order of 10 % of the vertical forces on the hull and seem to increase with speed (Migeotte and Hoppe, 1999). In the case of trimarans, the foils will span from the main-hull to the outrigger and therefore reduce the strength of the trailing vortices due to the end plate effects of the hull or struts.

Chapter 3 Trimaran and Hydrofoil Design

The results of this project can be compared to that of a hydrofoil-supported-watercraft (HYSUWAC) type hydrofoil-assisted catamaran with a similar displacement of 161 tonnes and an overall length of 40 m. The HYSUWAC type hydrofoil configuration is explained in section 3.2.1. The catamaran model has the same hull shape and overall length as the main-hull of the trimaran model tested in this project. The shape of the hull underneath the free surface and the waterline length are different for the two vessels due to the different drafts. Each catamaran hull displaces 80.5 tonnes. Therefore, the main-hull of the trimaran is nearly double loaded than in the case of the catamaran, because the outriggers only carry a small percentage of the total displacement. This, however, does not allow a favorable resistance comparison as the heavier loaded hull will have a higher resistance and especially at hump speed, due to two different systems being compared. The comparison between the catamaran and the trimaran are still, nonetheless, made to determine superiority for equal displacement. The length-displacement ratio of the main-hull of the trimaran is 7.36, but of the catamaran demi-hull is 9.27. Again, the catamaran would have an advantage in resistance. A hydrofoil-assisted catamaran was tested previously and resistance data exists for this case. Therefore, the design of the trimaran and the trimaran's hydrofoil system are compared to that of the previously tested catamaran and its hydrofoil system.

3.1 Trimaran Design

The configuration of the trimaran is the most important factor in the preliminary stages of the design. A certain hull form was specified for the center hull of the trimaran. This was done to provide direct comparison with a catamaran of similar dimensions. The hull for the outriggers was specified to be geometrically similar as the center hull, but scaled down. The size of the outriggers changed due to certain adjustments that had to be made to provide an optimum hydrofoil-assisted trimaran configuration.

The configuration of a trimaran depends on the shape, size, displacement of the outriggers and main-hull, the design speed and the position of the outriggers with regards to the center hull.
The well-known design spiral used to design a vessel was clearly present in this design. A trimaran consists of ten parameters that can vary for different vessel applications (Armstrong and Holden, 2003). These parameters are illustrated in table 3.1. The parameters for a catamaran and a mono-hull are also shown.

	Mono-hull	Catamaran	Trimaran
Waterline length, WL	√	√	√
Displacement	√	√	√
Trim	√	√	√
Length/beam ratio	√		√
Angle of entrance at waterplane	√	√	√
Wetted surface area, WSA	√	√	√
Clearance distance		√	
Waterline length of outrigger			√
Displacement of outrigger			√
Longitudinal location of outrigger			√
Transverse location of outrigger			√

Table 3.1: Parameters associated with vessel type configuration

The catamaran and mono-hull each have five and six parameters respectively, compared to ten of the trimaran. This, however, makes the optimisation of a trimaran design much more complicated and difficult than a catamaran or a mono-hull (Armstrong and Holden, 2003). The trimaran has ten thousand million variations, compared to the 46656 of the catamaran.

The software packages used to determine the hydrostatics and hydrodynamics of the trimaran were Maxsurf Academic Version 11 and Michlet Version 6.05 respectively. Maxsurf Academic Version 11 is a powerful three-dimensional surface modeling system for use in the field of marine engineering. Michlet Version 6.05 is a numerical method used for investigations into some aspects of ship hydrodynamics. The fundamental theory behind these packages is discussed in chapter 5.

The center hull and the outrigger of a trimaran are very slender. The more slender a vessel is, the lower the wave resistance will be. Both the center hull and the outriggers have a hard chine and a

small spray rail that increases in size towards the transom stern. This helps with the planing effect and therefore reducing the wetted surface area of the vessel. The basic hull shape used in this project is illustrated in figure 3.1.

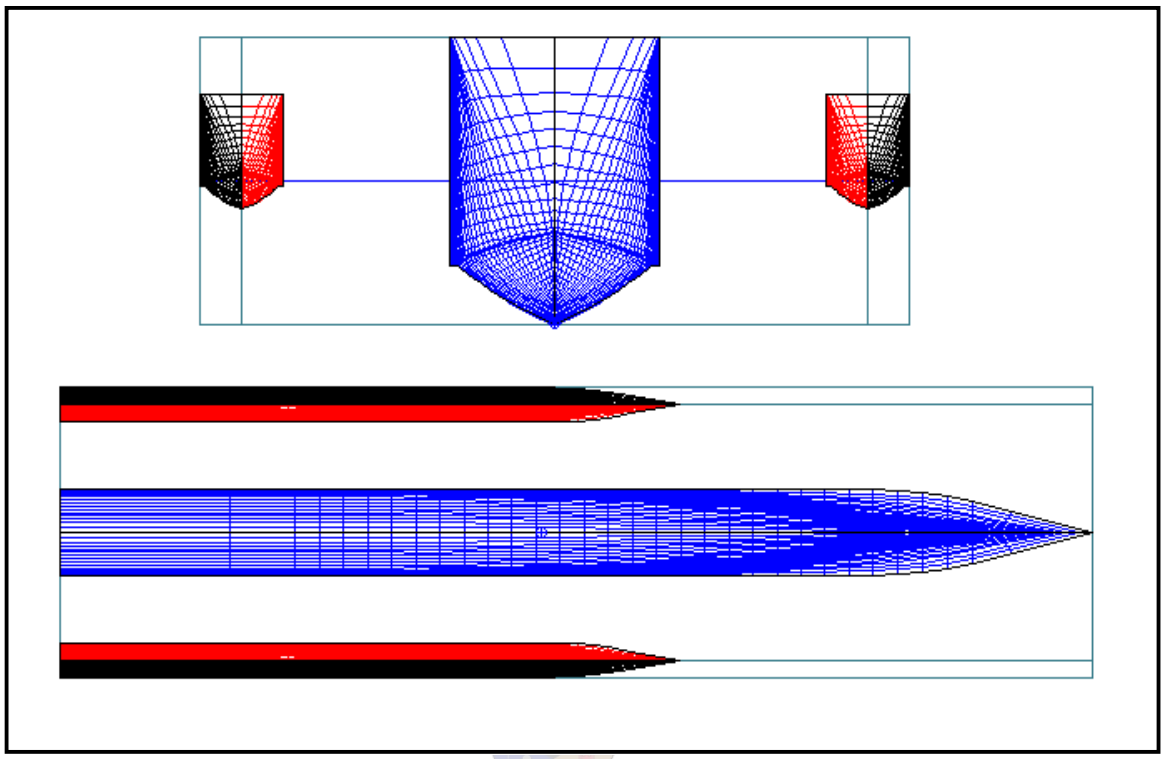

Figure 3.1: Basic hull shape of a trimaran

3.1.1 Hydrostatics

A crucial aspect of hydrostatics is the static stability of the vessel. The center hull in the case of a trimaran is very slender as mentioned previously, but unstable. The outriggers are added to increase the stability of the vessel, but maintaining a low overall resistance for the vessel. The water plane area influences the second moment of inertia of the vessel and therefore the static stability (Dubrovsky, 2004). The position and the size of the outriggers influence the stability of the vessel. The further the outriggers are positioned in the transverse direction from the center the more stable the vessel will be.

However, an increase in water plane area increases the wetted surface area and therefore creating a higher viscous resistance. The outriggers should also be at such a position that the interference effect between the hulls is at a minimum, unless the vessel has a specific application that requires a certain position for the outriggers.

The static stability of a vessel is determined by the value of the transverse GM. GM is the distance between the center of gravity of the vessel and the metacentric height and should be positive to ensure stability. The higher the value of GM, the more stable the vessel will be. The GM should actually be as low as possible, but still large enough to ensure vessel stability, to provide superior comfort due to the low rolling acceleration (Armstrong and Holden, 2003).

The second moment of inertia of the main-hull's waterplane drops with an increase in slenderness. This means that the contribution of the main-hull to the transverse stability of the entire ship depends strongly on the main-hull's beam at the waterplane (Dubrovsky, 2004). Generally, the intact stability of outriggered ships is similar to that of comparable mono-hulls. The stability of a trimaran and the accompanying terms are illustrated in figure 3.2.

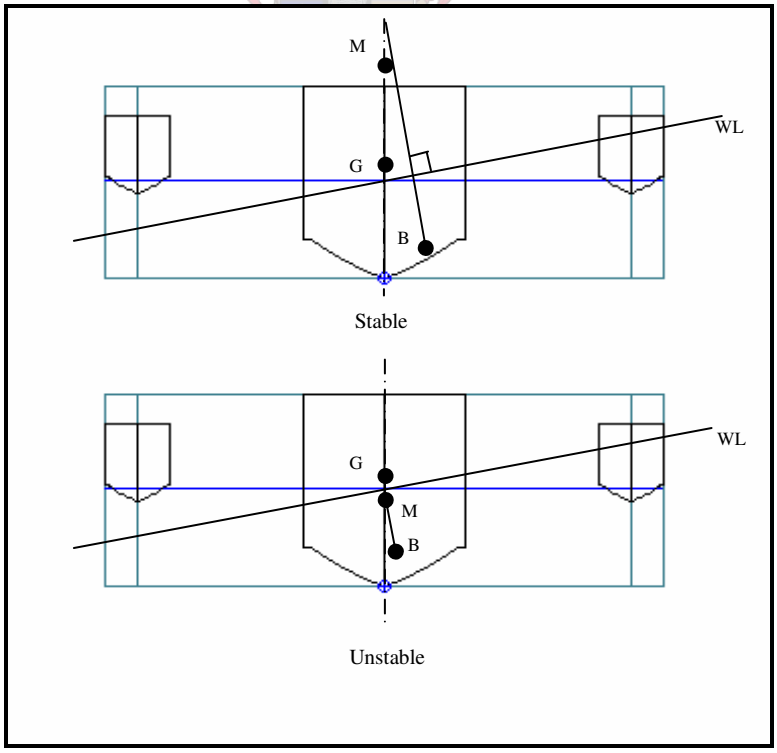

Figure 3.2: Stability of a trimaran

The vessel is kept horizontal and the waterline is inclined at a certain heel angle. This allows for a clearer understanding of figure 3.2. The notation for the center of buoyancy, metacenter and the center of gravity of the vessel are respectively given as B, M and G. The buoyancy force acts through the center of buoyancy perpendicular to the waterline. The point where the line, through which the buoyancy force acts, intersects with the center plane of the vessel is the metacenter. Therefore, if the center of gravity is below the metacenter, then the vessel is stable. Otherwise the vessel is unstable. It should be noted however that a change in the overall width has a much greater impact on the lateral metacenter height than the outriggers dimensions (Dubrovsky, 2003).

The center of gravity of a vessel is determined by all the major weight components of the vessel. This includes the mass of the hull, propulsion system and machinery. Due to this project focusing mainly on the hydrodynamics of a hydrofoil-assisted trimaran the weight of the ligthship was unknown and therefore, the center of gravity was unknown.

The damaged stability of a multi-hull vessel usually needs to be determined to satisfy the safety regulations of the 2000 High-Speed Craft (HSC) Code if it is to be used as a passenger ferry. No results were determined for the stability in damaged conditions of the vessel under investigation, since this was considered to fall outside the scope of the project.

A trimaran will most of the time be stable due to the increased righting moment created by both of the outriggers if the vessel heels. If an outrigger emerges from the water, the other outrigger will naturally be submerged even more, creating a greater righting moment. This is only true if the displacement and position of the outrigger is sufficient.

3.1.2 Hydrodynamics

The hydrodynamic parameters of importance are the resistance, rise/sinkage and trim of the vessel. The resistance of a vessel can be broken down into the components given in figure 2.6. In the case of a trimaran or any multi-hull vessel, there is an interference effect between the hulls.

This effect causes an increase or decrease in the resistance of the vessel. The hydrodynamics of a trimaran will be influenced not only by the dimensions of the main-hull, but also by the size, displacement and position of the outriggers.

Accurate resistance predictions are still very difficult to determine even today. The best possible solution is to do model tests that provide resistance data, optimization of foil position, foil angle-of-attack and establishing the stability limits of a vessel. The problems associated with model tests are scaling effects, blockage and shallow water effects. These effects will be discussed in subsequent sections.

The theoretical model that is presented by Dubrovsky (2004) for estimating a trimarans resistance is based on an interaction coefficient *I* determined through model testing. Different type of outrigger configurations and hull shapes were used to obtain a database for resistance predictions. This theoretical model is, however, not suited for design purpose due not only to the results that were obtained, but also because of different hull shapes and configurations used in this project.

3.1.3 Hydrofoil-Assisted Trimaran Configuration

The configuration of the trimaran is more complicated than a catamaran. The design spiral is implemented several times to achieve the best possible configuration. The main considerations that should be taken into account when designing a trimaran are the displacement of the center hull and also the outriggers, the position of the outriggers compared to the center hull, the length of the outriggers and the positioning of the hydrofoil system. These were the main parameters that were considered to achieve the best possible configuration taking a hydrofoil system into account. If one of the parameters were changed due to certain results obtained, then the whole iteration process, the so-called design spiral, was repeated. The rest of the parameters in table 3.1 were established after the main parameters were determined. The design process is a complex process and certain results will affect the outcome of the other parameters.

Outrigger displacement

The displacement of the outriggers is very important when designing a trimaran. The resistance of the vessel is influenced by the size and position of the outriggers according to most previously published research. Therefore, to ensure that the vessel has the least amount of resistance the outriggers must be as small as possible, but still be big enough to ensure stability. The specification of the trimaran was that the vessel should have a displacement of 161 tons. Therefore, the outriggers should carry a certain percentage of the overall displacement.

According to previously published research on the static transverse stability of a trimaran shows that the outriggers volume compared to the center hulls volume can vary between 0.06 and 0.11 for the vessels resistance to be a minimum, depending on the hull shape for both the main-hull and outriggers (Armstrong and Holden, 2004). But the research done by Austal Ships in Australia has shown that the displacement of the outriggers can be as low as 0.025 and therefore enable the vessel to achieve better speeds (Armstrong and Holden, 2004). These values may differ for different types of hull shapes.

The outriggers that were first considered had a length of equal to 40 % of the center hulls length. The other dimensions were scaled down accordingly. This ensured a large enough water plane area (WPA) for the outriggers for the trimaran to be stable. The WPA of a vessel is one of two main parameters that determine the static stability of a vessel (Dubrovsky, 2004). The outrigger length was later increased to 60 % of the main-hulls length due to the hydrofoil configuration and all the following results and calculations are based on this length.

According to the design of the vessel, the trimaran will only be stable if the displacement of the outriggers is more than 0.8 % of the center hulls displacement and positioned at least at a clearance distance of 4.9 m from the centerline of the center hull to the centerline of an outrigger. The 4.9 m is an arbitrary value that represents what the displacement shall be if the outriggers have a clearance distance of 4.9 m. Anything below this mentioned displacement value and clearance distance would result in the vessel to capsize. The further the outriggers are positioned form the center hull the lower the value for the least amount of displacement for the outriggers

becomes to ensure static stability and vice versa. Figure 3.3 shows the stability of the trimaran according to the percentage displacement of the outriggers with a clearance of 4.9 m and the unstable center hull at 0 % outrigger displacement with a negative GM value. The location of the center of gravity is unknown, therefore an assumption is made that the center of gravity is situated unrealistically high above the waterline where it generally would not be. This unrealistic value is twice the draft height of the main-hull measured from the keel (KG = 4.16 m). This, however, would result in an under-estimated value of GM.

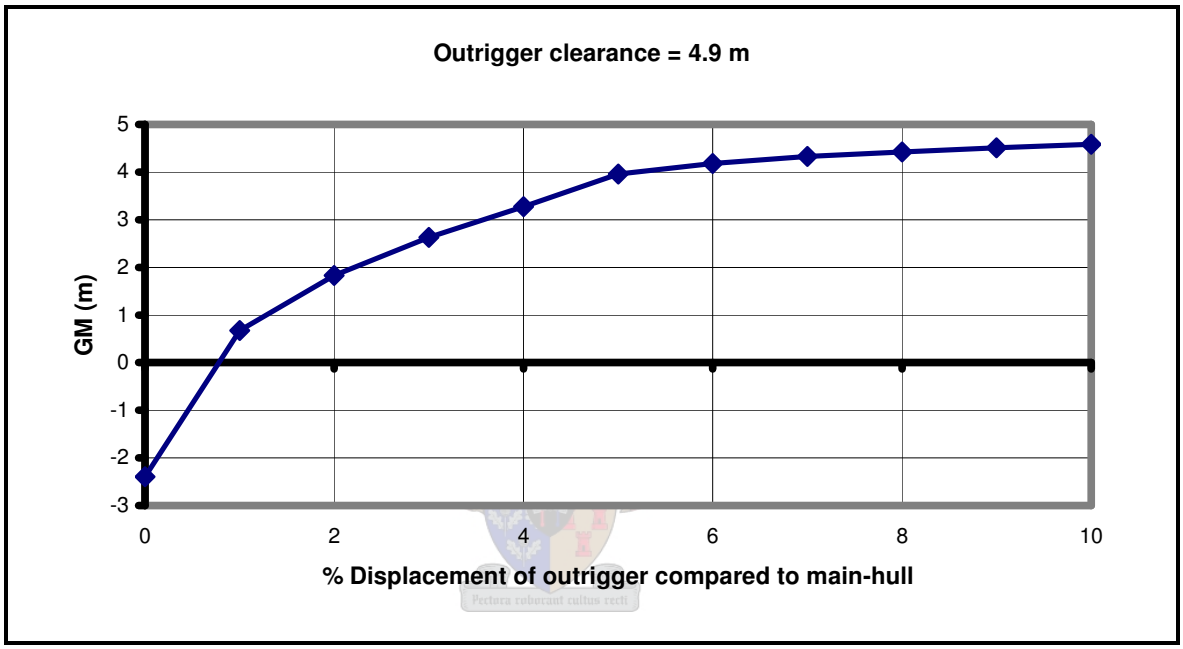

Figure 3.3: GM versus the % displacement of the outriggers

According to the results presented here clearly shows that a 6 % outrigger displacement will be stable at a clearance distance of 4.9 m. An optimum clearance distance can therefore be determined through another main parameter.

Outrigger length

The initial design assumed outriggers that had a length of 40 % of the main-hull's length. The other dimensions were scaled down accordingly for the outrigger to be geometrically similar to the main-hull. Previously published research suggested that the outriggers should be typically

between 30 % and 40 % of the main-hull's length for the vessel to have a minimum resistance (Doctors and Scrace, 2003).

A problem with the 40 % length was that for the hydrofoil configuration being investigated could not have a feasible configuration. Another length was considered: a 60 % main-hull length for the outrigger. The other dimensions were kept the same as for the 40 % case. The 40 % and 60 % length outrigger will from now on be referred to as configuration A and configuration B respectively. Figure 3.4 illustrates the different outrigger lengths of both configurations. Table 3.2 gives the appropriate dimensions.

	Outrigger Length compared to the Main-Hull		
	40 % length	**60 % length**	
	Configuration A	**Configuration B**	**Units**
Length wl	14.505	22.359	m
Beam wl	1.268	1.265	m
Draft	0.518	0.4	m
Wetted surface area (WSA)	21.402	27.689	m^2
Water plane area (WPA)	14.372	21.325	m^2

wl = water line

Table 3.2: The dimensions for configuration A and B at static conditions

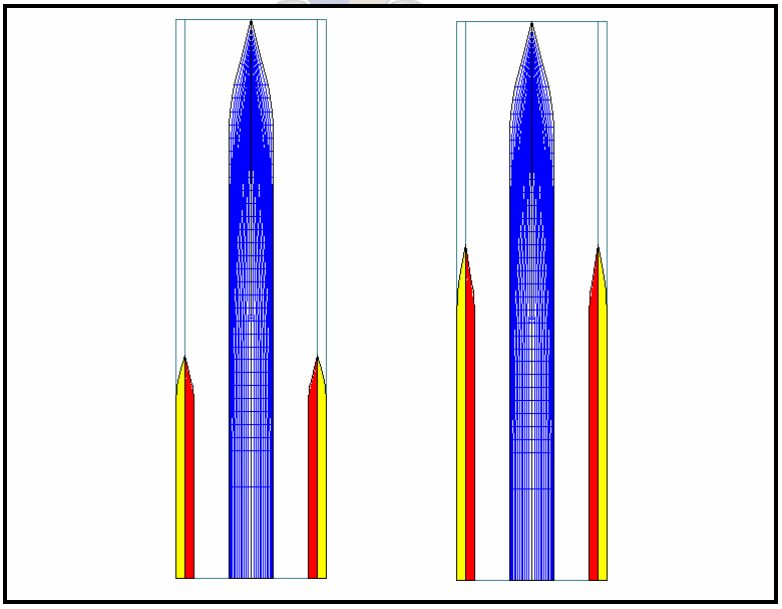

Figure 3.4: Configuration A and configuration B on the left and right respectively

Resistance data had to be determined on the vessel with different outrigger clearances. The results show that the clearance, according to this particular design, did not have a huge influence on the total resistance. The wave interference resistance for the vessel differs with a variation in clearance positions, but not with any significant effect on the total resistance. Therefore, the outriggers can be positioned anywhere to support the best possible hydrofoil system configuration.

The resistance determined for configuration A and B does not show any significant difference according to the results determined in Michlet Version 6.05 as can be seen in figure 3.5. The problem associated with these results is that no rise/sinkage or trim values were used in the calculations. Model tests should initially be performed to determine the trim and rise/sinkage values of the vessel at a certain speed and then be imported into Michlet Version 6.05 for calculations. The resistance will certainly change due to the dynamic lifting force created at higher speeds and due to the change in trim of the vessel.

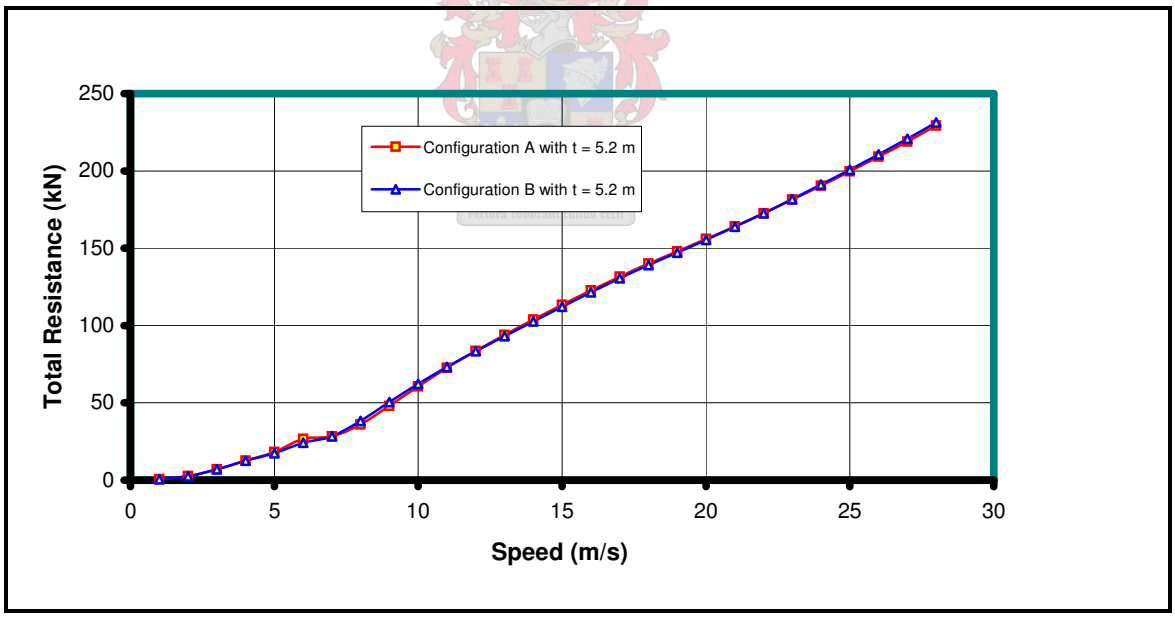

Figure 3.5: Total resistance for configuration A and B without hydrofoil assistance

The displacement of the outriggers of both configurations is kept constant at 6 % of the total vessel displacement, as was determined in section 3.1.3. This resulted in a larger wetted surface area (WSA) for configuration B and therefore a higher frictional resistance, but lower residual

resistance (Tulk and Quigley, 2004). Considering hydrofoil assistance will result in a faster decrease in WSA for configuration B than for configuration A due to the shallower outrigger draft of configuration B.

The advantages of configuration B are the increased stability due to a larger water plane area and more potential to support a hydrofoil system.

Outrigger clearance

The positioning of the outriggers with regards to the center-hull is very important with regard to the wave interference resistance of a vessel according to previously published research. The transverse and longitudinal distance of the outriggers from the center-hull is referred to by many researchers as clearance and stagger respectively. The type of hull shape (for both the center-hull and the outriggers) and the design speed also influence the wave interference resistance of the vessel. However in this study only one hull shape was considered for the center-hull and two configurations for the outriggers. The two configurations referred to are described in the previous section.

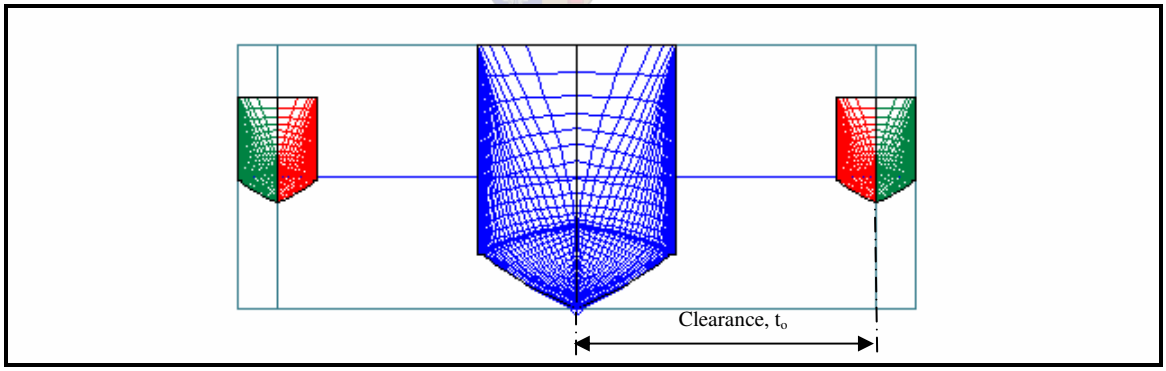

Figure 3.6: Clearance

The clearance is measured from the centerline of the main hull to the centerline of an outrigger as illustrated in figure 3.6. The stagger, however, was taken as zero due to being most practical for hydrofoils. This means that the transoms of both the outriggers and the main-hull are inline.

Previously published research states that the wave interference resistance is at a minimum if the longitudinal position of the outriggers (stagger) is close to zero (Doctors and Scrace, 2003).

The stability is also influenced by the clearance of the outriggers and the results are shown in figure 3.7. The outriggers are positioned at different clearances from the center hull. The clearance is measured from the centerline of the center hull to the centerline of an outrigger. The geometry of the model was imported into Maxsurf Academic Version 11 and the calculations were based on the outriggers having a 60 % main-hull length. The interference line is the closest distance the outriggers can be positioned before it comes into contact with the center hull.

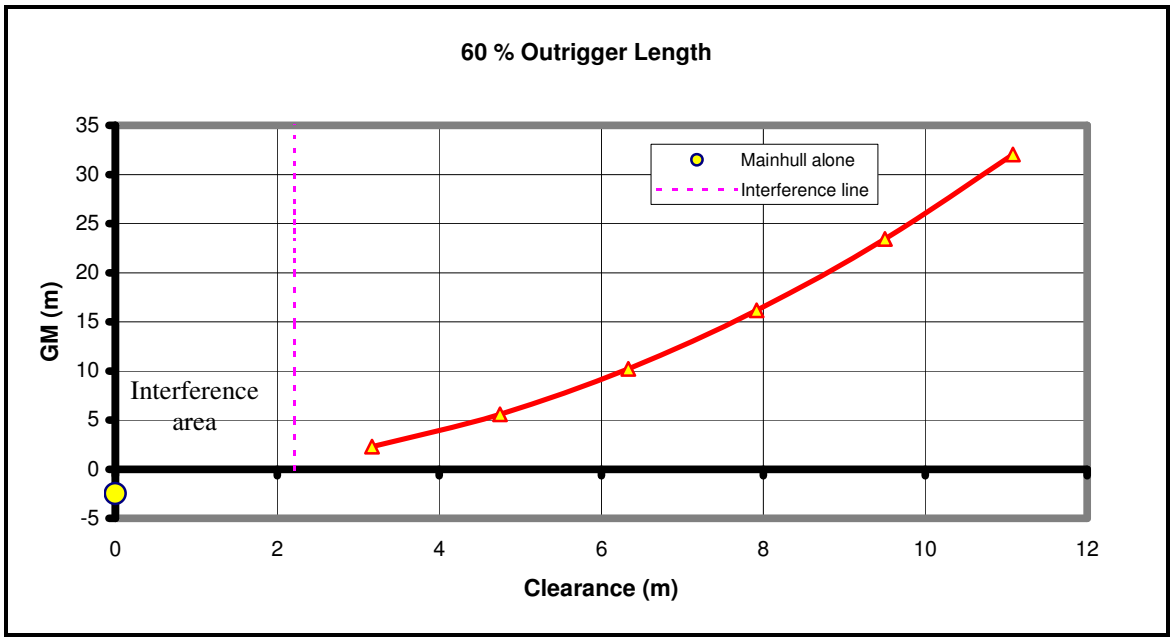

Figure 3.7: 6 % Outrigger displacement with different clearances

The results also show that the center hull is unstable on its own with a GM of approximately -2.4 m. This value can be seen at a clearance of 0 m. As soon as the outriggers are added and positioned as close as possible to the center hull the vessel becomes stable. The interference area is difficult to determine due to unknown displacement of the outriggers as they start combining with the center hull. Therefore this area is not shown. Clearly the results confirm that the further the outriggers are positioned from the center hull the more stable the vessel becomes and that there is no prescribed limitations on outrigger position with regards to static stability.

This section however does not take into account the effect of the hydrofoil support. The results are determined according to the hull shape and the trimaran configuration. The results are also for the full-scale vessel.

The results of figure 3.8 show the wave interference resistance for different outrigger clearances. It is clearly visible that the wave interference resistance decreases, as the outriggers are moved further away from the center-hull. The results for a catamaran with a clearance of 8.5 m are also shown. There is a difference in the wave interference resistance at speeds below 25 knots between the catamaran and the trimaran with different outrigger clearances, but this, however, is where the hump resistance approximately occurs for the catamaran. The vessel is designed to operate at a design speed of 50 knots and therefore, the results show that the trimaran with a clearance of more than 6 m has a lower wave interference resistance than a catamaran. The catamaran has the same overall length and total displacement as the trimaran.

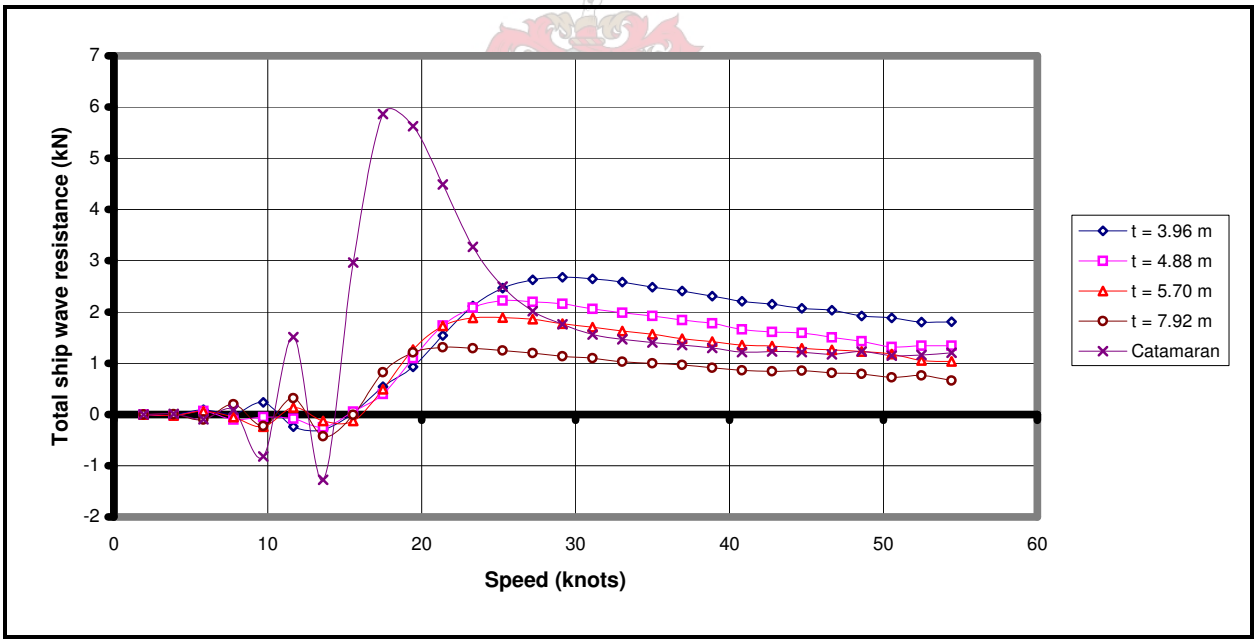

Figure 3.8: Wave interference resistance for different outrigger clearances

The results, however, of the trimaran vessel with different outrigger clearances show no remarkable differences in the total resistance as can be seen in figure 3.9 due to no experimental trim and rise/sinkage values. The wave interference resistance calculated does not have any

significant effect on the total resistance according to the results determined in Michlet Version 6.05.

The results of a catamaran with a clearance of 8.5 m between the two hulls are also shown in figure 3.9. This gives a reasonable indication of the difference in total resistance between a catamaran and a trimaran without experimental determined trim and rise/sinkage values for both.

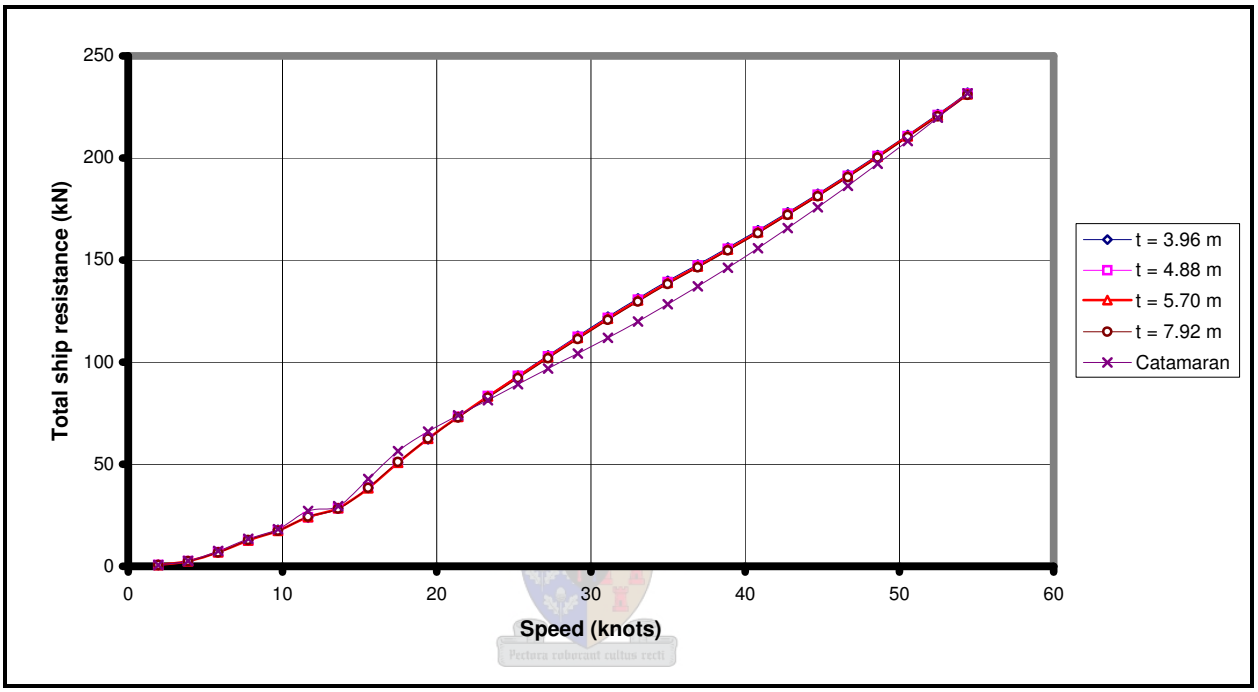

Figure 3.9: Total resistance for different outrigger clearances

The trimaran demonstrates excellent potential of benefiting from a hydrofoil system. The deeper draft will result in a higher rapid reduction of WSA and wave system compared to a catamaran is some of the beneficial characteristics of a hydrofoil-assisted trimaran.

Given that the static stability considerations as well as the interference effects having a small effect on the total resistance, it was possible to choose the spacing based on considerations for the hydrofoils.

To obtain a good direct comparison with the HYSUWAC catamaran, the spacing between the hulls of the trimaran was taken as the distance from the inner side of the hull to the centerline of

the vessel along the waterline of the catamaran. This distance is denoted by *s* and illustrated in figure 3.10. The reason for this is to have a similar aspect ratio for both hydrofoil systems. Therefore, a reasonable good comparison will be achieved according to the clearance between the hulls. Figure 3.10 points to a distinguishing feature of trimarans, namely that the draft of the main-hull tends to be deeper than that of a catamaran. The stabilizing outriggers are mostly precisely that, i.e. not tri-hulls as opposed to the demi-hulls of the catamaran, which equally share the displacement. Figure 3.11 clearly illustrates the zero stagger position of the outriggers.

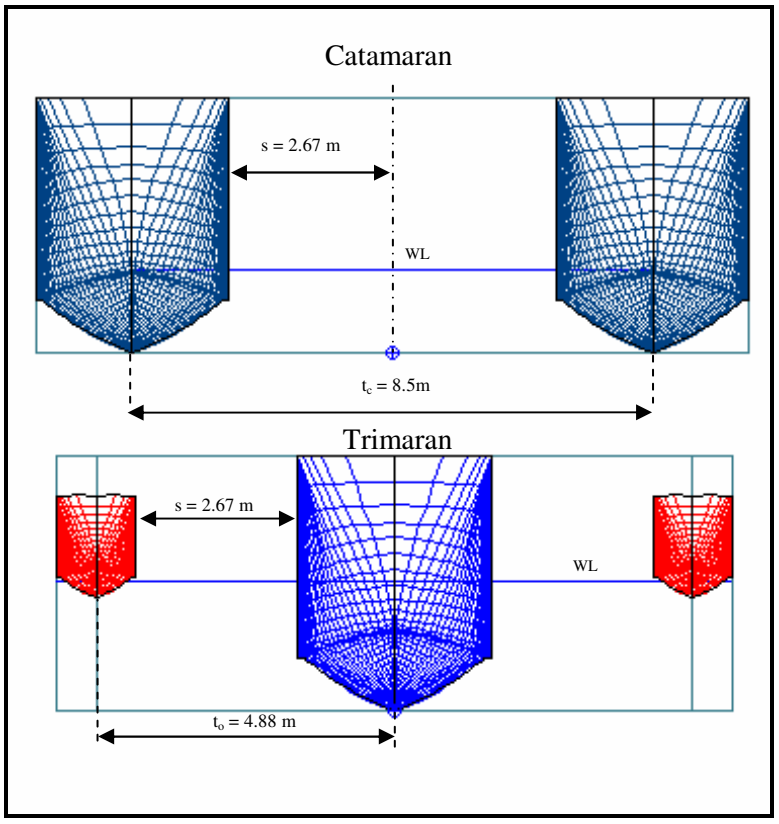

Figure 3.10: Clearance distance specified for optimal supported hydrofoil design configuration

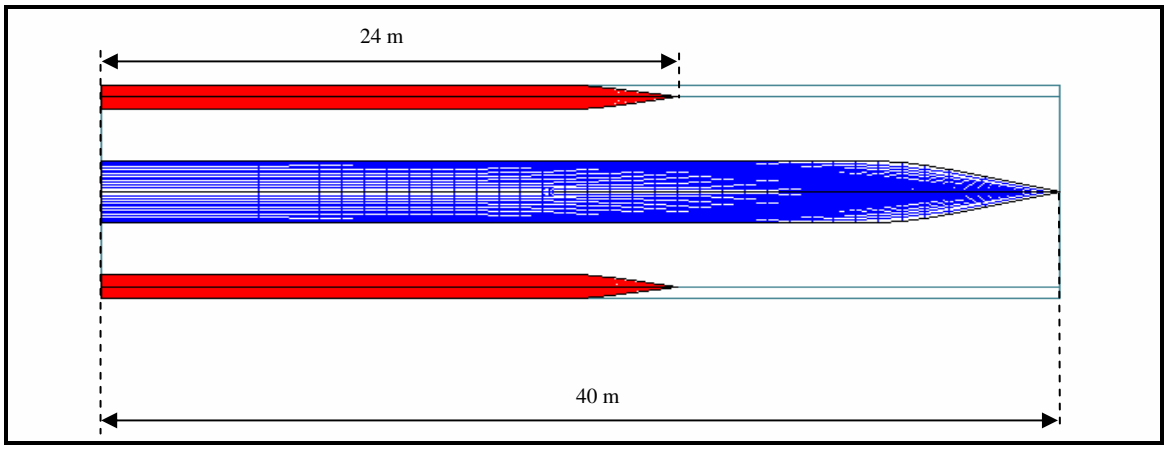

Figure 3.11: Top view of trimaran configuration

3.1.4 Final Trimaran Design and Configuration

The final design parameters resulting from the above considerations are given in the following table. These parameters and dimensions are given in table 3.3 for the whole vessel, the center hull and an outrigger.

	Trimaran	Center-Hull	Outrigger	
Displacement	161000	151342	4830	kg
Volume	157.1	147.7	4.7	m^3
Draft to Baseline	2.09	2.09	2.09	m
Immersed depth	2.09	2.09	0.4	m
L_{wl}	37.29	37.29	22.36	m
Beam waterline	11.03	3.17	1.27	m
WSA	248.86	193.48	27.69	m^2
Max cross sect area	5.91	5.31	0.30	m^2
Waterplane area	139.73	97.09	21.33	m^2
C_p	0.71	0.75	0.71	
C_b	0.36	0.60	0.41	
C_m	2.59	0.80	0.59	
C_{wp}	0.66	0.82	0.75	
LCB from zero pt	-4.47	-4.10	-10.31	m
LCF from zero pt	-4.97	-2.84	-9.81	m
KB	1.31	1.27	1.96	m
BM_t	6.94	0.47	0.49	m
BM_l	73.19	59.57	134.19	m
KM_t	8.25	1.73	2.44	m
KM_l	74.50	60.84	136.15	m
Immersion (TPc)	1.43	1.00	0.22	tonne/cm
Clearance			4.88	m

Table 3.3: Hydrostatic characteristics of the trimaran

3.1.5 Conclusion

Given that there is no significant difference in the clearance, stability and resistance of the two types of configurations considered without experimental trim and rise/sinkage values incorporated into the results, the hydrofoil system is the only parameter that remains to increase the effectiveness of the vessel. This project's main focus is to evaluate the hydrodynamics of a hydrofoil-assisted trimaran and not the hydrostatics. Hence, further work will focus on the determination of the optimum configuration of the hydrofoil system for the selected trimaran configuration.

3.2 Hydrofoil Design

The design of a hydrofoil system specifically needs to incorporate the hydrodynamic characteristics concerning the tunnel width and hull shape of the vessel. The hydrofoil design alone can be ideal, but the addition of the system to a vessel can reduce the performance significantly due not only to the interaction effects between the hulls and the foils, but also the interference effect the front foil can have on the rear foil.

The hydrofoil design is also very complex due to conflicting design requirements in each of the three different operating phases (displacement, transition and planing) and will be discussed later in this section (Migeotte, 2001).

The hydrofoil system design for this project was done by Dr. G. Migeotte, managing director of CAE Marine (South Africa) and co-promoter of this study due to the scope limitations of this project. The important aspects regarding hydrofoil design will still be discussed.

Different types of catamaran foil configurations have been developed over the last couple of years, but only two familiar configurations shown in figure 3.12 which have been tested at the *Department of Mechanical Engineering* of the *University of Stellenbosch* will be considered. Both these hydrofoil-systems are patents of the *University of Stellenbosch*. The characteristics of both will be discussed briefly and these are the HYSUCAT and HYSUWAC configurations. Only one of these foil configurations was slightly modified to suite the trimaran design.

The best possible method of determining the effects that a hydrofoil has on a vessel and optimizing the foil configuration is by doing model testing. The problem associated with foil-assisted models is that the viscous scale effect cannot be properly accounted for in the scaling procedure (Migeotte, 2001). At slower model speeds, however, cavitation is less of an issue, allowing higher angles-of-attack and spectacular results to be achieved that can generally not be realized at full-scale (Tulk and Quigley, 2004).

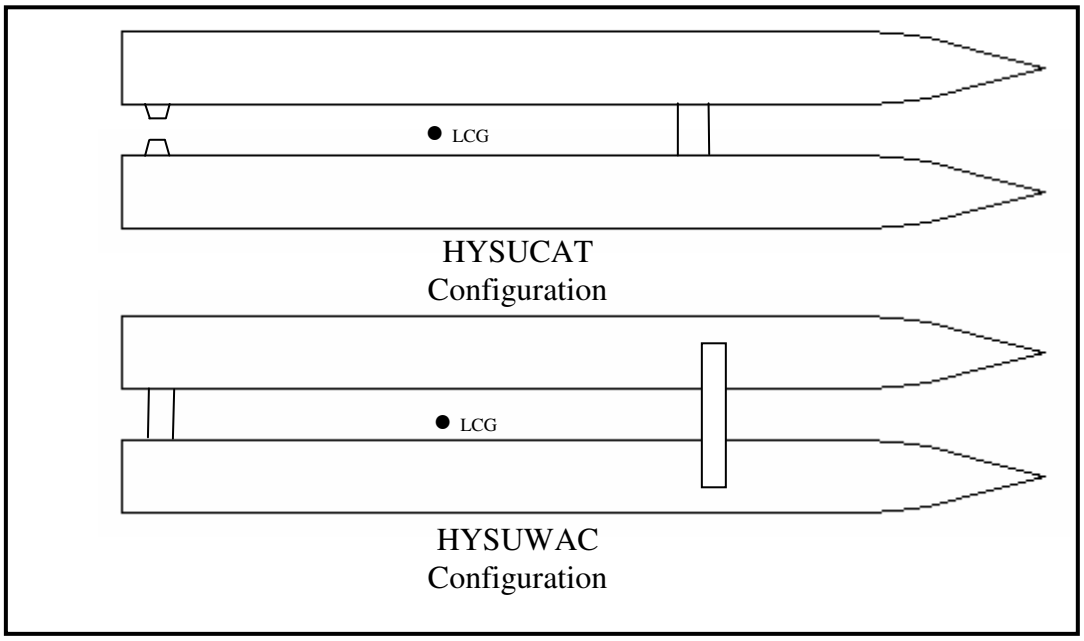

Figure 3.12: Foil configurations

3.2.1 Foil Configuration

HYSUCAT configuration

The HYSUCAT (hydrofoil-supported-catamaran) or "avion" foil configuration has a main-foil spanning the tunnel width and two small foils acting as auto-trim-stabilizers near the stern. The auto-trim-stabilizers allow the vessel to be designed so that the most efficient trim conditions are met at design speed (Migeotte, 1997). The vessel will therefore operate at the trim angle of least resistance, while the main-foil operates at the optimum lift-to-drag ratio.

The main-foil is the primary load carrying foil and is positioned slightly in front of the longitudinal center of gravity (LCG). Consequently the foil lifting force creates no unfavorable large moments. The vessel may become very unstable if the lifting force shifts behind the LCG (Migeotte, 1997).

The auto-trim-stabilizers operate in extreme free surface effect. If the vessel trims positively (with the bow lifting) the auto-trim-stabilizers generate more lift due to operating less in the free surface effect and at a higher angle-of-attack therefore returning the vessel to an acceptable trim angle. If the vessel trims negatively the auto-trim-stabilizers moves closer to the free surface, the angle-of-attack decreases, resulting in a reduction of the lift force while the drag increases returning the vessel once again to an acceptable trim angle.

HYSUWAC configuration

HYUWAC stands for hydrofoil-supported-watercraft and applies to mono-hulls, catamarans and trimarans. Both foils should be positioned as far apart as possible to limit the interference effect caused by the front foil on the rear foil and to dampen the pitching motion (Migeotte, 1997). The rear foil will operate in the downwash of the front foil if the foils are in close proximity to each other. The foils are both considered carrying a large part of the load due to their relatively high lift-to-drag ratio. This foil system was specifically developed for the larger fast ferries with semi-displacement hulls and patented in 1998 by the US.

Long slender vessels that are heavily loaded will benefit from a tandem foil configuration due to the large portion of the load that is carried by both foils and the large potential spacing between the foils (Migeotte, 1997). A sufficient tandem configuration not only reduces the interference effect between the foils, but also enhances the pitch stability of the vessel due to the large lifting forces created near the bow and the stern.

3.2.2 Foil Profile

The profile of the foil will influence the pressure distribution around the foil associated with the amount of lift and drag. The chord length, thickness and chamber line are some of the influential parameters concerning foil profile design. The profile for the front and rear foils can differ in a tandem foil configuration. It is usual to make use of circular arc profiles for hydrofoils as these have shapes that are close to optimum for hydrofoils as well as providing ease of construction.

3.2.3 Foil Positioning

The horizontal and the vertical positions of a foil are very important in foil design. It is beneficial to position the foils in the wetted perimeter of the vessel due to foil protection ensured by the hulls. Some foil arrangements situated below the keel have proven to enhance the foil performance, creating more potential to lift the vessel higher out of the water. The position of two tandem foils is important to the already mentioned downwash created by the front foil. The position of the main-foil near the LCG is of great concern for any foil configurations (Migeotte, 1997). The foils should be attached 90 degrees to the hull to minimize foil-hull interference.

3.2.4 Planform Considerations

Aspect ratio

The hydrofoil efficiency is greatly associated with the aspect ratio (Migeotte, 2001). The higher the aspect ratio the more lift will be generated as well as, but a less significant, increase in drag (Hoppe, 1992). The span of the foil is limited by the distance between the outrigger and the main-hull somewhat limiting the aspect ratio.

Sweep and dihedral

Swept foils delay the onset of cavitation by increasing the pressure on the suction side of the foil and improving the dynamic stability during maneuvering, as swept foils induces the craft to bank into the turn (Migeotte, 2001). According to research done on hydrofoil-assisted catamarans, increased sweep angles have proven to be beneficial in reducing spray and water disturbance when the foil is close to or breaking the free surface (Hoppe, 1980). According to Calkins (1981), dihedral foils enhance the roll stability and rough water capability of a vessel.

Angle-of-attack

A favorable angle-of-attack will generate sufficient lift at the design speed. If the rear foil is operating in the downwash caused by the front foil the angle-of-attack of the rear foil will be affected and should be increased.

The fixed foil system will move with the vessel as the vessel trims, therefore changing the angle-of-attack of the foils. This can result in unfavorable angle-of-attacks and flow separation may occur and increase the drag of the foils.

3.2.5 Final Hydrofoil Design

The trimaran hydrofoil design is similar to a HYSUWAC hydrofoil design used for a catamaran with equal displacement. This will give a good resistance comparison between the hydrofoil-assisted trimaran and the hydrofoil-assisted catamaran. Figure 3.13 and figure 3.14 show respectively the foil arrangement and both exaggerated foil profiles. The aspect ratio for the front and the rear foil are respectively 6.60 and 5.31. The sweep angle of the front foil is 53.8 degrees. The angle-of-attack for the front and the rear foils are respectively –0.7 degrees and 0.4 degrees after conducting experimental tests that will be explained in chapter 4.

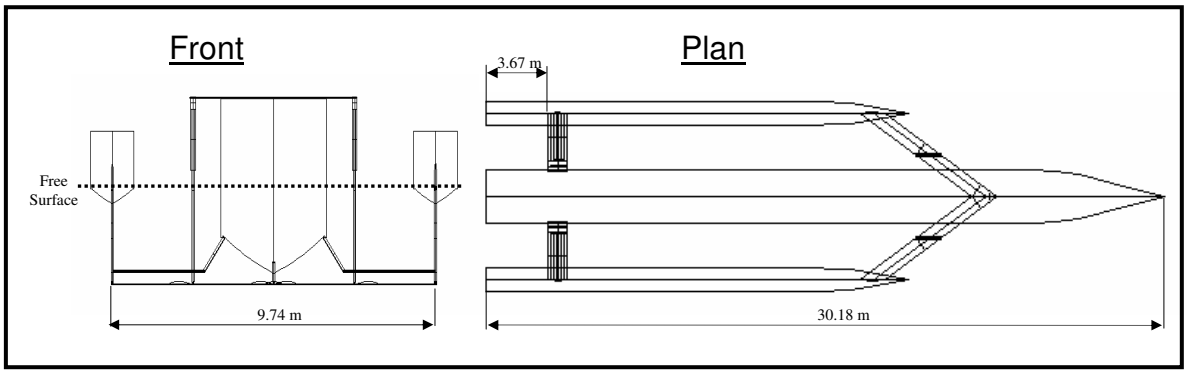

Figure 3.13: Front and plan view of foil arrangement

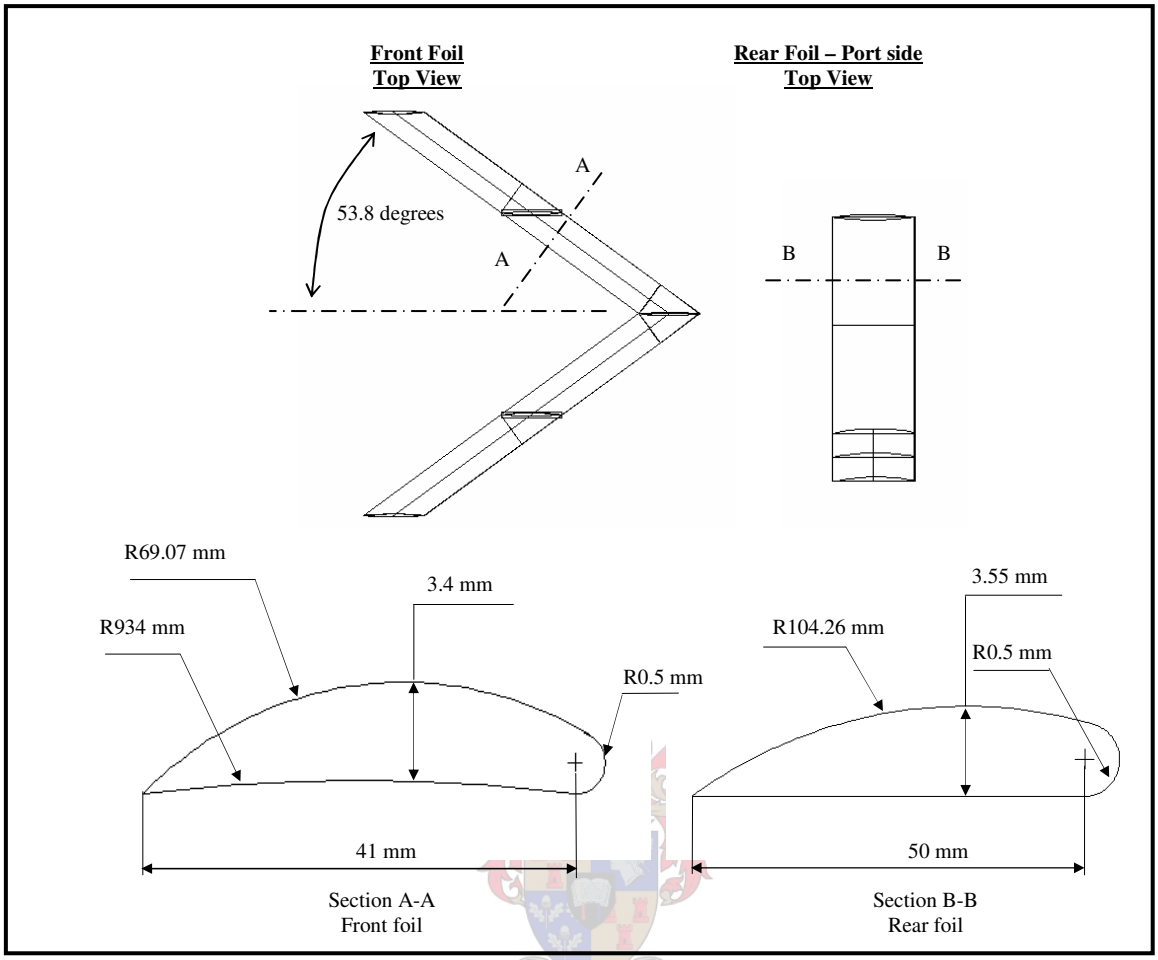

Figure 3.14: Front and rear foil profiles

Chapter 4 Model Testing

4.1 Introduction

Model testing provides reasonable results for predicting a ship hydrodynamic characteristics and performance. The scaling laws for conventional ships are well established and the procedure correlates model and ship with a high level of accuracy. The same scaling laws can generally be applied to high speed craft, such as a trimaran, but some fundamental problems may arise that will lead to small inaccuracies. Surface tension (spray), viscous forces and moments and cavitation are some of the fundamental problems that cannot be accounted for during scaling. These problems will be discussed later in the report.

The trimaran model was tested with and without hydrofoils at specified outrigger transverse clearance positions. A specific outrigger transverse clearance position, as determined in chapter 3, of the hydrofoil-assisted trimaran is used to obtain a reasonable comparison with a hydrofoil-assisted catamaran. The validity of comparing these two systems is explained in chapter 3. Three different outrigger transverse clearance positions were also tested to determine the importance of the interference resistance between the main hull and the outriggers.

4.2 Towing Tank

The *Department of Mechanical Engineering* of the *University of Stellenbosch* has a towing tank with the following dimensions:

Length: 92 m
Breadth: 4.5 m
Depth: 2.7 m

Figure 4.1 shows the towing tank with the trolley that is used to tow the models. The trolley can reach a maximum speed of 8.2 m/s.

Figure 4.1: Towing tank and trolley

4.3 Model Dimensions

Figure 4.2 shows the main dimensions of the trimaran model with and without hydrofoils that was used for testing. The scaling factor is 20.997 and the overall mass of the model is 17.39 kg.

Three different outrigger positions are tested to determine if the interference resistance between the hulls influences the performance of the model. The three different transverse clearances are shown in figure 4.3. The hydrofoils will be fitted to the model with the outriggers positioned at setup C.

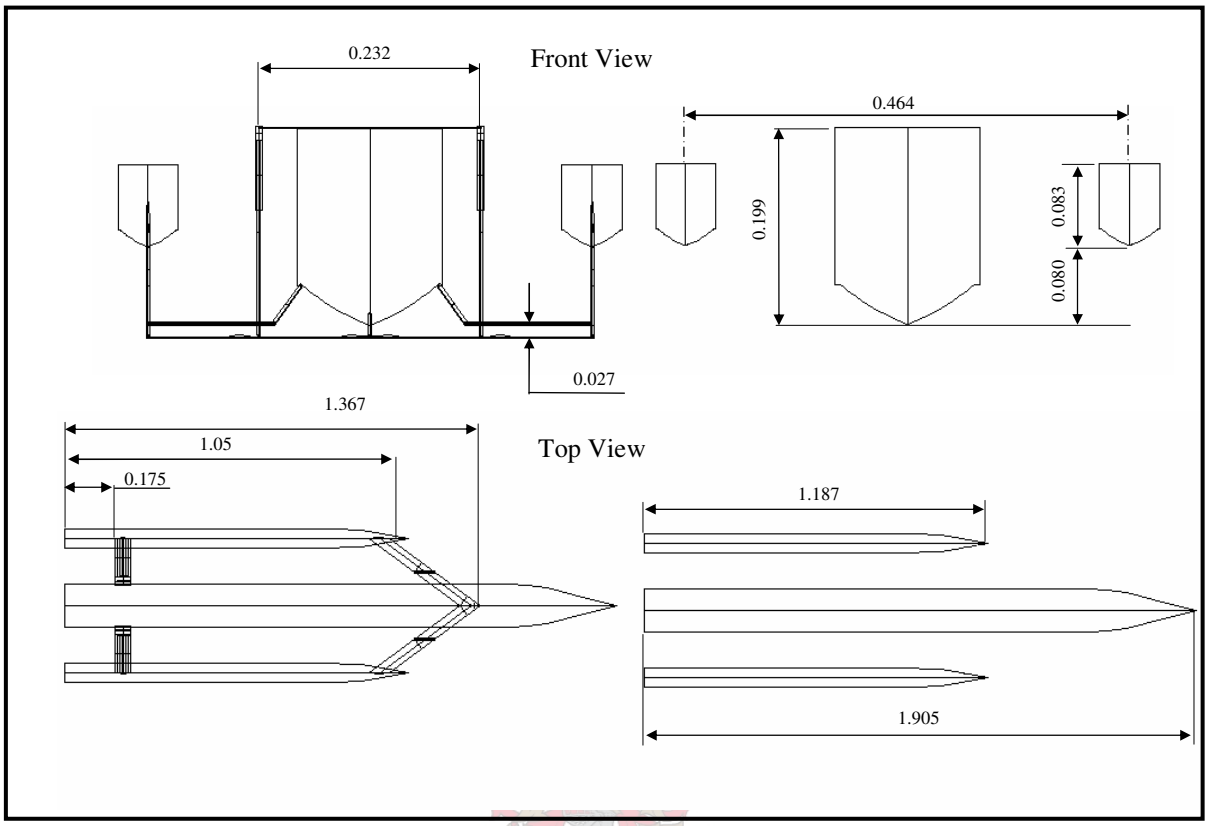

Figure 4.2: Main trimaran model dimensions with and without hydrofoils

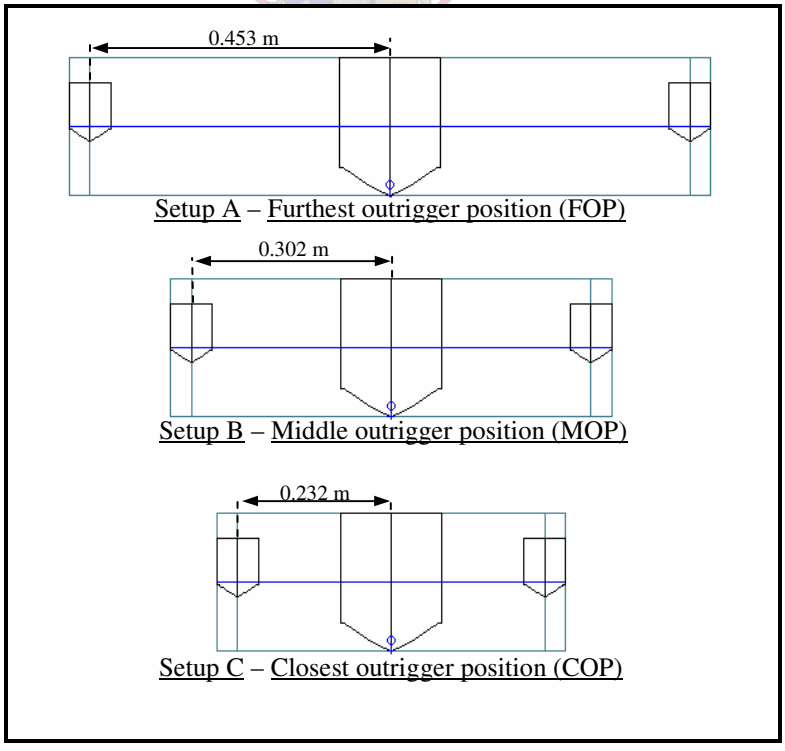

Figure 4.3: Different outrigger transverse clearance positions

4.4 Model Setup

Figure 4.4 illustrates the basic model setup with the measuring sensors that determine the total model resistance, front trim and rear trim. The front trim and rear trim together determines the amount of rise or sinkage and the trim angle generated by the dynamic forces. The longitudinal center of gravity (LCG) of the model is determined before each set of tests. The LCG of a vessel is influenced by the weight of different major components in the vessel. The major weight components are: hull structure, propulsion plant, electric plant and auxiliary systems. Three different LCG positions of the model are tested, due to unknown weight of the major weight components and to determine which LCG gives better performance results.

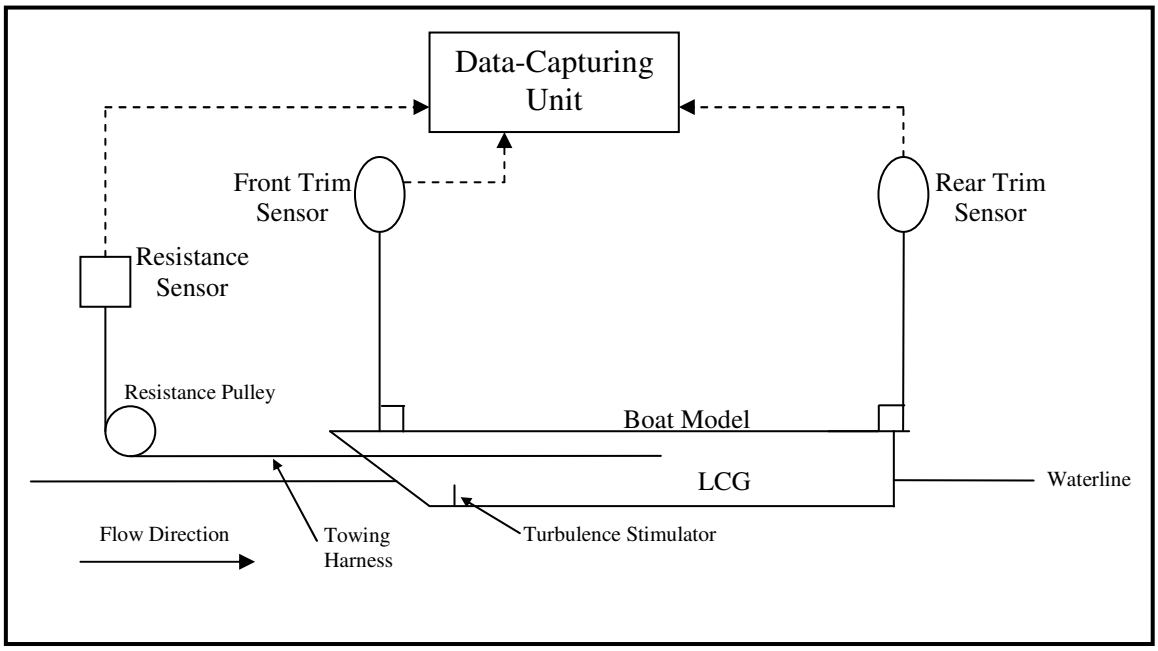

Figure 4.4: Model setup

The resistance pulley can be adjusted vertically, because the towing harness that runs underneath the resistance pulley and coupled to the model must be horizontal and near the LCG. If the towing harness is not horizontal, then the measurements will give inaccurate results due to a vertical force created by the rope while towing the model. This will influence the trim angle of the model. The trim sensors must be coupled to the model perpendicular as shown in figure 4.4.

The data-capturing unit consists of a computer and a data acquisition device (DAQ). The DAQ converts the analogue signal (produced by the measuring sensors) into a digital signal that feeds into the computer. Two linear displacement sensors measure the front and rear trim. A load cell determines the resistance measurement.

Models operate at considerably lower Reynolds numbers than there corresponding prototypes. This means that the transition from laminar to turbulent flow occurs relatively further aft resulting in lower frictional resistance for the model than the full-scale ship. Froude's laws of scaling require the flow condition on the model to be similar to that of the prototype i.e. turbulent flow. Therefore, the model is equipped with turbulent stimulators (sandpaper strips) near the bow. In practice, the transverse stimulators are sometimes placed further aft, creating a longer laminar flow region that compensates for the added resistance created by the transverse stimulator.

4.5 Model Calibration

The resistance sensor is calibrated by measuring a known weight. The data-capturing unit displays the weight measured. The weight displayed and the known weight must be exactly the same before testing may begin. The measurement is accurate enough when the error that is involve when calibration is less than 0.001 kg. The front and rear trim sensors are calibrated by determining the height where the sensors are attached to the stationary model in the towing tank with the towing harness taut to simulate the model is being towed. The data-capturing unit measures a zero point for each trim sensor at that position where the model is kept still and with the towing harness taught. The measurement here is accurate enough when the error that is involved when calibrating is less than 0.0005 m. Therefore, the measurements method is reasonably accurate. The total error involved with the results after scaling to full-scale is between 5 % and 10 % (Migeotte, 2005).

4.6 Testing Procedure

Each set of tests includes a LCG position, six different measuring speeds and three different measuring speeds to determine the wetted surface area. Three sets (due to different LCG positions) are tested for each outrigger clearance position.

The LCG positions are taken as 34 % LCG, 32 % LCG and 30 % LCG. The percentage indicates the distance taken from the main-hulls length measured from the transom in relation to the waterline length. The 34 % LCG is where the model is at even keel (at static conditions with a zero trim angle). It was first assumed to measure at 36 % LCG, 34 % LCG and 32 % LCG, but a number of test runs showed that the model at even keel is generating too much spray and created a very large bow wave, therefore the next LCG position should rather be shifted towards the transom than towards the bow. The LCG positions where determined by lifting the model out of the water and hanging the model by two vertical ropes on the starboard and port side. The weights inside the model are adjusted until the model is hanging perfectly horizontal. This will result in a certain trim angle at static condition when the model is not at even float.

According to volumetric Froude scaling, the maximum speed that is tested is 5.8 m/s. Therefore, six different speeds were tested in intervals of 1 m/s over a speed range of 0 m/s to 6 m/s. At each speed the total resistance, front trim and rear trim are measured.

Painted vertical lines in front of each measuring station on the main-hull and the outriggers before a test and the paint traces are examined after a test to determine the wetted surface area. As the model is towed the paint smudges where the water is forced on the side of the hull due to the velocity and shear forces according to the wave and trough generation created by the hulls. This can be seen in figure 4.5. The total wetted surface area can then be determined for a specified speed. The wetted surface area is used to calculate the viscous friction resistance.

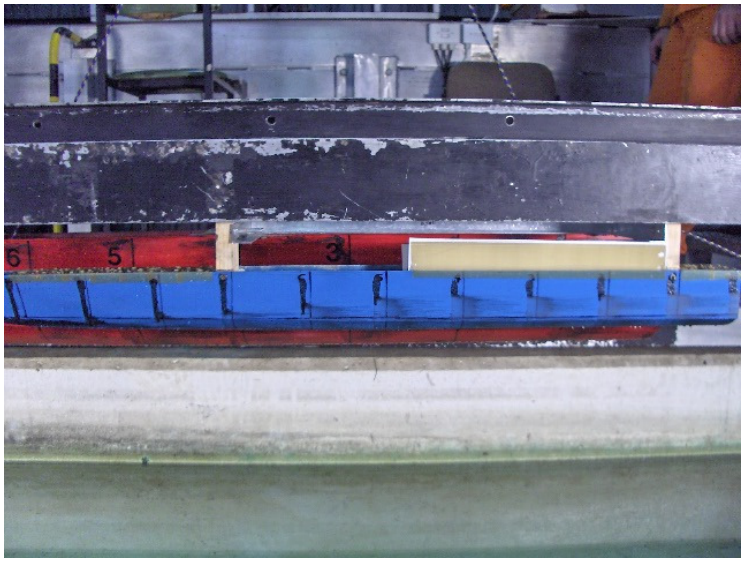

Figure 4.5: Smudge marks for calculating wetted surface area

4.7 Problems for Fast and Unconventional Ships

Model testing is an excellent means of predicting full-scale resistance, but there are some inaccuracies that may arise due to towing tank size, cavitation, scaling errors, air resistance and wetted surface area, which have to be accounted for and which shall be explained in the following sections.

4.7.1 Model Tank Restrictions

The size of the towing tank may influence the measurements gained from model testing to that of actual full-scale resistance. Valid full-scale predictions in unrestricted water are only possible if the tank is sufficiently large. Blockage and shallow water effects are two characteristics that are associated with insufficient tank size. Blockage is the ratio of the submerged cross sectional area of the model to the cross sectional area of the tank (Bertram, 2000). Therefore, the size of the tank can restrict the size of the model. The size of the model should be as large as possible to minimize the viscosity scaling effects. Blockage will generally be very low for high-speed ships. Shallow water effect depends on the model speed and the depth of the towing tank.

Shallow water effect

The resistance of a ship will increase when operating in shallow waters. Two distinct speed regimes exist in shallow waters: sub-critical regime and super-critical regime. These regimes are separate by the critical speed. The critical speed is the maximum wave speed in shallow waters at a certain depth. A ship's speed is therefore sub-critical when it is less than the critical speed and vice versa for the super-critical speed. In the sub-critical regime, a normal Kelvin wave pattern exists on the water surface. At critical speed the wave-making resistance increases considerably which gradually decreases in the super critical speed range. At super-critical speeds there is a decrease in resistance associated with a diverging wave system whose apex angle is related to ship speed in a similar manner to the supersonic Mach wave in aerodynamics (Millward, 1982). The critical speed is important to vessels operating on rivers and inland waterways and also for models tested in towing tanks with restricted dimensions. The critical speed is related to depth as follows (Dubrovsky, 2002):

$$V_{crit} = \sqrt{gd} \tag{4.1}$$

where d is the water depth. The critical speed is characterized by great energy losses due to the growth of the wave-generating component of the resistance. When the vessel is moving at less than the critical speed wave-making resistance tends to be higher and vice versa for speeds above the critical speed (Migeotte, 1997). The changes in wave making resistance is presented as a function of Froude depth number:

$$Fn_d = \frac{V}{\sqrt{gd}} \tag{4.2}$$

Figure 4.6 shows typical effects of Froude depth number on the residual resistance characteristics of a high-speed vessel and is reproduced from Millward (1982). According to figure 4.6, the residual resistance coefficient can be corrected if shallow water effects are present.

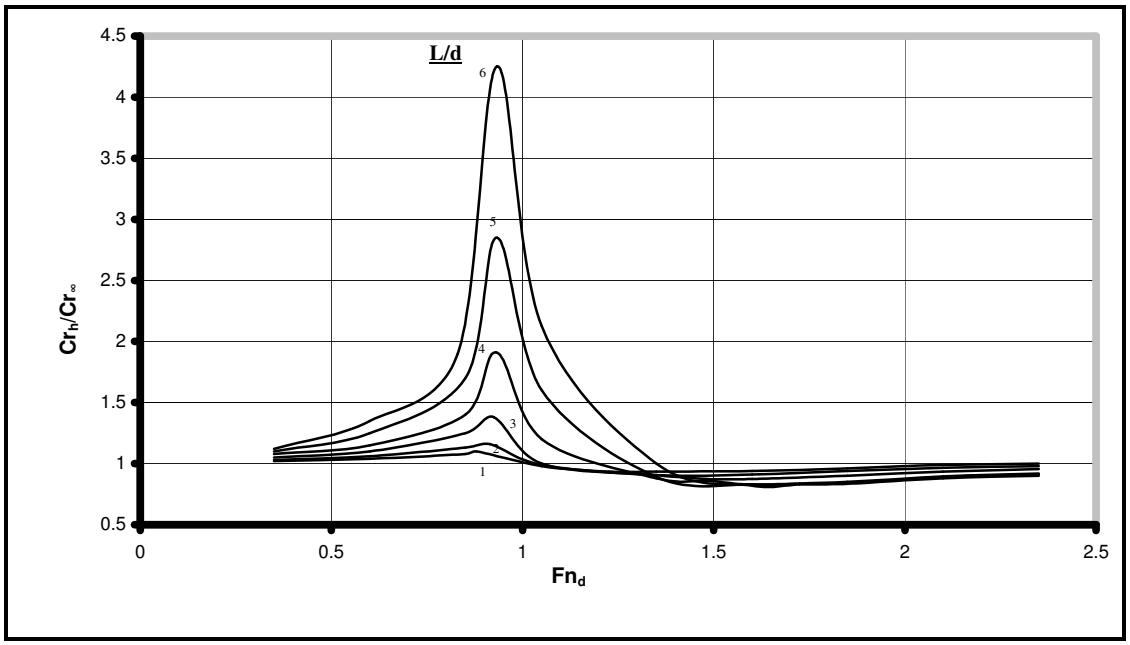

Figure 4.6: Changes in residuary resistance for high-speed craft if speed and water depth vary

The figure clearly shows that the resistance reaches a maximum just below the critical speed in the sub-critical region. If the length to depth ratio is less than unity, then the changes in wave resistance due to shallow water effects are very small and for all practical purposes can be neglected.

If shallow water effects are present, then empirical equations can be used to correct the shallow water effect given by the Society of Naval Architects and Marine Engineers (1988), but no correction exists for the super-critical speed regime. The L/d ratio that was encountered in this project was roughly 0.63, therefore the effect of shallow water was negligibly small and did not have any significant affect on test measurements.

Blockage

Blockage is caused by lateral restriction of the water in a narrow channel. This, however, increases the potential flow and therefore increases the frictional resistance or a loss in speed of the vessel. According to Landweber (who expanded the work of Schlichting), the principal factor controlling the loss in speed of a vessel due to blockage is presented in Lewis (1988) as follows,

$$\frac{\sqrt{A_x}}{R_H} \tag{4.3}$$

where A_x and R_H are the maximum cross-sectional area of the vessel and the hydraulic radius respectively. If the value for the factor in equation 4.3 is above 0.2, then blockage effect is increasing the resistance of the vessel (Migeotte, 1997). The hydraulic radius for a vessel in a rectangular channel can be determined from the following equation,

$$R_H = \frac{(b_c h_c - A_x)}{(b_c + 2h_c + p)} \tag{4.4}$$

where b_c, h_c and p are the channel width, channel depth and the vessel's wetted surface perimeter respectively. Landweber was able to deduce a single curve to determine the speed loss of the vessel or alternatively the increase in water velocity around the hull presented in Lewis (1988). This curve is reproduced and given in figure 4.7.

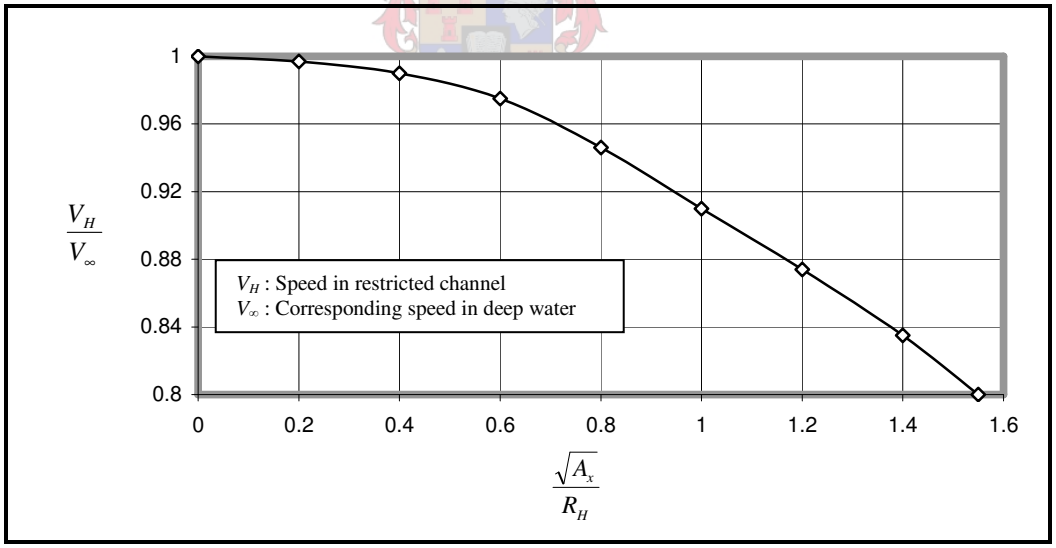

Figure 4.7: Curve for velocity ratios for calculating resistance in restricted channels

The following curve-fit equation provides useful approximation for figure 4.7 that can be used for the bounds of the figure (Migeotte, 1997),

$$\frac{V_H}{V_\infty} = a + b \cdot \frac{\sqrt{A_x}}{R_H} + c \cdot \left(\frac{\sqrt{A_x}}{R_H}\right)^2 + d \cdot \left(\frac{\sqrt{A_x}}{R_H}\right)^3 + e \cdot \left(\frac{\sqrt{A_x}}{R_H}\right)^4 + f \cdot \left(\frac{\sqrt{A_x}}{R_H}\right)^5 + g \cdot \left(\frac{\sqrt{A_x}}{R_H}\right)^6 \quad (4.5)$$

where,

a = 1.0000, b = -0.1081, c = 0.1176, d = -0.5855, e = 0.6406, f = -0.3101, g = 0.05726.

The increase in velocity around the hull due to the blockage can be determined. This increase in velocity results in an increase in frictional resistance of the vessel. Knowing the increase in velocity allows easy calculation of the correct frictional coefficient based on the corrected Reynolds number. No blockage was encountered in the current setup used for this project.

4.7.2 Cavitation

Cavitation may occur on the full-scale hydrofoil and not on the model hydrofoil being tested. Cavitation not only influences the lift and drag forces created by foils, but also cause material damage. The loading and the speed determine the amount of cavitation created. Significant cavitation will occur if the foil loading exceeds $6 \cdot 10^4$ N/m^2 (Bertram, 2000). Cavitation on the foil tips, joints, struts and other critical parts may be expected at speeds greater than 40 knots. Beyond 60 knots, cavitation will occur on a large part of the foil. Therefore, similarity of forces cannot be expected between full-scale and model if the prototype cavitate.

4.7.3 Hydrofoils

The foils used for model testing are geometrical similar. However, the forces created by the foils cannot be scaled precisely to full-scale. The forces on hydrofoils are largely driven by viscous effects with small to negligible gravity effects. According to Migeotte (2001), the model experience extra viscous pressure drag due to the thicker laminar boundary layer created across the foil compared to the full-scale thinner turbulent boundary layer. Some inaccuracies will arise

due to violation of Reynolds similarity. This is due to the flow being laminar over the hydrofoils that reduces the frictional resistance, but increases the profile drag as the laminar flow breaks off more easily at places of the profile curvature with positive pressure gradient (suction side) which increases the drag (especially for larger angles of attack) and reduces the lift (Hoppe, 1989). The Reynolds numbers achieved during testing range between $8.6 \cdot 10^4$ and $3.7 \cdot 10^5$. These values are mainly due to the carriage speed of the towing tank trolley and the size of the foils attached to the model. Reynolds numbers of at least $5 \cdot 10^5$ are needed to ensure turbulent flow past the foils that will minimize the error involved with scaling the forces of the foils.

A solution for this problem mentioned in the previous paragraph to ensure that the effect of the amount of lift generated by the model will have the same effect for the full-scale is to align the angle-of-attack of the prototype foil differently compared to the model angle-of-attack to ensure an identical lift coefficient for both (Loubser and Nieder-Heitmann, 1983). However, this solution is only adequate for a single speed and it generally occurs at the design speed.

Another means of determining the forces created by hydrofoils is to test them separately in a cavitation tunnel. This, however, will neglect the interaction between the hull and the foil and therefore, introduces other error margins. The best method would be to use a larger model ensuring turbulent flow across the foil, but this means a larger towing tank and is expensive. A high turbulent degree in the flow around the model foils will give better results and increased lift.

4.7.4 Air Resistance

The air resistance depends on the vessel's speed and the area and shape of the upper structure. In the case of wind, the resistance depends also upon the wind speed and its relative direction.

The method used limits the air resistance occurring and therefore does not have any significant effect on model testing, i.e. a vertical glass plate positioned ahead of the model removes any wind that might cause added resistance and with model testing the hydrodynamic aspect of the vessel is mainly considered. Therefore, the fast full-scale vessel might have an extra resistance that is

approximately between 10 % and 35 % of the total resistance due to air resistance that the model did not have. This, however, can be calculated theoretically and added later. It definitely cannot be neglected for a 50 knot craft. No air resistance, however, was assumed to be part of the full-scale results of the trimaran or the catamaran in the current study.

Chapter 5 Applicable Numerical Methods

This chapter outlines the assumptions, range of applicability and basic principles regarding the numerical programs predicting the hydrodynamics of the vessel and hydrofoils. A validation example will be given where possible. Both Michlet Version 6.05 and Autowing Version 3.0 cannot calculate the spray and wave-breaking resistance due to the high complexity of these phenomena.

5.1 Michlet Version 6.05

Michlet Version 6.05 is a computer workbench that can be used for investigations into some aspects of thin ship hydrodynamics. A text input file supplies the basic hull shape, multi-hull configuration, speed range, trim, sinkage and type of resistance prediction method to be used and an example is shown in appendix D. Michlet Version 6.05 cannot take a foil system into account. The experimental results of the trim and sinkage should be imported into Michlet Version 6.05 to account for the foil addition to the vessel.

The mathematical model representing the total resistance is the sum of the viscous drag, the wave drag and the hydrostatic pressure on the (dry) transom stern. The viscous drag is calculated using the ITTC 1957 ship correlation line. The wave drag is determined by Michell's integral (Michell, 1898). The resistance created by the transom stern is calculated similar to the infinite hollow model. A virtual appendage is added behind the transom that is based on the critical transom draft Froude number. For this project further assumptions were made that the vessel is operating in a calm sea state and that the flow is fully turbulent.

Michlet Version 6.05 calculates and adds the boundary layer thickness to the hull offsets, therefore influencing the wave and transom resistance. The wave drag is influenced regarding the change over from laminar to turbulent flow or if the flow should be fully turbulent, while the transom drag is calculated for the additional boundary layer thickness in conjunction with the

stern offsets to determine the shape and extent of the virtual appendages. The transom stern condition is very sensitive to the critical transom draft-based Froude number at which the transom will be running fully dry.

The resistance is also influenced by the trim and sinkage input values. These values can however only be determined from towing tank model experiments. The assumption is made, regarding the trim and sinkage that the portion of the hull shape above the waterline has the same shape as the waterplane area. Therefore, inaccuracies will result due to this simplification for vessels with large flared section when large trim and sinkage values are used.

No form factor must be used in conjunction with the boundary layer thickness method. The ITTC 1957 line is not a skin friction line, but a correlation line and as such it contains some allowance for the three dimensional effects. If a form factor is used there is a danger of double counting.

A previous example is given to prove that Michlet Version 6.05 is a valid numerical tool that can be used as a comparison method to experimental results. The following graph shows Michlet Version 6.05 estimates of the total resistance coefficient as a function of Froude number for a transom stern hull compared with experiments conducted at the *University of Southampton* for a mono-hull (Molland et al., 1994).

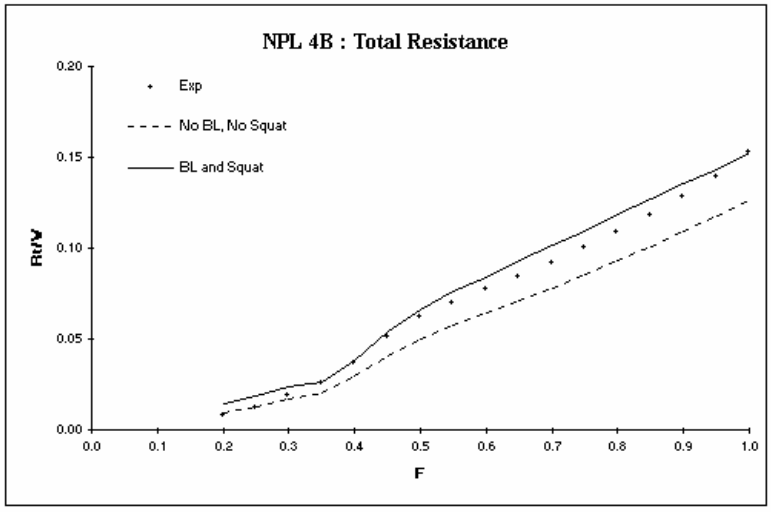

Figure 5.1: Michlet Version 6.05 validation example (Lazuaskas, 2000)

Clearly figure 5.1 show that the boundary layer plus squat model improves the agreement with experimental results. Michlet Version 6.05 finite hollow method with a critical transom-depth based Froude number differs for each LCG to account for transom stern effects. This was however, only estimated by observation of the experimental results. Note that no additional form factors were used in these predictions.

The main assumptions that are made in Michell's integral are:

- The body is thin, therefore the beam-to-length ratio is small
- The boundary conditions on both the free surface and the body can be linearised
- The fluid is inviscid

Since these assumptions are obvious simplifications, it is hardly surprising that Michell's integral does not always give acceptable estimates of the true wave resistance.

The range of applicability of Michlet Version 6.05 is given in table 5.1.

MICHLET Version 6.05: Range of Applicability	
Speed range (m/s)	0 - 40
Max. number of hulls	5
Max. Water depth (m)	10 000
Min. trim angle (degrees)	-10
Max. trim angle (degrees)	10
Max. sinkage	hull fully submerged
Min. sinkage	hull fully lifted above WL

Table 5.1: Michlet Version 6.05 range of application

5.2 Autowing Version 3.0

Autowing Version 3.0 is a powerful and efficient software package for doing hydrodynamic design of hydrofoils. The numeric tool is directed at solving the technical problems regarding the design of wing configuration of hydrofoils, design of wing configurations consisting of

hydrofoils and planing surfaces and design of a hydrofoil for a given pressure distribution (only in Autofoil extension). The two main factors concerning this project while using Autowing Version 3.0 is the lift-to-drag ratio and any signs of cavitation on the foil configuration. Autowing Version 3.0 two-dimensional and three-dimensional graphics quickly lend an intuitive understanding of hydrodynamic processes through visualization of results and input data

The three different methods that Autowing Version 3.0 uses to calculate the hydrodynamics of a hydrofoil are:

- Potential flow
- Large Froude numbers
- Viscid-inviscid interactions

Each of these methods is associated with certain assumptions, the accuracy required, essential results and also the computational time involved. Figure 5.2 illustrate the type of application for each method.

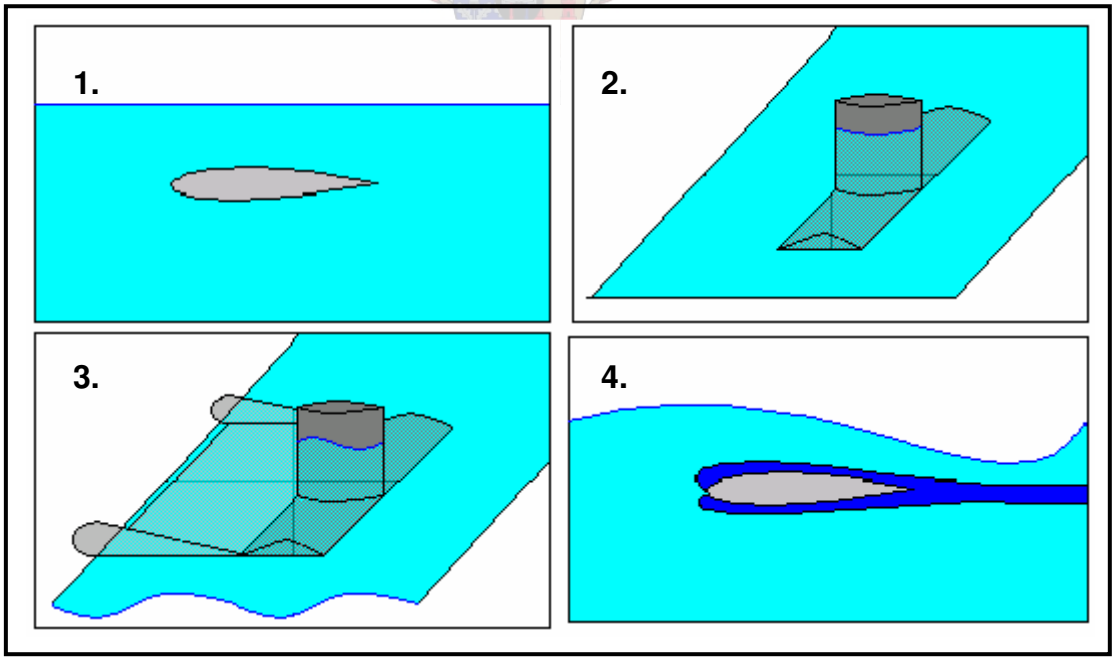

Figure 5.2: Application of each method: 1. large Froude number; 2. large Froude number; 3. potential flow; 4. viscid-inviscid interaction (Autowing, 2005)

The *Large Froude number* method provides the hydrodynamic calculation of the hydrofoil at large Froude numbers (Fn > 4.5). However, this method does not calculate the deformation of the free surface as the assumption that the free surface deformation at large Froude numbers, does not affect lift and drag.

The *Potential flow* or inviscid method calculates the hydrodynamic aspects of the hydrofoil as well as the free surface wave deformation and the vortex wake behind the foil. The viscous drag (both the pressure drag and the friction drag) is calculated using recommendations from a research paper (Kirkman and Kloetzli, 1980). This method offers the best compromise between computational time, numerical complexity and accuracy.

The *Viscid-inviscid interaction* method calculates the "exact" solution that takes into account the predominant viscous region inside the boundary layer. This method uses an iterative procedure that can lead to unfavorable computational time.

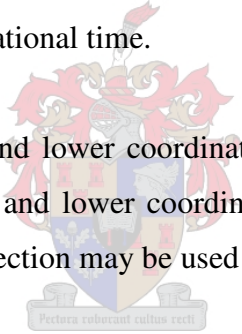

The foil profile consists of upper and lower coordinates. The number of points determines the accuracy of the section. The upper and lower coordinates cannot contain more than a hundred points each. More than one profile section may be used in the configuration of the hydrofoil.

The configuration of the hydrofoil includes the foil and the struts that are positioned accordingly. The foils use the profile section mentioned earlier and the span length is supplied by means of coordinates for the leading and trailing edges of the root and tip of the foil. The number of panels necessary for convergence for the lift and drag differs for deeply submerged foils and for foils close to the free surface. An investigation proved that the number of panels should be 50 and 30 in the chordwise and span direction respectively (Migeotte, 2001).

The wave parameters necessary for the free surface, especially the panel density, not only affect the shape of the free surface, but also the forces generated by the foils. The size of the wave panel on the free surface computational domain should be less than or equal to half of the hydrofoil's averaged aerodynamic chords (AAC). The span of the wave panel system (along the Z-axis) should not be less than two-and-a-half times the maximum positive Z-coordinate of the foil

configuration. Usually, the maximum positive Z-coordinate of the wing configuration is equal to its semi-span. The length of the wave panel system (along the X-axis) should be more than or equal to distance between leading and trailing edge of the tandem hydrofoil system plus five AAC.

The applicable range that Autowing Version 3.0 can be used for depends on the accuracy required and is limited by the number of panels on the lifting surfaces and on the free wave surface. No limit for the speed range has so far been encountered. Autowing Version 3.0 is, however, sensitive towards tandem foil configurations with surface piercing struts. The simplification of excluding the struts results in poorer accuracy regarding the drag and lift forces, but nonetheless reasonable results is still obtained. Only from experimental results can the amount of rise (or sinkage) and trim be determined considering the angles-of-attack for the front and rear foils before conducting Autowing Version 3.0 calculations. The foils of the tandem foil configuration cannot be considered individually due to the rear foil that is operating in the downwash created by the front foil. However, Autowing Version 3.0 is still used to determine the foils hydrodynamics separately not only to compare with theoretical results of chapter 2.2, but also to determine the reliability of both Autowing Version 3.0 and theoretical results.

Autowing Version 3.0 serves as a preliminary design tool not only to solve problems faster, cheaper and with less effort than conducting experiments, but also to estimate reliability and accuracy of experimental results. Autowing Version 3.0 is used by CAE-Marine as an active design tool and therefore can be considered as a feasible design tool for this project.

In this project the *Large Froude number* method was used to determine the lift, drag and cavitation of the foil-system. The method proved to be reasonably accurate considering the sizable amount of time to complete a calculation.

Chapter 6 Results

In this chapter, the experimental results for the resistance, trim and rise/sinkage are given for a trimaran with different outrigger positions, as well as for a trimaran with (figure 6.10 to figure 6.15) and without foils (figure 6.1 to figure 6.9). The different outrigger positions tested are: furthest outrigger position (FOP), middle outrigger position (MOP) and closest outrigger position (COP). The clearance distances from the centerline of the outrigger to the centerline of the main-hull for the three different outrigger positions are shown in figure 4.3.

The results obtained by Migeotte (2001) for a catamaran with a similar displacement and a LCG of 36 %, are compared to the trimaran results evaluated in this project. The theoretical and numerical results of the trimaran are shown in appendix A. Theoretical predicted values are only given for the COP position due to the inadequate interference factor capabilities as determined by Dubrovsky (2004). These theoretically predicted values are given for each LCG position, and they are illustrated with the vessel speed in knots. No results were obtained for the 34 % LCG position with foils due to an instability that occurred at high speeds. The reason for this instability is also discussed in this chapter.

The error involved with the results determined in this project can vary between 5 % and 10 % (Migeotte, 2005). This is mainly due to the scaling procedure implemented as well as the small error involved in the experimental measurement method. The same scaling procedure was used for the results determined for the hydrofoil-assisted catamaran and those determined for the hydrofoil-assisted trimaran, thereby allowing for a meaningful comparison.

The results are given in an orderly fashion. The resistance, trim and rise/sinkage of a trimaran without foils and different outrigger positions give a clear indication of the vessels behavior at a certain speed. The results regarding the addition of foils for a trimaran and catamaran start at figure 6.10. A numerical comparison indicates the amount of resistance due to the foil system and the vessel. The amount of lift the foil system produces at a certain speed is indicated in figure 6.19.

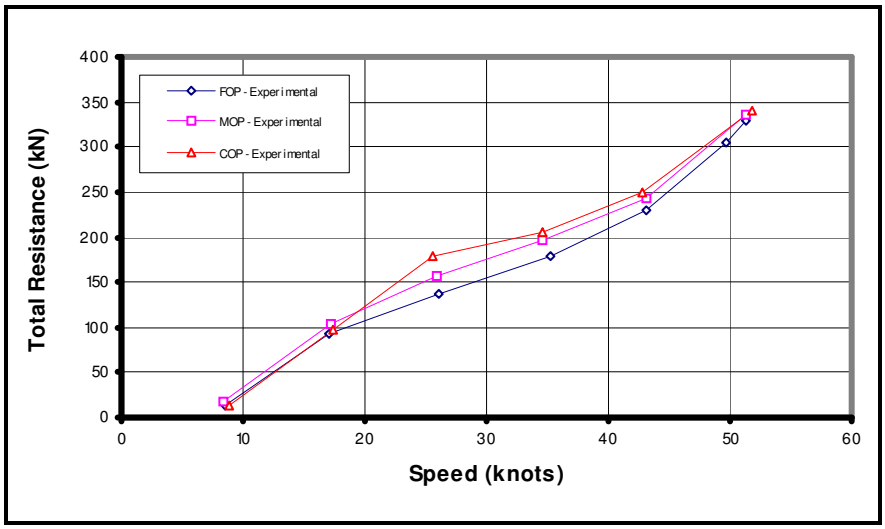

Figure 6.1: Total resistance versus speed for 34 % LCG of different outrigger positions

Figure 6.1 illustrates that there is a visible difference in resistance at the "hump" region, but not a significant difference at high speeds for different outrigger positions. The FOP does however, have the least amount of resistance at a LGG of 34 %. Figure 6.2 show that the "hump" region has a significant effect on the trim, especially at the COP. The "hump" region occurs between 20 knots and 30 knots.

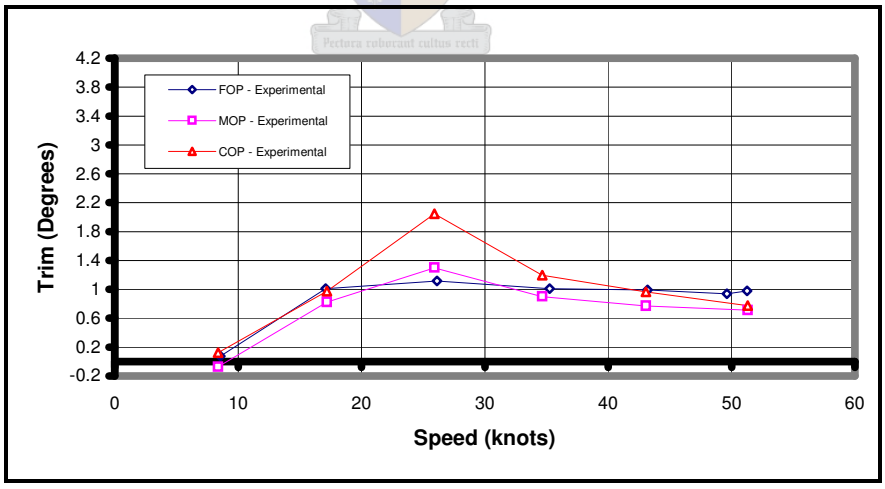

Figure 6.2: Trim versus speed for 34 % LCG of different outrigger positions

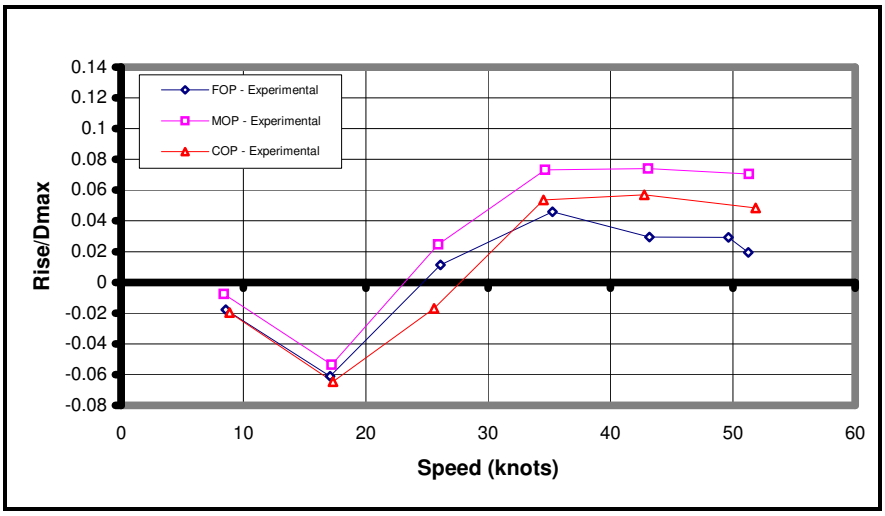

Figure 6.3: Rise-draft ratio versus speed for 34 % LCG of different outrigger positions

Planing occurs above 35 knots as shown in figure 6.3 and a difference in the amount of rise at high speeds is clearly visible for the different outrigger positions.

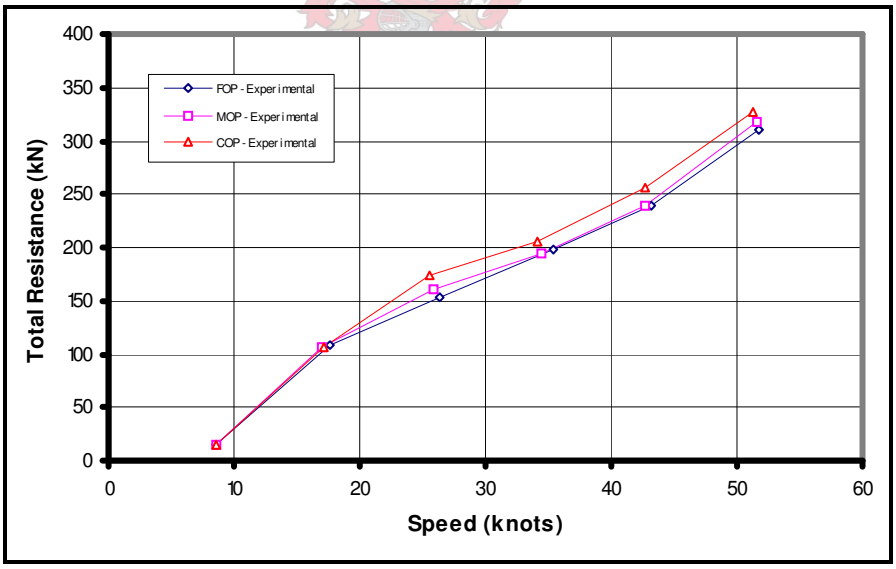

Figure 6.4: Total resistance versus speed for 32 % LCG of different outrigger positions

Figure 6.4 shows that the difference in resistance at the “hump” region for 30 % LCG are less than for the 34 % LCG. The resistance for the different outrigger positions also tends to differ at high speeds.

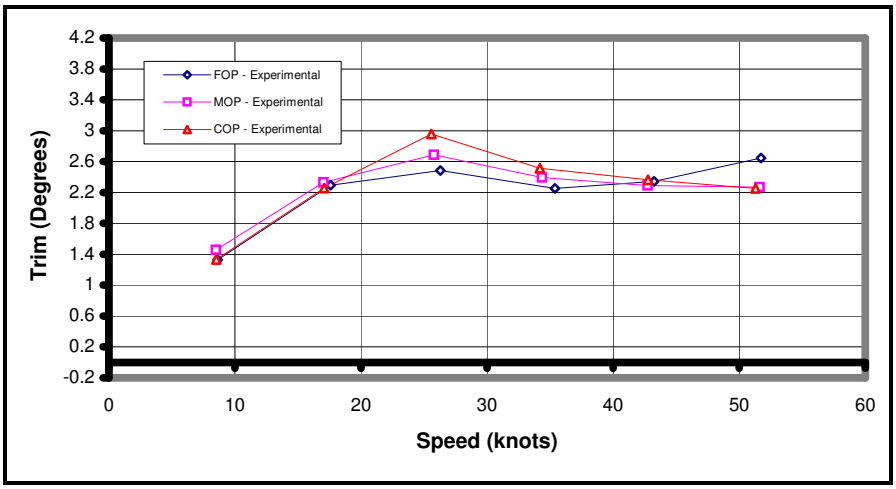

Figure 6.5: Trim versus speed for 32 % LCG of different outrigger positions

Figure 6.5 shows that the "hump" region significantly affects the trim at the COP, but has less effect when it is compared to the 34 % LCG as in figure 6.2. The trim is higher due to the LCG position that has shifted aft.

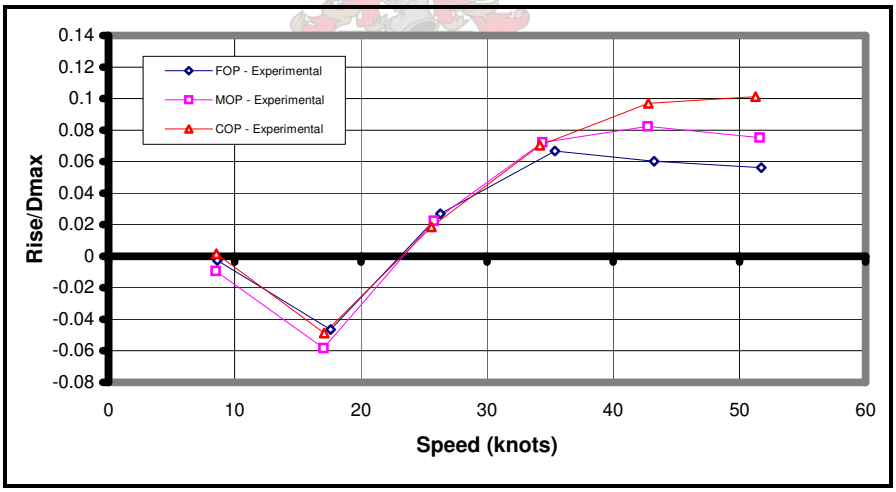

Figure 6.6: Rise-draft ratio versus speed for 32 % LCG of different outrigger positions

The vessel is lifted higher with the 32 % LCG as shown in figure 6.6, but there is still a significant amount of rise difference between the different outrigger positions above 35 knots. This illustrates the amount of lift at which the vessel is planing for each outrigger position. Note that the COP shows the highest rise indicating a strong interaction between outriggers and main-hull that results in more lift being generated.

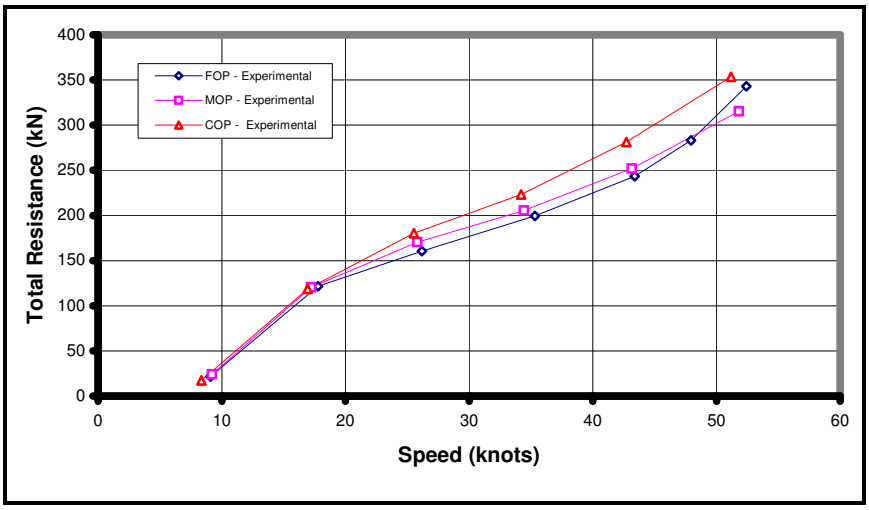

Figure 6.7: Total resistance versus speed for 30 % LCG of different outrigger positions

Figure 6.7 shows that the difference in resistance at the "hump" region is less when compared to both the 32 % LCG and 34 % LCG. The resistance for the different outrigger position also tends to differ more at high speeds than the previously mentioned LCG. The 34 % LCG has the least amount of resistance overall for each outrigger position. A reason for this is that the transom for the other LCG positions is submerged deeper and creates a larger wave system behind the transom. This results in the addition of energy that causes the higher resistance.

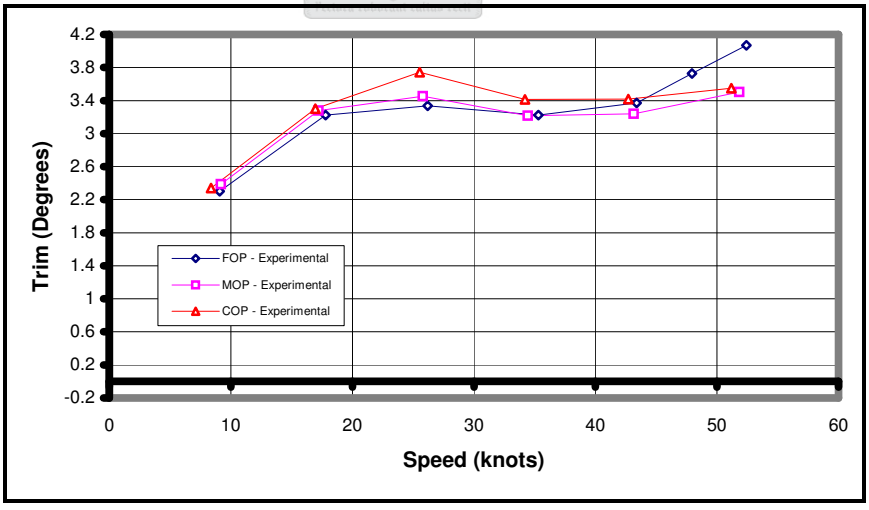

Figure 6.8: Trim versus speed for 30 % LCG of different outrigger positions

The trim is again affected less by the "hump" region according to figure 6.8, although the trend of the trim to increase for the FOP at high speeds is clearly visible.

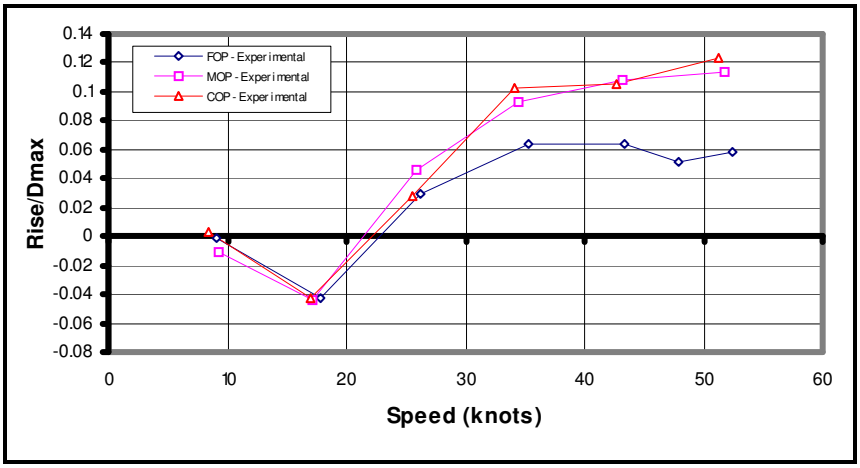

Figure 6.9: Rise-draft ratio versus speed for 30 % LCG of different outrigger positions

Figure 6.9 shows a slightly different tendency to the results of other LCG positions. The figure shows that the rise of MOP is relatively high. This indicates that there is a strong and highly non-linear interaction between the outriggers and the main-hull that is a function of outrigger clearance, speed and LCG.

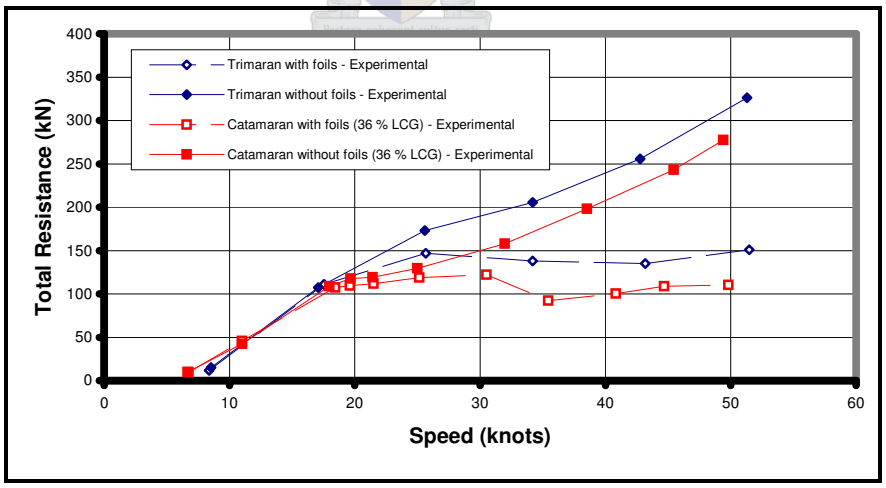

Figure 6.10: Total resistance versus speed for 32 % LCG with foils compared to the catamaran

Figure 6.10 clearly illustrates the reduction in resistance due to the addition of foils for both trimaran and catamaran. The reduction in resistance for the trimaran and catamaran is

approximately 55 % and 60 % respectively at design speed of 50 knots. The resistance of the catamaran without foils is lower compared to the trimaran without foils; this is mainly due to the lower wetted surface area of the catamaran and a slightly more efficient hydrofoil-system on the catamaran. The "hump" region also occurs at a lower speed for the catamaran.

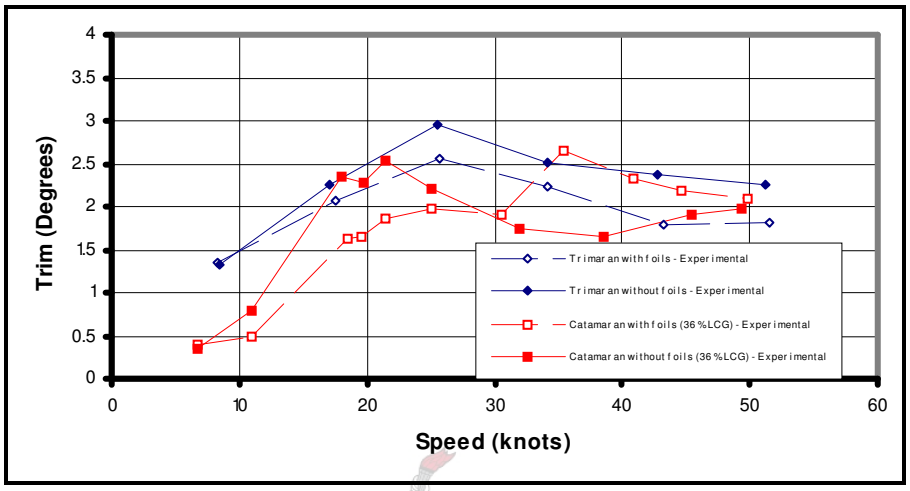

Figure 6.11: Trim versus speed for 32 % LCG with foils compared to the catamaran

Figure 6.11 illustrates that the hydrofoil-assisted trimaran has a gradual transition to planing compared to the hydrofoil-assisted catamaran. The hydrofoil-assisted catamaran has a steep transition from 30 knots to 35 knots and this results in the abrupt transition to planing.

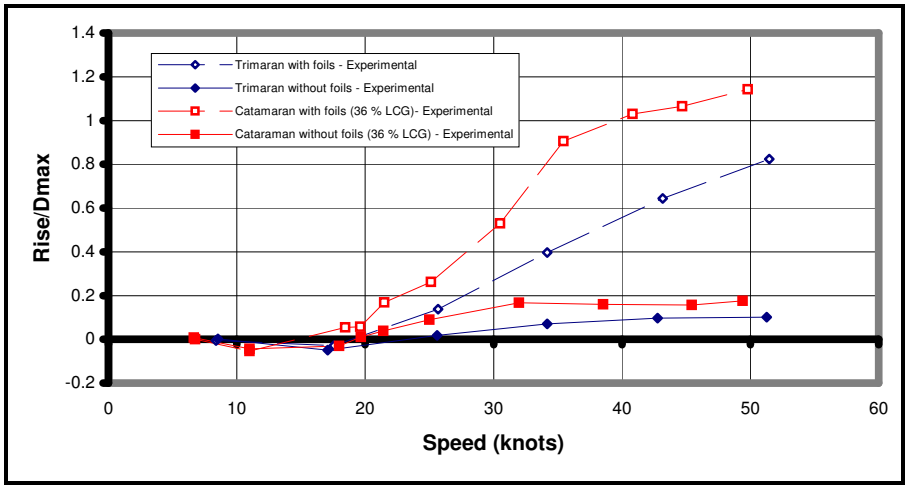

Figure 6.12: Rise-draft ratio versus speed for 32 % LCG with foils compared to the catamaran

The lift of the trimaran is less than that of the catamaran (figure 6.12). This is due to the lower trim values of the trimaran (figure 6.11) as well as to the different LCG positions.

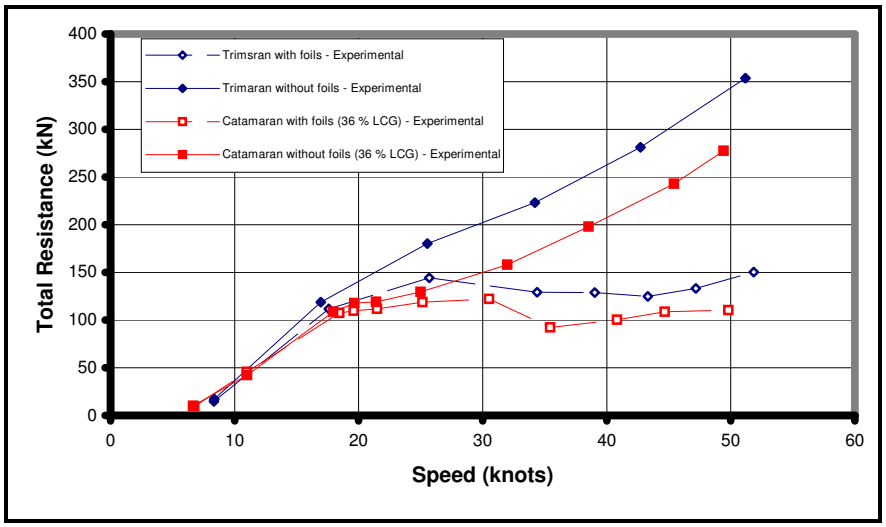

Figure 6.13: Total resistance versus speed for 30 % LCG with foils compared to the catamaran

According to figure 6.13 the reduction in resistance of the trimaran is approximately 57 % at the design speed of 50 knots. This improved the reduction compared to the 32 % LCG. 30 % LCG is therefore the optimum for this type of foil configuration.

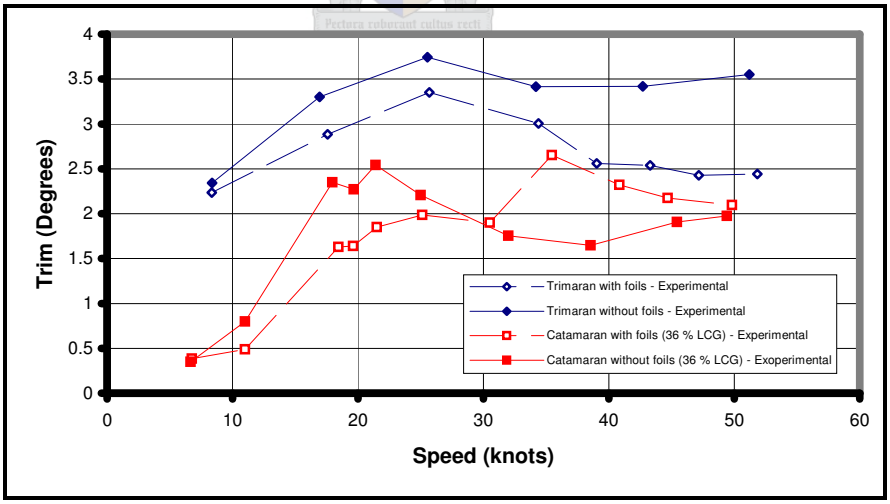

Figure 6.14: Trim versus speed for 30 % LCG with foils compared to the catamaran

The addition of the foils results in the visible difference in trim of the trimaran and catamaran as shown in figure 6.14. The strong rear foil created a significant amount of lift, and this is

responsible for the difference between a hydrofoil-assisted trimaran and a trimaran at high speeds. Again the steep transition to planing can be noticed for a hydrofoil-assisted catamaran. The lift of the trimaran is less than the catamaran as shown in figure 6.15. This is due to the trim values of the trimaran (figure 6.14) as well as the different LCG positions.

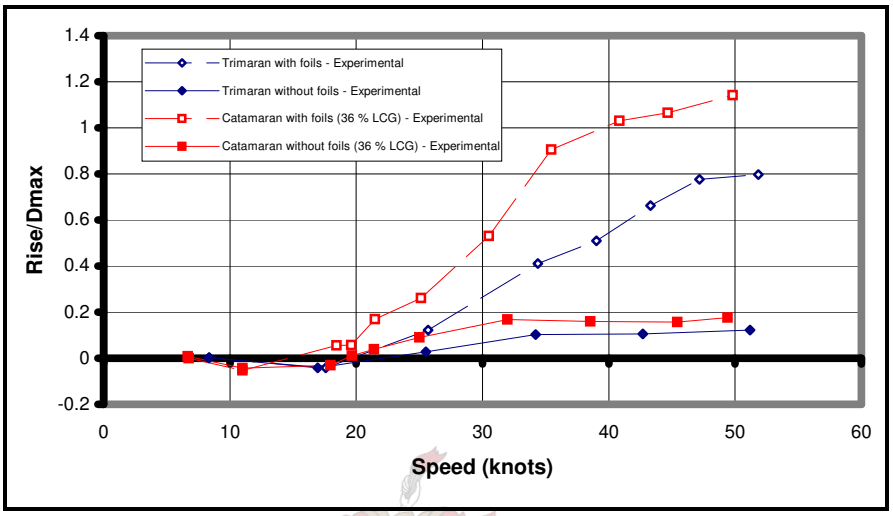

Figure 6.15: Rise-draft ratio versus speed for 30 % LCG with foils compared to the catamaran

The following figure illustrates the breakdown of the resistance component of the trimaran with foils and that of the foil-system. The summation of both these resistance components gives the total numerical resistance prediction for the hydrofoil-assisted trimaran. The experimental values are also shown in figure 6.16 and figure 6.17.

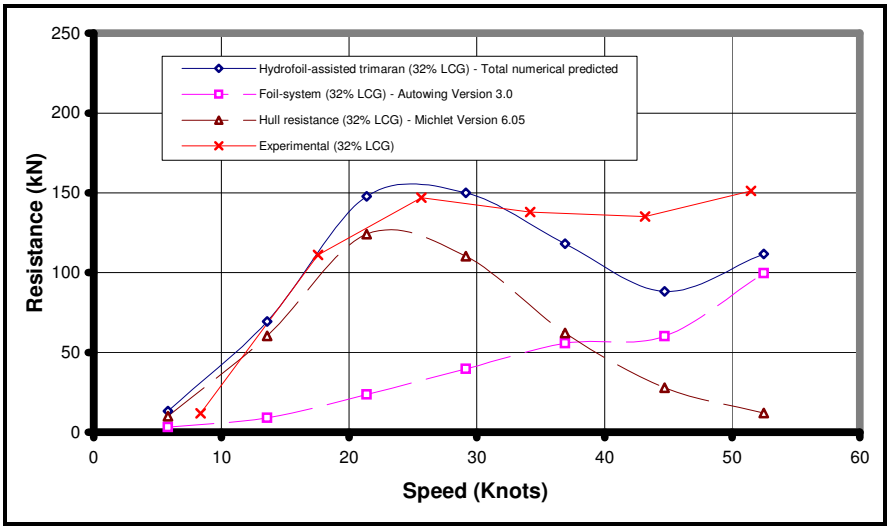

Figure 6.16: Resistance breakdown for 32 % LCG position

The total numerically predicted values correspond reasonably well with the experimental values at the "hump" region in figure 6.16 and figure 6.17. At high speeds effects like spray and interference cannot be accounted for in the numerical prediction. The numerical prediction regarding the foil resistance does not take into account the free surface deformation caused by the foils and the vortices shedding off the foils. These additional resistance components would effectively increase the drag at high-speeds. At 40 knots, approximately 60 % of the resistance is due to the drag of the foils. The numerical predicted values of the hydrofoil-system consider the whole hydrofoil-system when calculating. This means that the rear foils operate in the downwash the front creates.

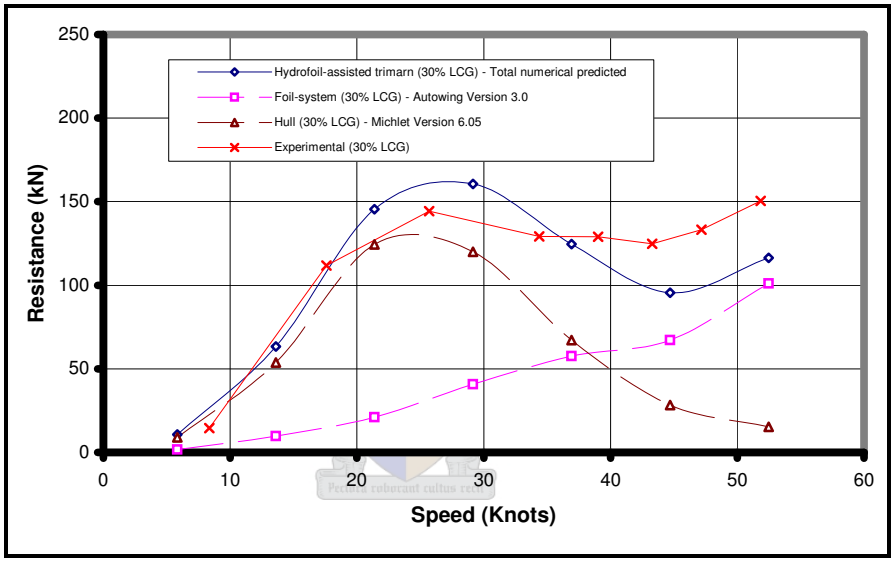

Figure 6.17: Resistance breakdown for 30 % LCG position

Figure 6.18 illustrates the significant amount of spray occurring at the rear foils that is responsible for the resistance difference at high speeds. There is no simple theory to account for this additional component. A future refinement of this foil system should address this problem.

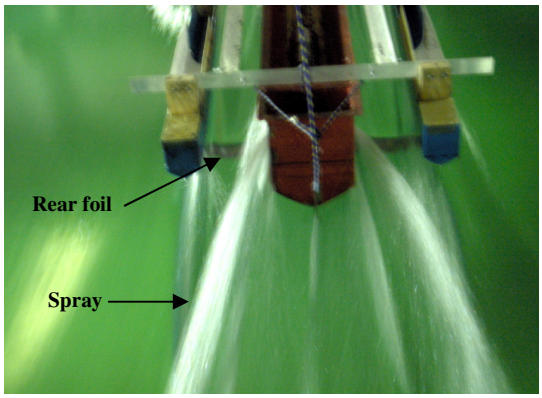

Figure 6.18: A significant amount of spray occurring at the rear foils

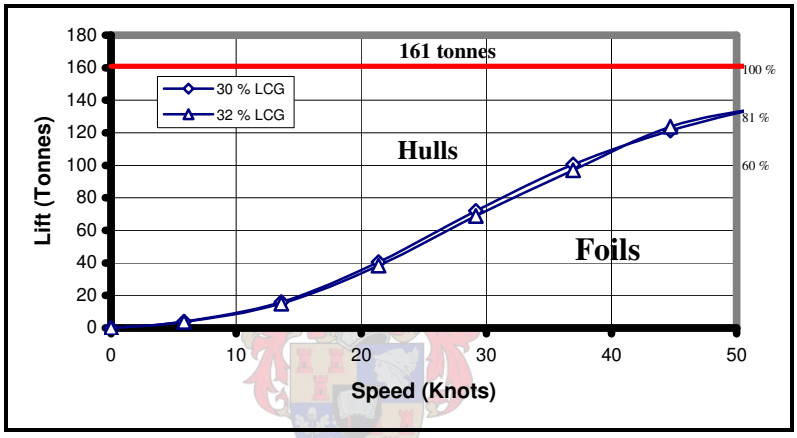

Figure 6.19: The load the foil-system and hulls are carrying at a certain speed

Figure 6.19 illustrates the load that the foil-system and the hulls are carrying as the speed is increased. At 40 knots and 50 knots the foil-system carries approximately 69 % and 81 % of the vessels displacement load respectively.

The center of pressure of the foil system was determined using Autowing Version 3.0 and is shown in figure 6.20. The distance for each of the three different LCG positions is also shown in figure 6.20. According to Hoppe (1992), the center of pressure of the HYSUCAT (that consists of a single main-foil and two stabilizers near the midship and the stern respectively) should be ahead of the LCG position of the hydrofoil-assisted vessel for the vessel to be stable. If this is not the case, an instability will occur that will limit the vessel of getting into the planing mode and course instabilities will occur.

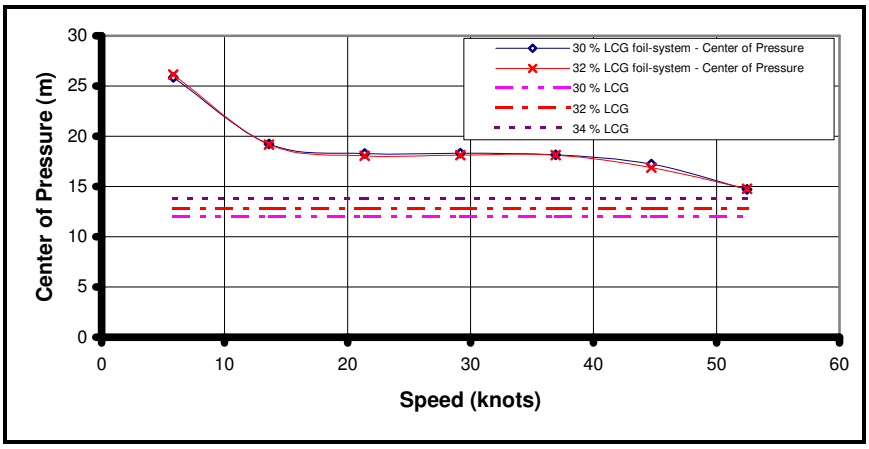

Figure 6.20: Center of pressure of the foil-system calculated in Autowing Version 3.0

Figure 6.20 clearly shows that the center of pressure is in close proximity to the 34 % LCG. This was confirmed in model tests as no results could be determined for the 34 % LCG position due to the vessel that became unstable.

Figure 6.21 clearly illustrates the visible difference of the trimaran model with and without the hydrofoil-system. It is also clearly visible that the bows of the main-hull and the outriggers are completely lifted above the water surface.

Figure 6.21: Trimaran model without and with foils shown left and right respectively

The theoretical results show the visible onset of cavitation in figure 6.22 and cavitation beginning at a speed of 37 knots. The white patches on the foils illustrate the cavitation. There is a significant amount of cavitation occurring across the whole span of the rear foil at 52 knots

according to the calculations done in Autowing Version 3.0. No cavitation is occurring on the front foil. As a further refinement of the rear foil the thickness-to-chord ratio should be decreased to avoid cavitation occurring at high speeds.

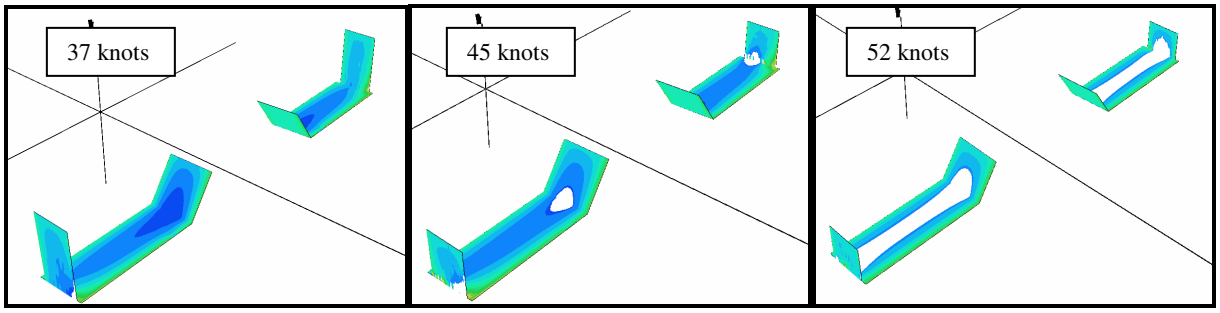

Figure 6.22: Onset of cavitation

The following sequence of photographs (figure 6.23) shows the lifting capability of the model hydrofoil-system at certain speeds. The top, middle and bottom photographs respectively illustrate the three operating regimes as discussed in chapter 2.

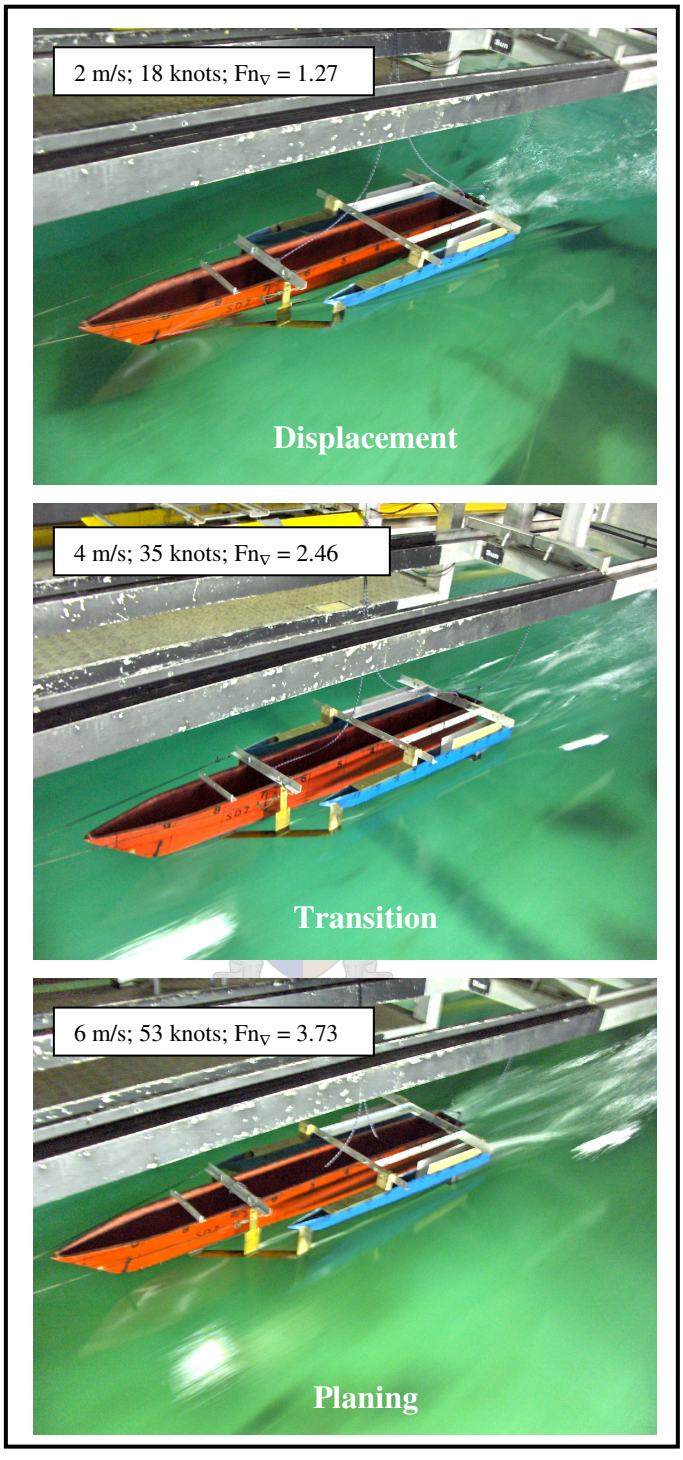

Figure 6.23: Sequence of photographs of model at certain speeds

Chapter 7 Conclusion

A suitable trimaran design and hydrofoil system was developed and manufactured to allow for sufficient experimental towing tank testing. The configuration of the outriggers (which includes the 6 % outrigger displacement and the clearance distance selected) proved to be adequate for this project, but should be improved to enhance the performance of a hydrofoil-assisted trimaran. Observations suggest, while conducting experimental tests, that the draft of the outriggers should be increased to ensure that the outriggers stay in contact with the free surface. An increased outrigger draft would result in the vessel remaining more stable in roll.

The results presented for the three different outrigger clearances of the trimaran indicate that the FOP has the least amount of total resistance, together with the 34 % LCG position. This confirms that the interference effect between the hulls is a minimum for the FOP. The numerically and theoretical predicted values are presented in Appendix A. The numerically predicted values correspond reasonably well with the experimental values in the 32 % LCG case as shown in Figure A.2. The theoretical method of Dubrovsky (2004) does not compare well with both the numerical and experimental values and cannot be used as a design tool due to the limitations of this method.

A feasible scaling procedure for the trimaran model has been developed according to the method of Froude. The scaling procedure takes into account the different sized hulls of the trimaran and is supplied in Appendix C.

The main objective of the project was to determine if the addition of foils could successfully decrease the resistance of a trimaran by at least 40 % at a design speed of 50 knots. This was accomplished successfully where a reduction of 57 % in resistance was determined. The hydrofoil system of the trimaran can be improved to achieve better resistance results. The angle-of-attack of the front and rear foil was not sufficiently optimised. Results were obtained for the 32 % LCG and the 30 % LCG. The instability that occurred at the 34 % LCG was substantiated by numerical investigation, when the center of pressure and LCG are in close proximity of each

other as explained in chapter 6. The instability that occurred at the 34 % LCG position is regarded as a better result, especially for future related work. Therefore, the angle-of-attack was not sufficiently optimised to ensure a stable vessel throughout the different LCG positions.

The catamaran with a similar displacement proves to be superior compared to the trimaran with and without foils. Further refinement of the trimaran concept is still needed. The difference in total resistance between the trimaran and the catamaran with and without foils can clearly be seen in figure 6.10 and figure 6.13. The catamaran outperforms the trimaran in both cases. Some reasons for this might be that the hydrofoil system of the catamaran is matured and well developed. Another reason could be that due to the new concept of hydrofoil-assisted trimaran, the configuration of the hydrofoil is not completely sufficient for the trimaran configuration. This would result in the significant amount of spray that occurred at high-speeds and resulted in increased resistance of the rear foil shown in figure 6.18. The final reason is that the main-hull of the trimaran for this project has a length displacement ratio of 7.36 and the demi-hull of the catamaran is 9.27, although research has shown that the length displacement ratio of the main-hull of a trimaran can be as high as 18.2 (Mizine and Amromin, 1999). The deeper draft of the main-hull of the trimaran, when compared to the catamaran, does however result in a larger wave-resistance occurring at the bow at low speeds, and a higher transom resistance at high-speeds.

The lifting capability of the hydrofoil system increases with increased speed, as would be expected. The hydrofoil system carries 81 % of the total displacement of the hydrofoil-assisted trimaran.

The hydrofoil-assisted catamaran is more stable than the trimaran. This is due to the counter balancing moment the hulls of the catamaran configuration create. The trimaran cannot create this moment when the outriggers are lifted above the water surface in roll. The foils of the trimaran cannot also stabilise the vessel, as they are still too deeply submerged. Only foils in close surface effect could stabilise the craft. Outriggers that run clear of the water surface at high-speeds results in the trimaran behaving like a hydrofoil-assisted mono-hull.

Recommendations that can be made for future work are the optimisation of the hydrofoil system of the trimaran to eliminate the occurring instability as mentioned in the previous chapter. This could be done by shifting the center of pressure of the hydrofoil-system further forward and increasing the slenderness ratio of the main-hull. Also refining the foil design to improve its efficiency and eliminate the excessive spray generated by the rear foil should be considered.

References

Abbott I.R. and Von Doenhoff A.E. (1958), Theory of Wing Sections: Including a Summary of Airfoil Data, Dover Publications, New York, p. 72

Armstrong N.A. (2004), Coming soon to a port near you: The 126m trimaran, *RINA Conference Proceedings*, CD, London

Armstrong T. and Holden K. (2003), A new generation of large fast ferry – From concept to contract reality, *FAST 2003 Conference Proceedings*, Ischia, Italia, Keynote Lecture, p. 75 to p. 84

Austal (2005), http://www.austal.com/product-range/ferries-vehicle-passenger.cfm, 24 June 2005

Autowing (2005), Hydrodynamic and Aerodynamic Problems solving with the Autowing version 3.0 (licensed to G. Migeotte), Autowing version 3.0, 22 July

Bertram V. (2000), Practical Ship Hydrodynamics, Butterworth Heinemann, Oxford

Bricknell D. and Carlisle C. (2004), Power and propulsion systems for the new naval trimarans, *RINA Conference Proceedings*, CD, London

Calkins D.E. (1981), HYCAT: Hybrid hydrofoil catamaran, *AIAA 6th Marine Systems Conference*, September, Washington, Seattle

Daskovsky M. (2000), The hydrofoil in surface proximity - theory and experiment, *Ocean Engineering 27*, p. 1129 to p. 1159

Degiuli N., Werner A. and Zotti I. (2005), An experimental investigation into the resistance components of trimaran configurations, *FAST 2005 Conference Proceedings*, St. Petersburg, Russia

Doctors L.J. and Scrace R.J. (2003), The optimisation of trimaran sidehull position for minimum resistance, *FAST 2003 Conference Proceedings*, Ischia, Italy, Keynote Lecture, p.1 to p.12

Dolphin Ulsan (2005), http://www.nwbs.com.au/tri/html, 24 June 2005

Du Cane P. (1973), High Speed Small Craft, David and Charles: Newton and Abbot, London

Dubrovsky V. and Lyakhovitsky A. (2001), Multi-Hull Ships, Backbone Publishing Company, Fair Lawn, USA

Dubrovsky V. (2004), Ships with Outriggers, Backbone Publishing Company, Fair Lawn, USA

e-motion (2005a), http://www.yachts.nwbs.com.au/, 24 June 2005

e-motion (2005b), http://www.yachts.nwbs.com.au/expansive.htm, 24 June 2005

e-motion (2005c), http://www.yachts.nwbs.com.au/efficiency.htm, 24 June 2005

Fast (2005), Fast Ferry International, May 2005

Hoerner S. (1965), Fluid Dynamic Drag, 2nd Edition, Published by the author, New Jersey, p. 8 to p. 10

Hoppe K.G. (1980), The hydrofoil supported catamaran, *Progress Research Report 1980-2*, Mechanical Engineering Department, University of Stellenbosch, South Africa

Hoppe K.G. (1989), The HYSUCAT development, *Research Report*, Mechanical Engineering Department, University of Stellenbosch, South Africa

Hoppe K.G. (1991), The Hysucat developments, *Research Report*, University of Stellenbosch, Stellenbosch, South Africa

Hoppe K.G. (1992), The HYSUCAT development, *The South African Mechanical Engineer*, Volume 42, South Africa, October

Hoppe K.G. (1995), Ship Fluid Dynamics: Additional Notes and Data Collection, Mechanical Engineering Department, University of Stellenbosch, South Africa

Hoppe K.G. (1999), Hydrofoil catamaran developments in South Africa, *HIPER'99 Conference Proceedings*, *1st International Conference on High Performance Marine Vehicles,* Zevenwacht, Cape Town, p. 92 to p. 101

Houghton E.L. and Boswell R.P. (1969), Further Aerodynamics for Engineering Students, Edward Arnold, London, p. 68

Houghton E.L. and Carpenter P.W. (1993), Aerodynamics for Engineering Students, 4th Edition, Arnold, London, p. 43

Insel M. and Molland A.F. (1991), An investigation into the resistance components of high-speed displacement catamarans, *RINA Conference Proceedings*, Transactions of the Royal Institute of Naval Architects

Irens (2005), http://www.nigelirens.demon.co.uk/nid_power2.htm, 24 June 2005

Kirkman K.L. and Kloetzli J.W. (1980), Scaling problems of model appendages, *Proceedings of 19th General Meeting of the American Towing Tank Conference*, Vol. 1, University of Michigan, Ann Arbor, Michigan, p. 129 to p. 154

Korvin-Kroukovsky B.V. and Wernick R.J. (1952), Lift and Drag of Hydrofoils: Application of Theory to Experimental Results, Report No. 438, New Jersey

Lazuaskas (2000), Verifications of predictions, Michlet version 6.05 supplementary document, 23 February

Lewis E.V. (1988), Principles of Naval Architects Second Revision, 3rd Edition, Volume 2, Society of Naval Architects and Marine Engineers, Jersey City, p. 46 to p. 47

Li B-Q (1981), A prediction method of foilborne performance characteristics of hydrofoil craft in calm sea, *Conference on High Speed Surface Craft*, London

Loubser J.B. and Nieder-Heitmann C (1983), Weerstandstoetse op die Hysucat en skaalmodel, MscEng thesis, Mechanical Engineering Department, University of Stellenbosch, South Africa

Lyakhovitsky A.G. (1973), Wave-making resistance of a multi-hull vessel in deep waters, *Transactions XX11, Krylov Conference Proceedings*, St. Petersburg, p. 39 to p. 40

Lyakhovitsky A.G. (1976), Triple-Hull ship, *Invention certificate of USSR No 501921*, Patent Bulletin No 5

Marshall R. (2002), All About Powerboats - Understanding Design and Performance, McGraw Hill, USA

Michell J.H. (1898), The wave resistance of a ship, *Phil. Magazine*, Volume 5, Number 45, London, p. 106 to p. 123

Migali A., Miranda S. and Pensa C. (2001), Experimental study on the efficiency of trimaran configuration for high-speed very large ships, *FAST 2001 Conference Proceedings*, Southampton, UK

Migeotte G. (1997), Development for hydrofoil supported catamarans with semi-displacement hulls, MScEng thesis, Mechanical Engineering Department, University of Stellenbosch, South Africa, December

Migeotte G. and Hoppe K.G. (1999), Developments in hydrofoil assistance for semi-displacement catamarans, *HIPER'99, International Conference Proceedings on High-Performance Marine Vehicles*, Zevenwacht, p. 631 to p. 642

Migeotte G. (2001), Design and optimization of hydrofoil-assisted catamaran, PhD thesis, Mechanical Engineering Department, University of Stellenbosch, South Africa

Migeotte G. (2005), Personal communication, Stellenbosch

Millward A. (1982), Resistance of a fast round bilge hull in shallow water, *AIAA Journal*, Vol. 20, No. 8. p. 1092 to p. 1096

Mizine I. and Amromin E. (1999), Large high-speed trimaran – concept optimization, *FAST '99 Conference proceedings*, Seattle, Washington USA, p. 643 to p. 655

Molland A.F., Wellicome J.F. and Couser P.R. (1994), An improved method for the theoretical prediction of the wave resistance of transom-stern hulls using a slender body approach, *Transactions of the Royal Institute of Naval Architects*, Volume 138a, p. 55 to p. 71

Roy J. and Gee N. (2003), The effects of length on the powering of large slender hull forms, *FAST 2003 Conference Proceedings*, Volume 1, Ischia, Italy, p. 23 to p. 30

Tulk R.J. and Quigley S.G. (2004), Development of the North West Bay Ships trimaran, *RINA 2004 Conference Proceedings*, London, CD

Walree F. (1999), Computational methods for hydrofoil craft in steady and unsteady flow, PhD thesis, Technische Universiteit Delft, Delft, Netherlands, March

Appendix A Additional Results

The differences between the theoretical, experimental and numerical total resistance results are shown in figure A.1 to figure A.3.

The difference in resistance between the experimental and the numerical results are due to the interference effects between the hulls and the extra resistance created due to the vortices created at the corner of a hard chine that cannot be accounted for in the numerical prediction. It is clearly visible that the numerical results under predict the resistance at high-speeds compared to the experimental results, but does however compare reasonably good at speeds below 30 knots. The numerical results of figure A.1 to figure A.3 tends to compare better with the experimental results when the LCG is shifted further aft. The reason for this is still unclear. The theoretical results in all three cases does not compare exceptionally well with the numerical or experimental results. Therefore, as mention in the chapter 7, the theoretical method of Dubrovsky cannot be used as a design tool. The hump resistance is clearly visible at all three LCG positions and occurs generally, according to the results, between 20 knots and 30 knots. The accuracy of these methods is explained in chapter 4 and chapter 5. These results conclude that the numerical and experimental values are reasonably accurate at speeds below 30 knots depending on the position of the LCG, due to the reasonable similar results.

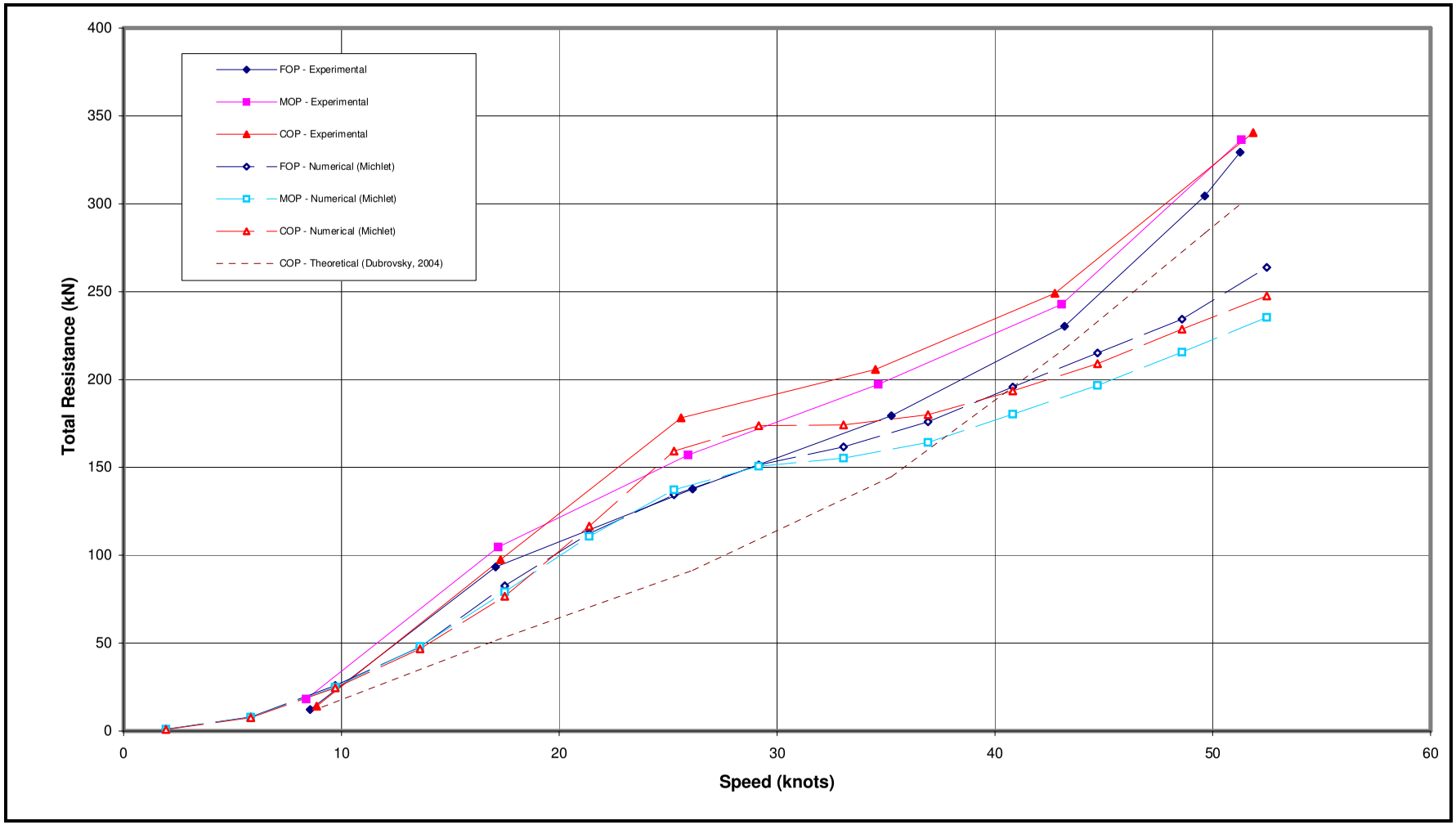

Figure A.1: Difference between theoretical, numerical and experimental for 34 % LCG

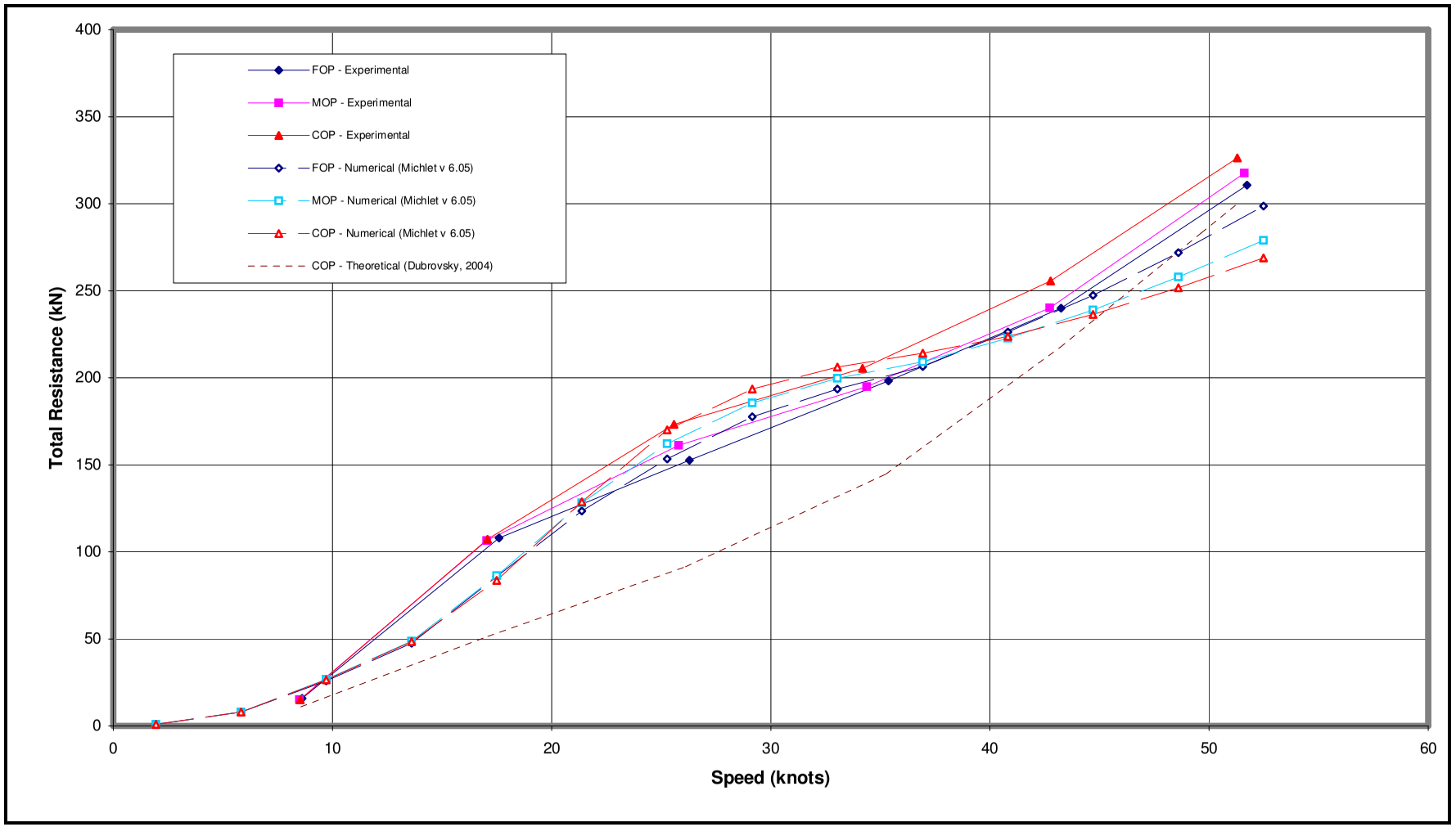

Figure A.2: Difference between theoretical, numerical and experimental for 32 % LCG

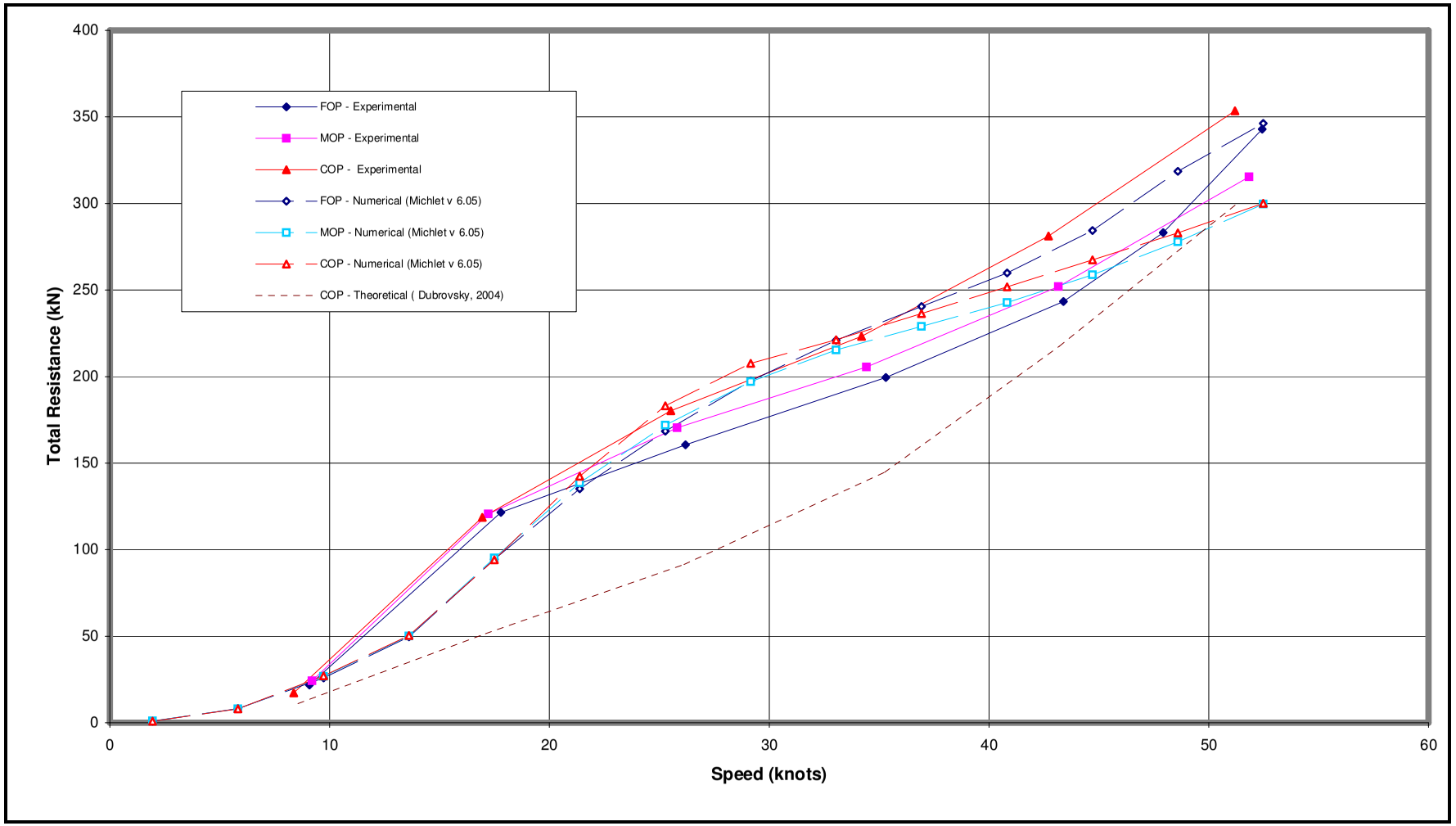

Figure A.3: Difference between theoretical, numerical and experimental for 30 % LCG

The results for the hydrodynamics of a hydrofoil that was discussed in chapter 2.2 are illustrated in the following figures. The front and the rear foil had to be calculated separately due to the nature of the theoretical method that is based on equation 2.4 to equation 2.20. Therefore, the interference and downwash the front foil creates on the rear foil is not taken into account. The following results are mainly to show that the results of the theoretical and numerical methods compare reasonably good. The lift and drag of the front foil without struts are illustrated respectively in figure A.4 and figure A.5. The lift and drag of the rear foil also without struts are illustrated in figure A.6 and figure A.7. The struts are ignored only to simplify the theory, due to the aspect ratio that can only be determined for a strut configuration illustrated in figure 2.19. Unfortunately no reasons can be given for the discrepancy between the theoretical and numerical values. These calculations are there to prove the reliability of both the theoretical method of chapter 2.2 and numerical predictions of Autowing Version 3.0.

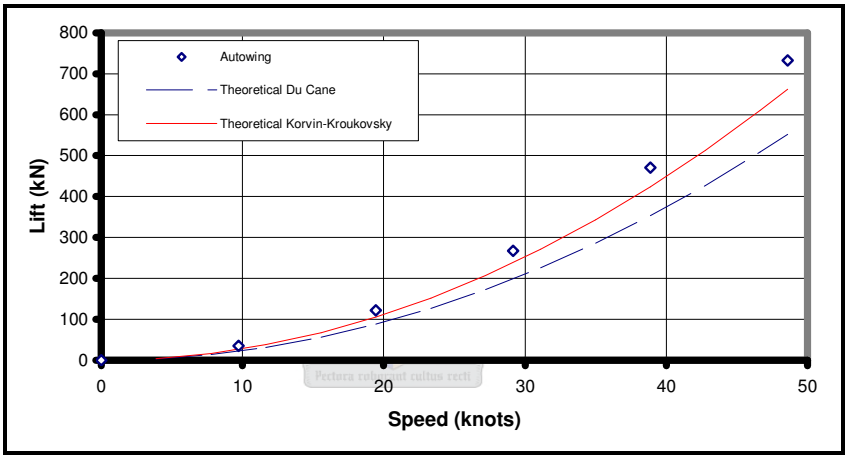

Figure A.4: Front foil lift at 0 degrees angle-of-attack

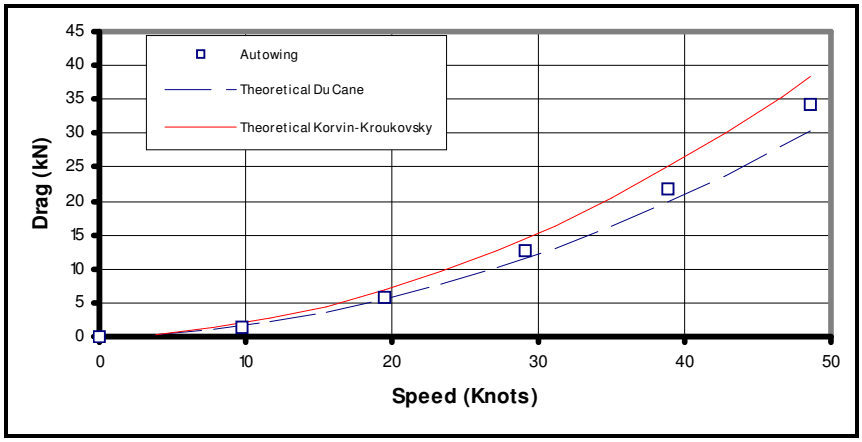

Figure A.5: Front foil drag at 0 degrees angle-of-attack

Two methods are used to determine the planform correction factor as discussed in chapter 2.2.1. Both these two methods namely: Du Cane and Korvin-Kroukovsky are illustrated. It is clearly visible that for the lift the method of Korvin-Kroukovsky compares better with the numerical values determined in Autowing Version 3.0 than the empirical equation developed by Du Cane. Figure A.5 illustrates the drag of the front foil and here can be seen that the method of Korvin-Kroukovsky over-predicts and the method of Du Cane under-predicts compared to the numerical values of Autowing Version 3.0. Figure A.6 and figure A.7 respectively show the results of the lift and the drag that the rear foil generates according to the theoretical methods and the values determined using Autowing Version 3.0.

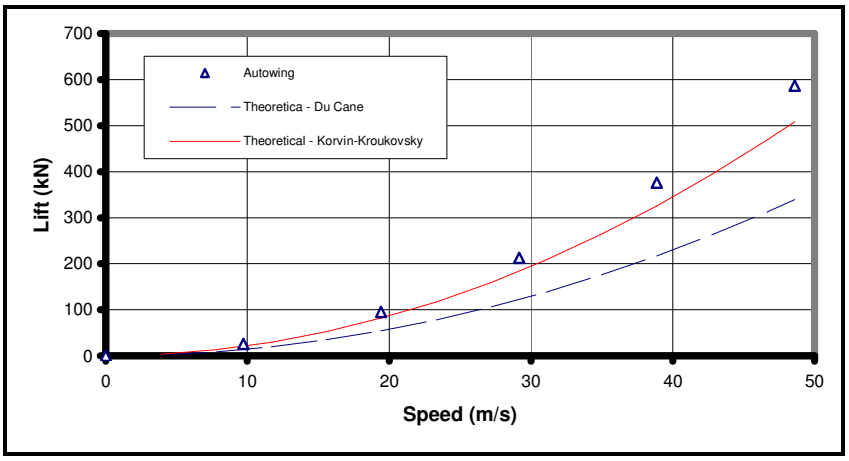

Figure A.6: Rear foil lift at 0 degrees angle-of-attack

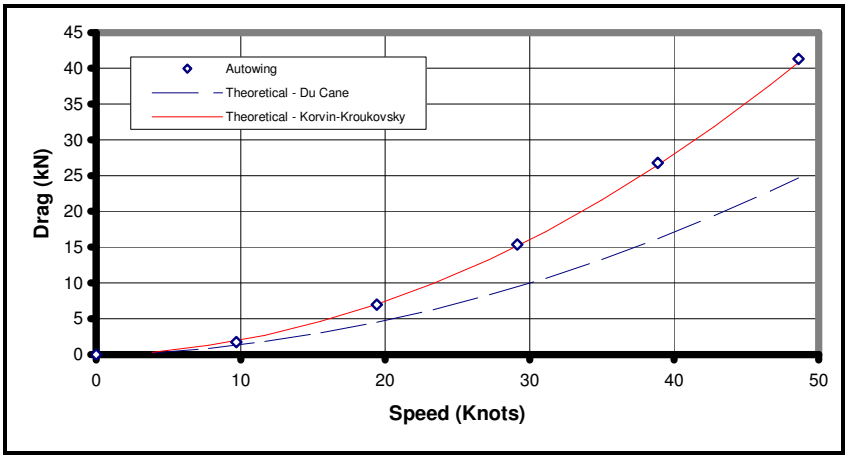

Figure A.7: Rear foil drag at 0 degrees angle-of-attack

Again, the theoretical method of Korvin-Kroukovsky to determine the planform factor compares better to the numerical predicted values than the method of Du Cane.

Appendix B Interference and Planform Factors

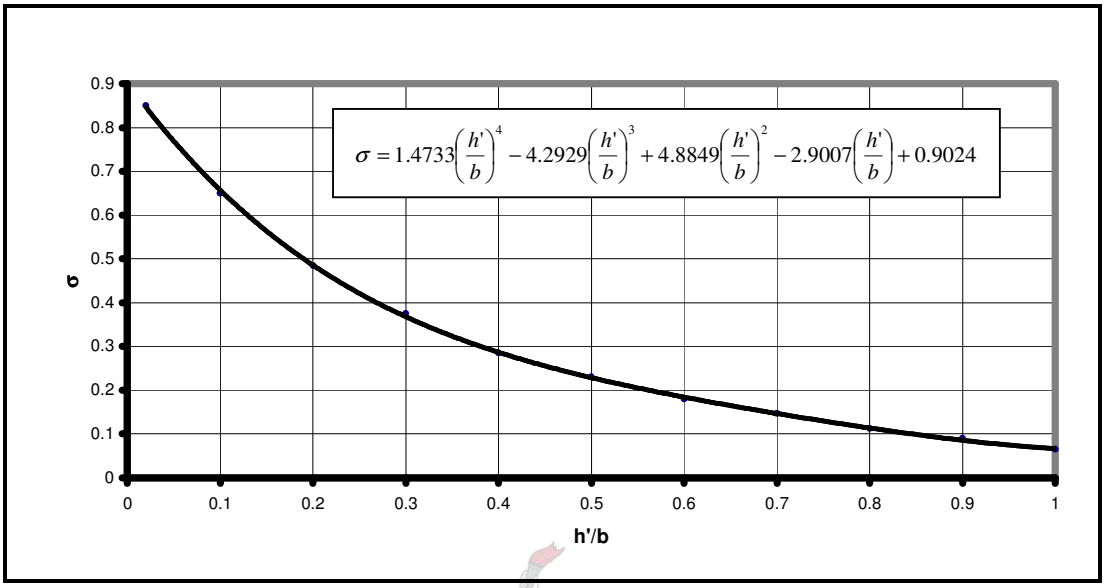

Figure B.1: Munk's interference factor

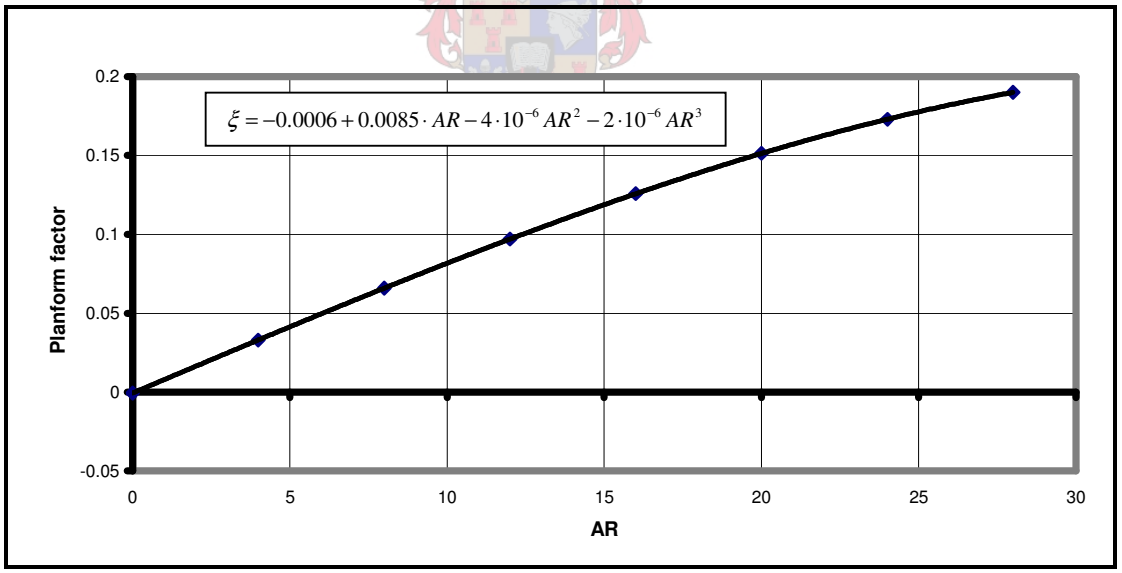

Figure B.2: Planform factor

Appendix C Scaling Procedure

Different scaling procedures are used for a vessel with foils and without foils. The laminar flow and separation of flow that is associated with low Reynolds numbers of the hydrofoil needs to be accounted for to satisfactorily scale hydrofoil resistance. The two different procedures are given below. Appendix E contains some results and values as an example of what the magnitude of the results and values were according to the scaling procedures.

C.1 Scaling Procedure without Foils

Ship resistance can be tested and measured according to Froude's law. Froude's law states that the ship resistance can be divided into frictional and residual resistance, but mainly wave--making resistance, with the wave-making resistance following his 'law of comparison' (Froude similarity) (Bertram, 2000). At present the wave-making resistance term has been modified to account for the interference effect, transom resistance and other related resistance components excluding the frictional resistance. This modified wave-making resistance term is called the residual resistance and is illustrated in equation C.1. Tests are performed keeping Froude similarity, where the Froude number of model and full scale are the same. The scale effect (error of not keeping the Reynolds similarity) is compensated by empirical corrections like the ITTC 1957 correlation line. The results obtained from model testing are the total model resistance, front trim, rear trim and wetted surface area. All of these parameters are measured at a certain speed.

The following equations, according to Froude, illustrate the model main resistance components for a conventional vessel,

$$R_T^* = R_F^* + R_R^* \qquad \text{(C.1)}$$

where R_T^*, R_F^* and R_R^* are respectively the total model resistance, the frictional model resistance and the residual model resistance.

Equation C.1 needs to be modified when considering a trimaran. The calculation of the frictional resistance of a trimaran differs due to the additional outriggers. Equation C.1 becomes,

$$R_T^* = \left(R_{F,MH}^* + 2R_{F,O}^*\right) + R_R^* \tag{C.2}$$

where $R_{F,MH}^*$ and $R_{F,O}^*$ are respectively the frictional resistance of the main hull and an outrigger. The frictional resistance of the model and the prototype can be calculated by the following equation,

$$R_{F,i}^* = C_{F,i}^* \left(\rho^* / 2\right) \left(V^*\right)^2 Sw_i^* \tag{C.3}$$

where V^* and ρ^* are the model speed and towing tank water density respectively. Sw_i^* is the wetted surface area of the main-hull or an outrigger of the model. The ITTC 1957 correlation line is used to calculate the frictional coefficient for both model and prototype by using the following equation that is a function of the Reynolds number only. The frictional resistance coefficient for the main-hull or an outrigger of the model are calculated by the ITTC 1957 formula as follows,

$$C_{F,i}^* = \frac{0.075}{\left(\log_{10} Rn_i^* - 2\right)^2} \tag{C.4}$$

where Rn_i^* is the Reynolds number of the main-hull or an outrigger. According to Bertram (2000), this formula already contains a global form effect increasing the value of C_F by 12 % compared to the value for flat plates.

The Reynolds number is calculated as follows,

$$Rn_i^* = \frac{V^* L_{wl\,i}^*}{\nu^*} \tag{C.5}$$

where $L_{wl\,i}^*$ and ν^* are the waterline length of the model main-hull and the viscosity (due to towing tank conditions) respectively. The same procedure is followed to obtain the frictional resistance for an outrigger of the model.

The total model resistance is measured in the experiment and the frictional resistance is calculated according to the ITTC 1957 correlation line; therefore, the residual model resistance is determined by modifying equation C.2,

$$R_R^* = R_T^* - \left(R_{F,MH}^* + 2R_{F,O}^*\right) \tag{C.6}$$

The residual resistance coefficient can be calculated as follows,

$$C_R^* = \frac{R_R^*}{\left(\frac{\rho^*}{2}\right)\left(V^*\right)^2 Sw_T^*} \tag{C.7}$$

where $Sw_T^* = Sw_{MH}^* + 2Sw_O^*$ and is the total wetted surface area of the model. But Froude's law of comparison states that the residual resistance coefficient for the prototype is the same as the models. Therefore,

$$C_R = C_R^* \tag{C.8}$$

The residual prototype resistance can now be determined by adjusting equation C.7 and converting arbitrary components to prototype values with the following equation,

$$R_R = C_R\left(\rho/2\right)\left(V\right)^2 Sw_T \tag{C.9}$$

where V and ρ are the full-scale speed and the water density the vessel will operate in respectively. Sw_T is the total wetted surface area of the trimaran.

The velocity is scaled according to the volumetric Froude number. The volumetric Froude number is used instead of the length Froude number, due to the number of hulls with different lengths. The following equation determines the volumetric Froude number,

$$Fn^* = \frac{V^*}{\sqrt{g\left(\nabla^*\right)^{1/3}}} \tag{C.10}$$

where ∇^* is the total model displacement. Keeping Froude similarity, $Fn = Fn^*$. Therefore, the speed of the full-scale vessel can be determined,

$$V = Fn\sqrt{g\nabla^{1/3}} \tag{C.11}$$

where ∇ is the total full-scale displacement. The waterline length and the wetted surface area are scaled according to the scaling factor λ. This is shown in equation C.12 and equation C.13 respectively,

$$Lwl_i = \lambda\left(Lwl_i^*\right) \tag{C.12}$$

$$Sw_i = \lambda^2\left(Sw_i^*\right) \tag{C.13}$$

Equation C.12 and equation C.13 can be used for the main-hull or an outrigger.

The frictional resistance for the prototype main-hull and an outrigger can be determined in the same manner as for the frictional resistance of the model. The prototype main-hull or outrigger frictional resistance can be determined using equation C.3 and the frictional resistance coefficient according to the ITTC 1957 correlation line formula.

The total frictional resistance of the prototype can now be calculated by the following equation,

$$R_F = R_{F,MH} + 2R_{F,O} \tag{C.14}$$

Therefore, the prototype total resistance can be determined in the same manner as the models by using equation C.2,

$$R_T = \left(R_{F,MH} + 2R_{F,O}\right) + R_R \tag{C.15}$$

Equation C.15 can be rewritten in terms of the resistance coefficients and the addition of a correlation coefficient will result in the following equation,

$$R_T = \left(\rho/2\right) V^2 \left[c_{F,MH} Sw_{MH} + 2c_{F,O} Sw_O + \left(c_R + c_A\right) Sw_T\right] \tag{C.16}$$

where c_A is the correlation coefficient and includes collectively all corrections, including roughness allowance, but also particularities of the measuring device and towing tank and the method used (Bertram, 2000). According to Bertram (2000), the correlation coefficient differs between various towing tanks. An example of such a formula for c_A is,

$$c_A = 0.35 \cdot 10^{-3} - 2L_{pp} \cdot 10^{-6} \tag{C.17}$$

where L_{pp} is the length between perpendiculars, but in this case the waterline length. The correlation coefficient ranges generally between 0.0002 and 0.0003 (Migeotte, 2005b).

C.2 Scaling Procedure with Foils

According to Hoppe (1995), the following empirical relation exists between prototype and model regarding the resistance-displacement ratio, ε:

$$\varepsilon = k_{corr} \varepsilon_m \tag{C.18}$$

where $\varepsilon = R_T / \Delta$. R_T and Δ are the total resistance and displacement mass respectively. The correlation factor for multiple foils for hydrofoil-assisted crafts according to Migeotte (2001) is:

$$k_{corr} = 1.0 - \frac{C_{Fhm} - C_{Fh} - C_A}{C_{Tm}} - \sum_i^n \frac{A_{FS_i}}{Sw} \frac{C_{Dm_i} - C_{D_i} - C_{Af_i}}{C_{Tm}} \tag{C.19}$$

where:

C_{Fhm}	frictional resistance coefficient of the model hull
C_{Fh}	frictional resistance coefficient of the prototype hull
C_A	roughness allowance for the prototype hull
C_{Tm}	total resistance coefficient of the model
A_{FS}	hydrofoil wetted area of the prototype
Sw	hull wetted area of the prototype
C_{Dm}	drag resistance coefficient of a foil of the model
C_D	drag resistance coefficient of a foil of the prototype
C_{Af}	roughness allowance for the model foils (Generally $C_{Af} \approx 0$)
n	the number of foils

The following relation developed by Kirkman et al. (1980) for estimating the drag coefficient takes into account laminar flow and separation of the flow associated with model foils. The drag coefficient is a function of Reynolds number and is given as follows:

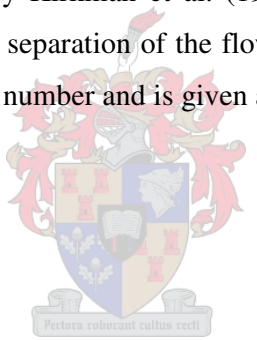

For $Rn < 5 \cdot 10^4$:

$$C_{DO_0} = 1.46 Rn^{-0.507}$$

$$C_{DO_{20}} = 0.466 Rn^{-0.259}$$

For $5 \cdot 10^4 \le Rn < 5 \cdot 10^5$:

$$C_{DO_0} = 0.172 Rn^{-0.310}$$

$$C_{DO_{20}} = 181 Rn^{-0.810}$$

For $5 \cdot 10^5 \le Rn < 1 \cdot 10^7$:

$$C_{DO} = 2.93 \cdot 10^{-3} \left[1 + 2\frac{t}{c} + 60\left(\frac{t}{c}\right)^4 \right]$$

For $Rn > 1 \cdot 10^7$:

$$C_{DO} = 0.03 Rn^{-0.1428} \left[1 + 2\frac{t}{c} + 60\left(\frac{t}{c}\right)^4 \right] \tag{C.20}$$

where t and c are the maximum foil thickness and the chord length respectively. C_{DO_0} represents values for $t/c = 0$ and $C_{DO_{20}}$ values for $t/c = 0.20$. Values for other thickness to chord ratios can be linearly interpolated from these (Migeotte, 2001).

Appendix D Input file of Michlet Version 6.05

The following is an input file for Michlet Version 6.05 that determines a hydrofoil-assisted trimaran with a 30 % LCG and a speed range of 0 knots to 52.5 knots.

```
======================================================================
                        MICHLET version 6
                             INPUT FILE
======================================================================
Note 1: Trimaran
Note 2: 161 tonnes
Note 3: With foils
Note 4: 30% LCG
Note 5: 0 m/s to 27 m/s
======================================================================
Course Particulars (0=None)
0
Number of Hulls (1, 2,..., 5)
3
Gravitational Acceleration (m/sec/sec) (min 9.6, max 9.9)
9.81
Water Density (kg/cubic metre) (min 995.0, max 1030.0)
1023.2
Water Kin. Viscosity (sq. m/sec * 10^-6) (min 0.8, max 1.31)
0.94251
Water Depth (metres) (max=10000.0)
10000.0
Sea State (0=Calm)
0
Ship Motion Method (0=None)
0
Minimum Speed (m/sec) (min 0.01, max 39.9)
1.0
Mximum Speed (m/sec) (max 40.0)
27
Number of Speeds (min 2, max 50)
14
Leeway Parameters (0=None)
0
Wave Drag Method (0=None, 1,ntheta=Michell, 2,ntheta,Re=Michell+BL)
2,1000,0.0
Skin Friction Method (0=None, 1=ITTC1957)
1
Form Factor Type (0=None, 1=Holtrop, 2=Scragg)
0
Transom Condition (0=Wet, 1=Dry, 2,Ftcrit=Simple Finite Hollow)
2,3.5
Added Resistance Method (0=None)
0
Pressure Signature Method (0=None)
0
Number of Offset Stations (rows) (odd integer: min 5, max 81)
11
Number of Offset Waterlines (columns) (odd integer: min 5, max 41)
39
Sectorial Wave Elevation Patch Parameters (R0,R1,Beta,Nr,Nbeta)
15,100,30,100,100
Rectangular Wave Elevation Patch Parameters (x0,x1,y0,y1,Nx,Ny)
16.0,60.0,-22.0,22.0,100,100
============================ FIRST HULL ==============================
Offsets
-1
Displacement Volume (cubic metres)
147.651
Length (metres)
37.291
Draft (metres)
2.092
Longitudinal Separation (metres) (0.0 for a monohull)
0.0
```

```
Lateral Separation Distance (metres) (0.0 for a monohull)
0.0
Loading Particulars (0=None)
0
Trim (0=None, 2=Exp)
2,2.104,1.911,1.883,2.155,2.427,2.653,2.877,2.764,2.609,2.311,2.101,2.073,2.0287,1.991
Sink (0=None, 2=Exp)
2,0.000,-0.001,0.005,0.023,0.041,-0.035,-0.113,-0.237,-0.366,-0.465,-0.574,-0.685,-0.746,-0.797
Heel (0=None)
0
Appendages (0=None)
0
Other Particulars (0=None)
0
============================ second HULL ==============================
Offsets
-1
Displacement Volume (cubic metres)
4.712
Length (metres)
22.359
Draft (metres)
0.4
Longitudinal Separation (metres) (0.0 for a monohull)
7.466
Lateral Separation Distance (metres) (0.0 for a monohull)
4.87
Loading Particulars (0=None)
0
Trim (0=None, 2=Exp)
2,2.104,1.911,1.883,2.155,2.427,2.653,2.877,2.764,2.609,2.311,2.101,2.073,2.0287,1.991
Sink (0=None, 2=Exp)
2,-0.001,-0.003,0.027,0.114,0.201,-0.175,-0.562,-0.761,-0.938,-0.999,-0.999,-0.999,-0.999,-0.999
Heel (0=None)
0
Appendages (0=None)
0
Other Particulars (0=None)
0
============================ third HULL ===============================
Offsets
-1
Displacement Volume (cubic metres)
4.712
Length (metres)
21.359
Draft (metres)
0.4
Longitudinal Separation (metres) (0.0 for a monohull)
7.466
Lateral Separation Distance (metres) (0.0 for a monohull)
-4.87
Loading Particulars (0=None)
0
Trim (0=None, 2=Exp)
2,2.104,1.911,1.883,2.155,2.427,2.653,2.877,2.764,2.609,2.311,2.101,2.073,2.0287,1.991
Sink (0=None, 2=Exp)
2,-0.001,-0.003,0.027,0.114,0.201,-0.175,-0.562,-0.761,-0.938,-0.999,-0.999,-0.999,-0.999,-0.999
Heel (0=None)
0
Appendages (0=None)
0
Other Particulars (0=None)
0
```

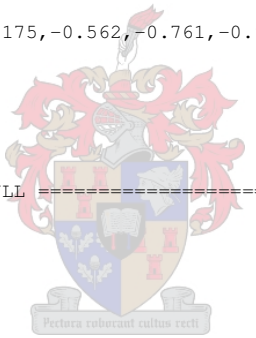

Appendix E Numerical Results Spreadsheet

E.1 Correlation Spreadsheet

The following are examples of spreadsheets containing the numerical values from experimental results scaled to full-scale values and all the necessary constants and values needed to achieve the full-scale values. The equations that are used in this section are given in appendix C. Two different correlation methods are used for the trimaran with and without foils.

E.1.1 Correlation method without foils

The following spreadsheet gives the correlation values for the trimaran with a 34 % LCG position and without foils.

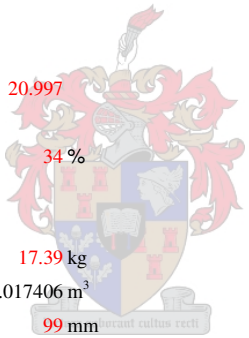

Scaling Factor:	20.997	
LCG :	34 %	
Model		
Displacement :	17.39 kg	
Displacement :	0.017406 m^3	
Draft :	99 mm	
Static Trim:	0 degrees	
Full Scale		
Displacement :	161000 kg	
Displacement :	157.349 m^3	
Draft :	2.079 m	
Water Conditions:		
Fresh Water		
Temperature:		14
	density [kg/m^3]:	999.155
	kinematic viscosity[cSt]:	1.170
Salt Water, 3.5% Salinity		
Temperature:		25
	density [kg/m^3]:	1023.206
	kinematic viscosity[cSt]:	0.943
Tank Dimensions:		
Width:	4.5 m	
Depth:	2.7 m	

Measurement Information:

Distances from transom

Rear trim meter [mm]:	-10
Forward trim meter [mm]:	1452
Model sinkage calculated at [mm]:	655

	MODEL (*) – Measured experimental data								
	V	Fn	Total Resistance	Front Trim	Rear Trim	Sw O	Sw MH	L_{wl} O	L_{wl} MH
	m/s		N	mm	mm	m^2	m^2	mm	mm
1	0.999	0.627	2.152	-0.3	-3.3	0.0777	0.4387	1077	1764
2	1.951	1.223	12.492	7.0	-17.7	0.0898	0.4394	1087	1752
3	2.884	1.809	23.512	26.4	-25.4	0.1099	0.4565	1074	1743
4	3.890	2.440	30.277	21.7	-8.5	0.1320	0.4760	1060	1733
5	4.818	3.022	39.567	18.9	-5.5	0.1332	0.5331	1054	1734
6	5.845	3.666	55.875	15.4	-4.1	0.1316	0.6020	1048	1737
7	0	0	0	0	0	0	0	0	0

Table E.1: Experimental measured input data

	MODEL (*)									
	Rn O	Rn MH	C_F O	C_F MH	R_F O	R_F MH	R_R	C_R	Trim	Sinkage
					N	N	N		Degrees	mm
1	919907.8	1507414	0.00477	0.00429	0.185	0.940	0.841	0.00283	0.12	-1.9
2	1812463	2923641	0.00413	0.00376	0.706	3.142	7.937	0.00674	0.97	-6.4
3	2648957	4298682	0.00383	0.00349	1.750	6.628	13.381	0.00476	2.04	-1.7
4	3524267	5764391	0.00362	0.00330	3.620	11.908	11.128	0.00198	1.19	5.3
5	4340468	7144382	0.00348	0.00318	5.387	19.687	9.104	0.00098	0.96	5.6
6	5236505	8678495	0.00336	0.00307	7.565	31.598	9.145	0.00061	0.77	4.8
7	0	0	0	0	0	0	0	0	0	0

Table E.2: Model data

	FULL SCALE									
	V	V	L_{wl} O	L_{wl} MH	Sw O	Sw MH	Rn O	Rn MH	C_F O	C_F MH
	kn	m/s	m	m	m^2	m^2				
1	8.86	4.561	22.603	37.039	34.2616	193.4269	109403703.7	179275209	0.00206	0.00192
2	17.31	8.905	22.813	36.799	39.5973	193.7290	215554413.8	347705647	0.00187	0.00175
3	25.59	13.164	22.554	36.601	48.4440	201.2819	315037738.2	511237938	0.00178	0.00167
4	34.51	17.755	22.248	36.390	58.1955	209.8556	419137546.2	685553123	0.00171	0.00160
5	42.75	21.994	22.120	36.410	58.7127	235.0409	516207464.6	849674048	0.00166	0.00156
6	51.86	26.677	22.002	36.464	58.0275	265.4263	622772243.1	1.032E+09	0.00163	0.00152
7	0	0	0	0	0	0	0	0	0	0

Table E.3: Prototype data

	FULL-SCALE					
	R_F O	R_F MH	R_R	R_T (without C_A)	C_A	R_T (with C_A)
	N	N	N	N		N
1	750.14	3949.48	7912.49	**13362.27**	0.000276	**14131.78**
2	3003.77	13777.67	74653.09	**94438.32**	0.000276	**97498.99**
3	7628.48	29740.21	125861.78	**170858.97**	0.000276	**178176.58**
4	16052.15	54322.55	104665.23	**191092.09**	0.000277	**205679.45**
5	24184.50	90862.83	85632.68	**224864.53**	0.000277	**249043.21**
6	34326.71	147345.44	86016.12	**302014.99**	0.000277	**340500.30**
7	0	0	0	**0**	0.00035	**0**

Table E.4: Different resistance components of the prototype

Correction due to BLOCKAGE and SHALLOW WATER EFFECT:

	V	A_x	p	R_H	Blockage Ratio	L/h	Fn(depth)
	m/s	m^2	m	m	< 0.2(no blockage)	< 1(no sh e.)	< 0.8(no sh e.)
1	0.999	0.0163	0.528	1.164	0.110	0.653	0.194
2	1.951	0.0203	0.614	1.154	0.124	0.649	0.379
3	2.884	0.0224	0.660	1.148	0.131	0.646	0.560
4	3.890	0.0178	0.559	1.156	0.115	0.642	0.756
5	4.819	0.0170	0.542	1.162	0.112	0.642	0.936
6	5.845	0.0166	0.533	1.163	0.111	0.643	1.136
7	0	0	0	0			
					No blockage	No shallow water effect	

Table E.5: Blockage and shallow water effect corrections

	Speed	R_T	Trim	Rise/Dmax
	m/s	kN	Degrees	
1	4.561	14.13	0.12	-0.019
2	8.905	97.50	0.98	-0.065
3	13.164	178.18	2.04	-0.017
4	17.755	205.68	1.19	0.054
5	21.994	249.04	0.97	0.057
6	26.678	340.50	0.77	0.049
7	0	#NUM!	0	0

Table E.6: Summary of prototype data

E.1.2 Correlation method with foils

The following spreadsheet gives the correlation values for the trimaran with a 32 % LCG position and with foils.

Scaling Factor: 20.997

LCG : 32 %

Model

Displacement : 17.39 kg

Displacement : 0.017406 m^3

Draft Main-hull : 99 mm

Floating Trim Angle : 1.25 Degrees

Draft Outrigger: 20 mm

Full Scale

Displacement : 161000 kg

Displacement : 157.349 m^3

Draft : 2.079 m

Water Conditions:

Fresh Water

Temperature: 12.4

density [kg/m^3]: 999.365

kinematic viscosity[cSt]: 1.221

Salt Water, 3.5% Salinity

Temperature: 25

density [kg/m^3]: 1023.206

kinematic viscosity[cSt]: 0.943

Tank Dimensions:

Width: 4.5 m

Depth: 2.7 m

Measurement Information:

Distances from transom

Rear trim meter [mm]:	-10.000
Forward trim meter [mm]:	1452.000
Model sinkage calculated at [mm]:	609.6

Foils:

Front Foil (model)

Chord length:	0.072 m
Circumference:	0.14 m
Thickness:	0.0034 m
Span:	0.786 m
Strut chord length:	0.072 m
Strut circumference:	0.141 m
Avg. Angle-of-Attack:	-0.7 Degrees
Planform Area (Model):	0.033 m^2
Planform Area (Prototype):	14.373 m^2

Rear Foil (model)

Chord length:	0.0505 m
Circumference:	0.102 m
Span:	0.184 m
Thickness:	0.0035 m
Strut chord length:	0.039 m
Strut circumference:	0.079 m
Avg. Angle-of-Attack (Starboard):	0.4 Degrees
Avg. Angle-of-Attack (Port):	0.4 Degrees
Planform Area (Model):	0.0093 m^2
Planform Area (Prototype):	4.100 m^2

	MODEL								
	V	Fn	R_T	Front Trim	Rear Trim	Sw O	Sw MH	L_{wl} O	L_{wl} MH
	m/s		N	mm	mm	m^2	m^2	mm	mm
1	0.944	0.592	2.74	0.8	-1.6	0.0646	0.4245	1032	1739
2	1.978	1.241	15.99	9.1	-11.7	0.0641	0.4098	1007	1722
3	2.892	1.814	21.28	32.7	-0.4	0.0480	0.3562	853	1674
4	3.852	2.416	20.88	53.4	28.7	0.0308	0.2988	689	1622
5	4.865	3.051	20.35	71.7	57.9	0.0119	0.1957	281	1271
6	5.801	3.638	21.27	89.6	75.4	0	0.1265	0	1020
7	0	0	0	0	0	0	0	0	0
8	0	0	0	0	0	0	0	0	0

Table E.7: Experimental measured input data

	Speed	Rn O	Rn MH	C_F O	C_F MH	C_T	Rn	Rn	C_F	C_F	Sw	C_T*
	m/s						Front foil	Rear foil	Front foil	Rear foil	m^2	
1	0.944	798286.0	1345063.1	0.00492	0.00439	0.01112	55676.488	39050.870	0.01056	0.01493	0.5536	0.0111
2	1.978	1631851.4	2789653.3	0.00422	0.00379	0.01520	116616.342	81793.406	0.00689	0.00994	0.5379	0.0152
3	2.892	2022190.0	3964708.6	0.00404	0.00354	0.01125	170499.078	119586.159	0.00561	0.00783	0.4522	0.0112
4	3.852	2174076.0	5118207.9	0.00398	0.00338	0.00781	227067.431	159262.574	0.00483	0.00657	0.3604	0.0078
5	4.865	1119305.3	5065817.3	0.00457	0.00338	0.00783	286787.676	201149.689	0.00429	0.00572	0.2195	0.0078
6	5.800	0	4844110.0	0	0.00341	0.00999	341937.180	239830.938	0.00393	0.00516	0.1265	0.0099
7	0	0	0	0	0	0	0	0	0	0	0	0
8	0	0	0	0	0	0	0	0	0	0	0	0

Table E.8: Model data

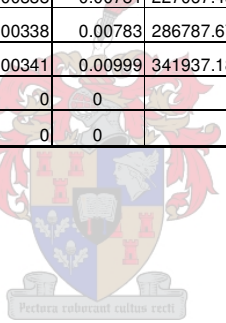

	Struts - Model			
	Rear Strut height	Front strut 1 height	Front strut 2 height	Front strut 3 height
	mm	mm	mm	mm
1	79	24	120	100
2	79	24	120	100
3	79	24	80	64
4	79	24	37	26
5	59	16	20	14
6	37	7	10	6
7	0	0	0	0
8	0	0	0	0
	Struts - Prototype			
	Sw (Rear Strut)	Sw (Front strut 1)	Sw (Front strut 2)	Sw (Front strut 3)
	m^2	m^2	m^2	m^2
1	9.056	5.079	25.395	21.166
2	9.056	5.079	25.395	21.346
3	9.056	5.079	16.897	13.608
4	9.056	5.079	7.758	5.485
5	6.725	3.340	4.335	2.859
6	4.205	1.459	2.157	1.374
7	0	0	0	0
8	0	0	0	0

Table E.9: Height and area of each strut (Model and prototype)

	Speed	Rn O	Rn MH	C_F O	C_F MH	C_A	Sw (Hulls)
	m/s						m^2
1	4.311	99148760.4	167059592	0.00209	0.00194	0.000276	244.110
2	9.030	202679297.3	346480657	0.00189	0.00175	0.000277	237.198
3	13.202	251160145.6	492424940	0.00183	0.00168	0.000279	199.411
4	17.582	270024698.6	635691915	0.00181	0.00162	0.000281	158.934
5	22.206	139020014	629184897	0.00199	0.00162	0.000296	96.801
6	26.477	0	601648392		0.00163	0.000307	55.790
7	0	0	0	0	0	0	0
8	0	0	0	0	0	0	0

Table E.10: Prototype data

	Struts			
	Rn (Front Strut)	Rn (Rear Strut)	C_F (Front strut)	C_F (Rear strut)
1	6915133.96	4850198.12	0.00321	0.00334
2	14483988.65	10158908.71	0.00311	0.00341
3	21176334.82	14852845.95	0.00295	0.00323
4	28202240.36	19780738.03	0.00283	0.00310
5	35619616.93	24983203.54	0.00274	0.00300
6	42469298.28	29787493.93	0.00267	0.00293
7	0	0	0	0
8	0	0	0	0
	Foils			
	Rn (Front foil)	Rn (Rear foil)	C_F (Front foil)	C_F (Rear foil)
1	6915133.95	4850198.12	0.00320	0.00334
2	14483988.65	10158908.71	0.00311	0.00341
3	21176334.82	14852845.95	0.00295	0.00323
4	28202240.36	19780738.03	0.00283	0.00310
5	35619616.93	24983203.54	0.00274	0.00300
6	42469298.28	29787493.93	0.00267	0.00292
7	0	0	0	0
8	0	0	0	0

Table E.11: Strut and foil data

	WITH STRUTS	
	k_{corr}	R_T Prototype (N)
1	0.463	11779.31
2	0.750	111179.06
3	0.746	147014.50
4	0.714	138001.54
5	0.717	135176.46
6	0.767	151098.91
7	0	0
8	0	0

Table E.12: Correction factor and total resistance of prototype

	Speed	Trim	Sinkage Main-hull	R_T With Struts	Sinkage Outrigger
	m/s	Degrees	%	kN	%
1	4.311	1.3	-0.006	11.78	-0.028
2	9.029	2.1	-0.028	111.18	-0.140
3	13.201	2.6	0.138	147.01	0.685
4	17.582	2.2	0.396	138.00	1.960
5	22.206	1.8	0.644	135.18	3.190
6	26.476	1.8	0.823	151.10	4.074
7	0	0	0	0	0
8	0	0	0	0	0

Table E.13: Summary of prototype data

E.2 Wetted Surface Area Spreadsheet

The following tables gives the data of the wetted surface area calculations for the trimaran with a 34 % LCG position and without foils.

LCG	34 %
Length of Station - Main Hull [mm]	180
Length of Station - Outrigger [mm]	Varies
Speed [m/s]:	2
l_{wl} - Main Hull [m]:	1752
l_{wl} - Outrigger [m]:	1087

SECTION	*Half Main Hull Sw [mm²]*	*Outrigger Sw [mm²]*	*Station*	*Outrigger Station Length*	*Main*	*Outrigger Outside*	*Outrigger Inside*	*Added Area Main*	*Added Area O/Outside*	*Added Area O/Inner*	*Total Area*	*Area single Outrigger mm²*	*Area Main Hull mm²*
A1	26280.00	7290.00	0	90	8	15	11	1170	1260	990	73980.00	9540.00	54900.00
A2	26280.00	8058.00	1	102	5	13	11	720	1275	1173	75012.00	10506.00	54000.00
A3	26280.00	7800.00	2	100	3	12	12	270	950	1200	73000.00	9950.00	53100.00
A4	26280.00	7546.00	3	98	0	7	12	-540	490	1078	69708.00	9114.00	51480.00
A5	25740.00	7650.00	4	102	-6	3	10	-1170	153	1020	66786.00	8823.00	49140.00
A6	24300.00	7446.00	5	102	-7	0	10	-1170	-153	510	61866.00	7803.00	46260.00
A7	22950.00	7280.00	6	104	-6	-3	0	-990	-364	-780	56192.00	6136.00	43920.00
A8	20700.00	5568.00	7	96	-5	-4	-15	-270	48	-1296	49500.00	4320.00	40860.00
A9	17100.00	4444.00	8	101	2	5	-12	180	858.5	757.5	46680.00	6060.00	34560.00
A10		3395.00	9	97	0	12	27	5610	1309.5	3977	17363.00	8681.50	
			10			15	55		1425	3325	20720.00	4750	11220
			Horizontal :		132	95	95			TOTAL	0.610807	0.0904335	0.44

Table E.14: Wetted surface area at 2 m/s

Speed [m/s]:			4										
l_{wl} - Main Hull [m]:			1732										
l_{wl} - Outrigger [m]:			1058										
SECTION	Main Hull Sw [mm^2]	Outrigger Sw [mm^2]	Station	Outrigger Station Length	Main	Outrigger Outside	Outrigger Inside	Added Area Main	Added Area O/Outside	Added Area O/Inner	Total Area	Area single Outrigger mm^2	Area Main Hull mm^2
A1	26280.00	7290.00	0	90	19	24	20	3060	2070	2970	83340.00	12330.00	58680.00
A2	26280.00	8058.00	1	102	15	22	46	1620	2244	5202	86808.00	15504.00	55800.00
A3	26280.00	7800.00	2	100	3	22	56	180	2100	5500	83720.00	15400.00	52920.00
A4	26280.00	7546.00	3	98	-1	20	54	-360	2058	5243	81534.00	14847.00	51840.00
A5	25740.00	7650.00	4	102	-3	22	53	180	2244	5151	81930.00	15045.00	51840.00
A6	24300.00	7446.00	5	102	5	22	48	1530	2142	5508	81852.00	15096.00	51660.00
A7	22950.00	7280.00	6	104	12	20	60	3600	2132	5928	83780.00	15340.00	53100.00
A8	20700.00	5568.00	7	96	28	21	54	5400	2064	4512	76488.00	12144.00	52200.00
A9	17100.00	4444.00	8	101	32	22	40	3060	2121	3535	60520.00	10100.00	40320.00
A10		3395.00	9	97	2	20	30	4872	1455	2037	13774.00	6887.00	
			10			10	12		825	891	13176.00	1716	9744
			Horizontal :		112	66	66			TOTAL	0.746922	0.1344	0.478104

Table E.15: Wetted surface area at 4 m/s

Speed [m/s]:			6										
l_{wl} - Main Hull [m]:			1737										
l_{wl} - Outrigger [m]:			1047										
SECTION	Main Hull Sw [mm^2]	Outrigger Sw [mm^2]	Station	Outrigger Station Length	Main	Outrigger Outside	Outrigger Inside	Added Area Main	Added Area O/Outside	Added Area O/Inner	Total Area	Area single Outrigger mm^2	Area Main Hull mm^2
A1	26280.00	7290.00	0	90	0	23	35	-450	2070	3600	77580.00	12960.00	51660.00
A2	26280.00	8058.00	1	102	-5	23	45	900	2550	5253	86082.00	15861.00	54360.00
A3	26280.00	7800.00	2	100	15	27	58	6480	2700	5850	98220.00	16350.00	65520.00
A4	26280.00	7546.00	3	98	57	27	59	12330	2695	5586	108874.00	15827.00	77220.00
A5	25740.00	7650.00	4	102	80	28	55	14850	2856	5253	112698.00	15759.00	81180.00
A6	24300.00	7446.00	5	102	85	28	48	15660	2805	4743	109908.00	14994.00	79920.00
A7	22950.00	7280.00	6	104	89	27	45	15390	2652	4160	104864.00	14092.00	76680.00
A8	20700.00	5568.00	7	96	82	24	35	12960	2208	3024	88920.00	10800.00	67320.00
A9	17100.00	4444.00	8	101	62	22	28	6570	1868.5	2272.5	64510.00	8585.00	47340.00
A10		3395.00	9	97	11	15	17	5616	727.5	1067	10379.00	5189.50	
			10			0	5		412.5	550	13157.00	962.5	11232
			Horizontal :		117	55	55			TOTAL	0.875192	0.1314	0.612432

Table E.16: Wetted surface area at 6 m/s

Calculations					
Speed	lwl Main	lwl O/Rigs	Area Tot	Area Outrigger	Area Main Hull
0.999	1764	1076	0.5893	0.0777	0.4387
1.951	1752	1086	0.6097	0.0898	0.4394
2.884	1743	1074	0.6709	0.1098	0.4565
3.890	1733	1059	0.7394	0.1319	0.4759
4.818	1734	1053	0.7994	0.1331	0.5331
5.845	1736	1047	0.8652	0.1316	0.6020
0	0	0	0	0	0

Table E.17: Summary of wetted surface area data

Appendix F Model Photographs

F.1 Model without Foils

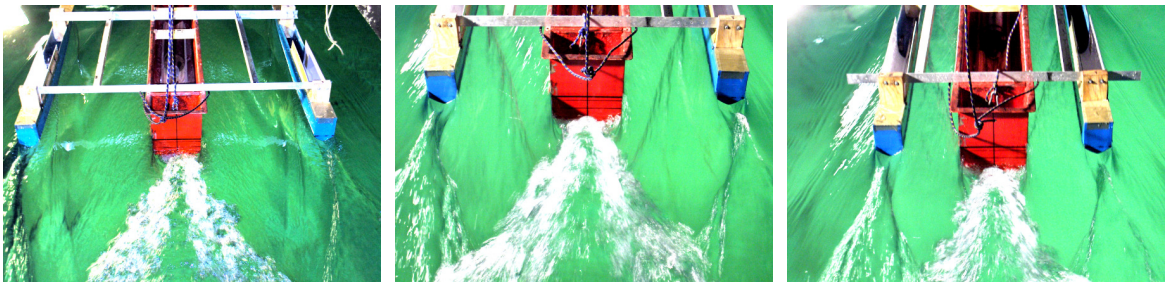

Figure F.1: Transom at 2 m/s with 34 % LCG (From left to right: FOP, MOP and COP)

Figure F.2: Transom at 4 m/s with 34 % LCG (From left to right: FOP, MOP and COP)

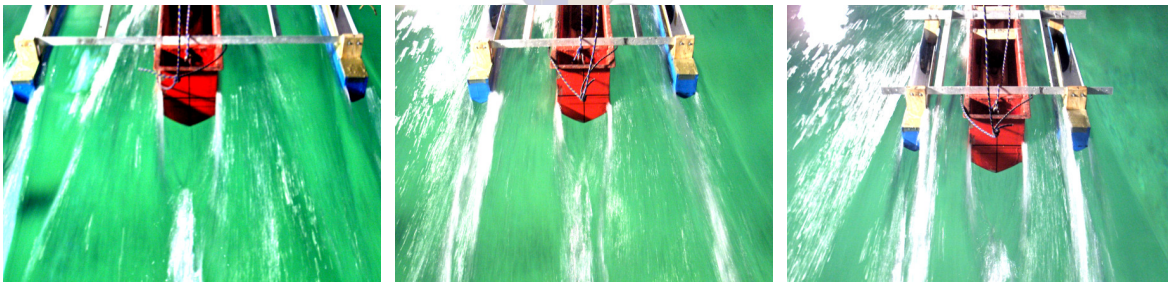

Figure F.3: Transom at 6 m/s with 34 % LCG (From left to right: FOP, MOP and COP)

Figure F.4: Transom at 2 m/s with 32 % LCG (From left to right: FOP, MOP and COP)

Figure F.5: Transom at 4 m/s with 32 % LCG (From left to right: FOP, MOP and COP)

Figure F.6: Transom at 6 m/s with 32 % LCG (From left to right: FOP, MOP and COP)

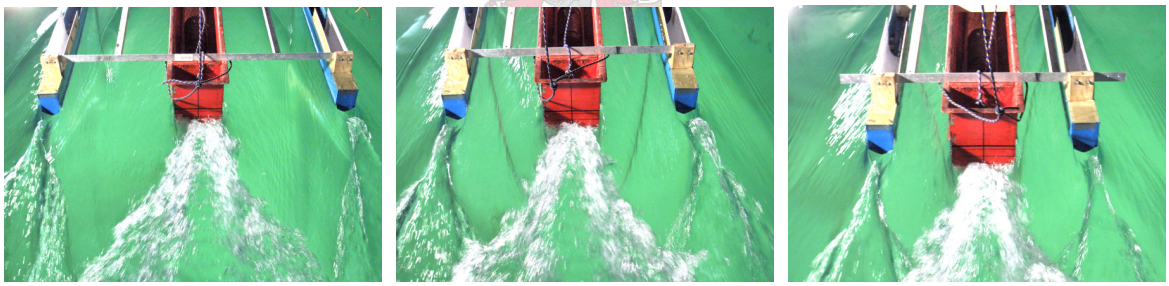

Figure F.7: Transom at 2 m/s with 30 % LCG (From left to right: FOP, MOP and COP)

Figure F.8: Transom at 4 m/s with 30 % LCG (From left to right: FOP, MOP and COP)

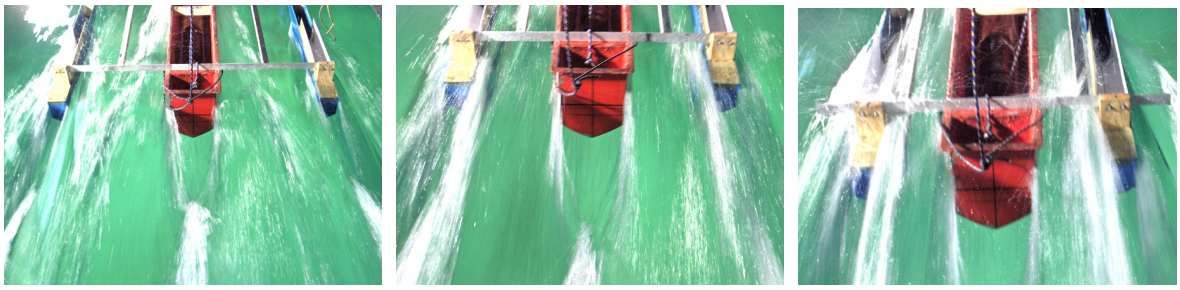

Figure F.9: Transom at 6 m/s with 30 % LCG (From left to right: FOP, MOP and COP)

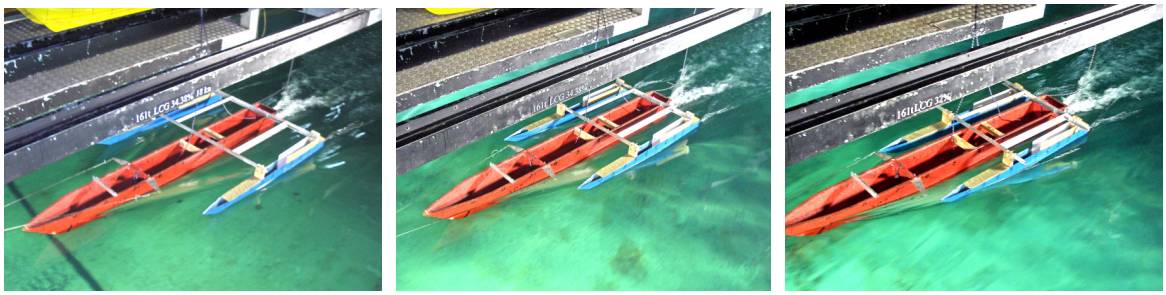

Figure F.10: Model at 2 m/s with 34 % LCG (From left to right: FOP, MOP and COP)

Figure F.11: Model at 4 m/s with 34 % LCG (From left to right: FOP, MOP and COP)

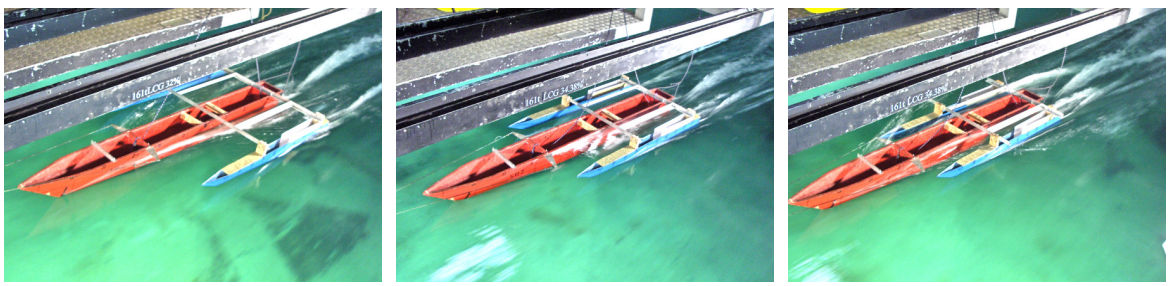

Figure F.12: Model at 6 m/s with 34 % LCG (From left to right: FOP, MOP and COP)

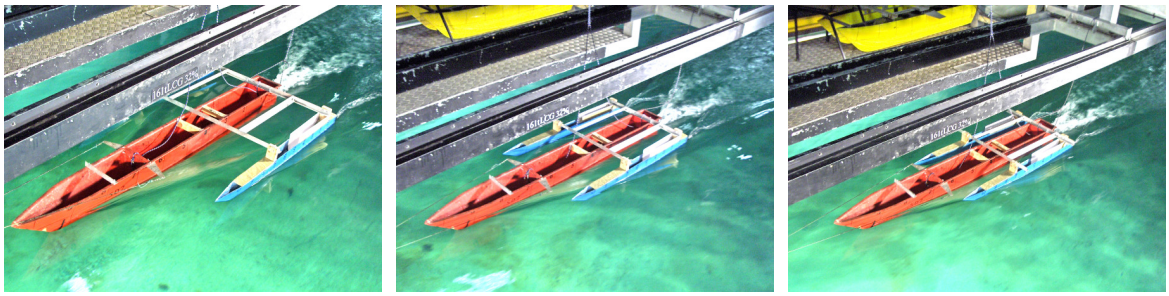

Figure F.13: Model at 2 m/s with 32 % LCG (From left to right: FOP, MOP and COP)

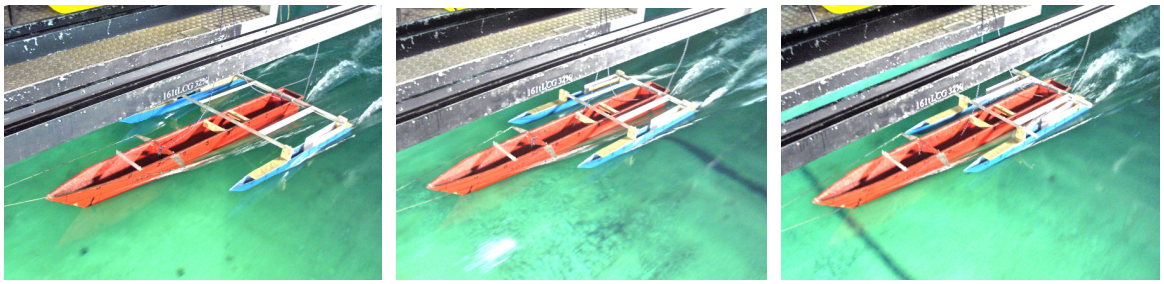

Figure F.14: Model at 4 m/s with 32 % LCG (From left to right: FOP, MOP and COP)

Figure F.15: Model at 6 m/s with 32 % LCG (From left to right: FOP, MOP and COP)

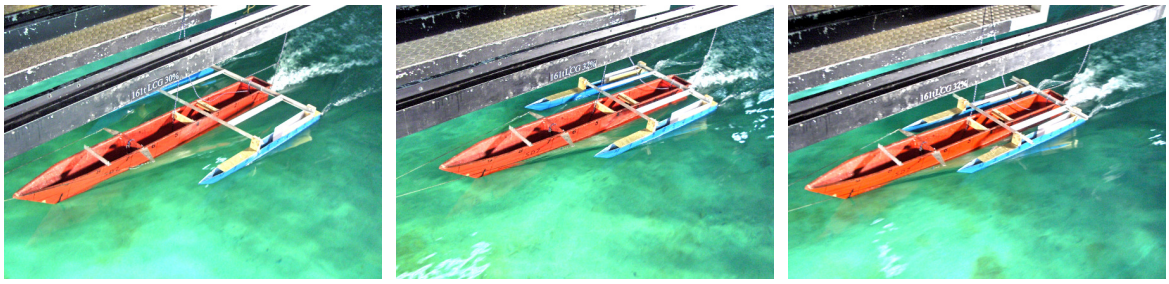

Figure F.16: Model at 2 m/s with 30 % LCG (From left to right: FOP, MOP and COP)

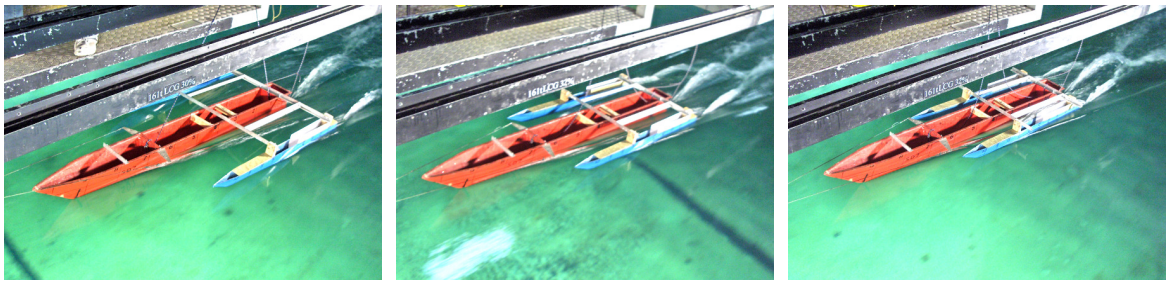

Figure F.17: Model at 4 m/s with 30 % LCG (From left to right: FOP, MOP and COP)

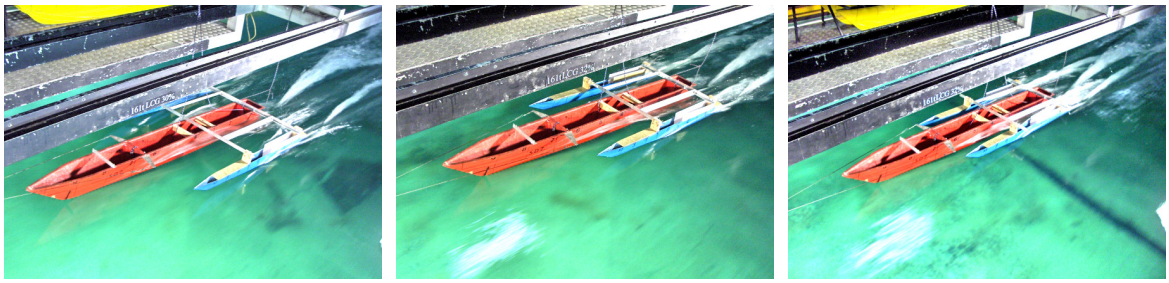

Figure F.18: Model at 6 m/s with 30 % LCG (From left to right: FOP, MOP and COP)

F.2 Model with Foils

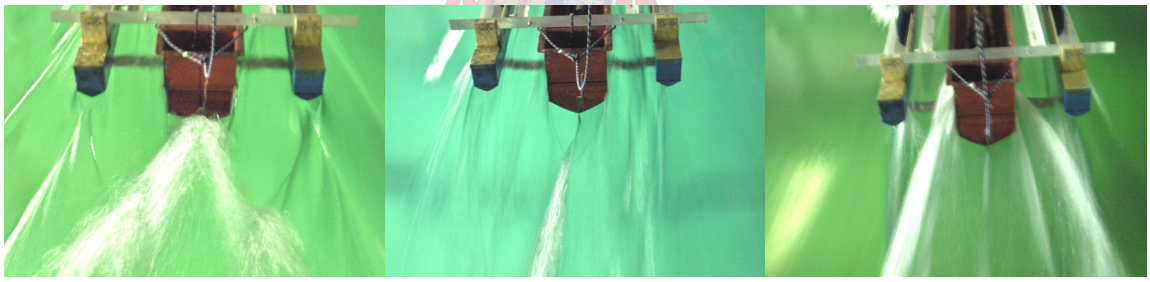

Figure F.19: Transom with 32 % LCG (From left to right: 2 m/s, 4 m/s and 6m/s)

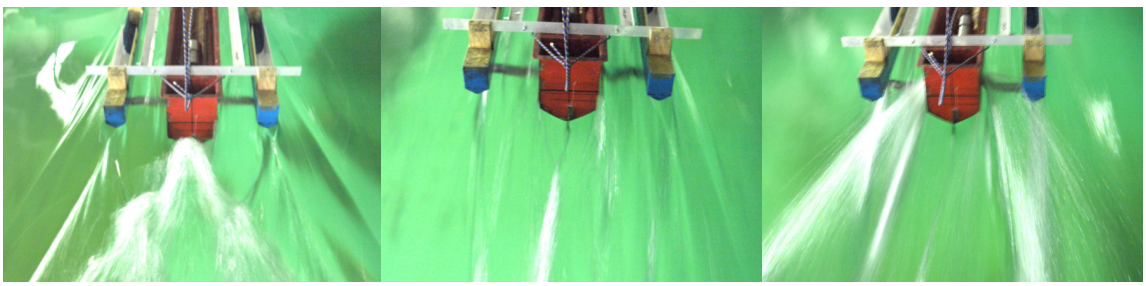

Figure F.20: Transom with 30 % LCG (From left to right: 2 m/s, 4 m/s and 6m/s)

Figure F.21: Model with 32 % LCG (From left to right: 2 m/s, 4 m/s and 6m/s)

Figure F.22: Model with 30 % LCG (From left to right: 2 m/s, 4 m/s and 6m/s)